



**GEOFORSCHUNGSZENTRUM POTSDAM**  
STIFTUNG DES ÖFFENTLICHEN RECHTS

---

# Scientific Technical Report

ISSN 1610-0956

# **Boron as a tracer for material transfer in subduction zones**

---

verfasst von  
Martin Siegfried Rosner  
geboren am 14.07. 1972 in Kassel

Dissertation  
zur Erlangung des akademischen Grades  
Doktor der Naturwissenschaften  
- Dr. rer. nat. -

eingereicht an der  
Mathematisch- Naturwissenschaftlichen Fakultät  
der Universität Potsdam

Potsdam, Januar 2003

Hiermit erkläre ich das die vorliegende Arbeit an keiner anderen Hochschule eingereicht wurde und von mir selbstständig und nur mit den angegebenen Hilfsmitteln angefertigt wurde.

Potsdam den 6. Januar 2003

**Gutachter:**      **Prof. Dr. Jörg Erzinger (Universität Potsdam)**  
                         **Prof. Dr. Gerhard Franz (Technische Universität Berlin)**  
                         **Prof. Dr. Roland Oberhänsli (Universität Potsdam)**

## Table of contents

<b>ERWEITERTE ZUSAMMENFASSUNG</b>	<b>1</b>
<b>CHAPTER I - Methodology of boron isotope and concentration analyses</b>	
<b>I.1 Introduction</b>	<b>7</b>
<b>I.2 Reagents and laboratory equipment</b>	<b>10</b>
<b>I.3 Boron concentration analyses</b>	<b>11</b>
<b>I.4 Methods of boron isotope analysis</b>	<b>12</b>
I.4.1 Mass spectrometric methods	12
I.4.1.1 Thermal ionisation mass spectrometry (TIMS)	13
I.4.1.1.1 PTIMS: The $\text{Cs}_2\text{BO}_2^+$ -graphite method	13
I.4.1.1.2 NTIMS: The $\text{BO}_2^-$ method	14
I.4.1.2 MC-ICP-MS and SIMS	14
<b>I.5. Sample preparation</b>	<b>15</b>
I.5.1 Dissolution methods	15
I.5.1.1 Carbonate fusion	16
I.5.1.2 Acid attack	16
I.5.2. Boron separation by ion exchange chromatography	17
I.5.2.1 Ion exchange chromatography after alkaline fusion	19
I.5.2.1.1 Purification after $\text{K}_2\text{CO}_3$ fusion (first separation step)	19
I.5.2.1.2 Removal of major cations (second separation step)	20
I.5.2.1.3 Purification of boron (third separation step)	21
I.5.2.2 Ion exchange chromatography after HF attack	22
<b>I.6 Loading techniques for TIMS</b>	<b>22</b>
<b>I.7 Mass spectrometry and data reduction</b>	<b>24</b>
I.7.1 PTIMS measuring procedure and data reduction	24
I.7.2 NTIMS measuring procedure and data reduction	26
<b>I.8 Analytical boron blank</b>	<b>28</b>
I.8.1 NIST SRM 952 as the spike material	28
I.8.2 Air-derived boron-blank	30
I.8.3 Reagent blanks	32
I.8.4 PTIMS loading blank	33
I.8.5 PTIMS procedure blanks	33
I.8.6 Overall blank effect on the "true" $\delta^{11}\text{B}$ value of a sample	35
<b>I.9 Summary of new methodological developments</b>	<b>36</b>

## **CHAPTER II - Boron isotopic composition and concentration of ten geological reference materials**

<b>II Abstract</b>	<b>38</b>
<b>II.1 Introduction</b>	<b>38</b>
<b>II.2 Samples</b>	<b>40</b>
<b>II.3 Analytical methods</b>	<b>41</b>
II.3.1 Boron concentration analyses	41
II.3.2 Boron isotope analyses	41
II.3.2.1 PTIMS: The $\text{Cs}_2\text{BO}_2^+$ -graphite method	41
II.3.2.2 NTIMS: The $\text{BO}_2^-$ method	42
II.3.3 Boron blank	42
<b>II.4 Results and discussion</b>	<b>43</b>
I.4.1 Boron concentrations	43
I.4.2 Boron isotopic compositions	44
I.4.2.1 NIST SRM 951	44
I.4.2.2 Influence of chemical separation	45
I.4.2.3 Silicate reference material	47
<b>I.5 Conclusions and recommended values</b>	<b>51</b>

## **CHAPTER III - Slab-derived boron isotope signatures in arc volcanic rocks from the Central Andes and evidence for boron isotope fractionation during progressive slab dehydration**

<b>III Abstract</b>	<b>53</b>
<b>III.1 Introduction</b>	<b>54</b>
<b>III.2 Geological setting</b>	<b>54</b>
<b>III.3 Boron behavior in subduction zone processes</b>	<b>57</b>
<b>III.4 Samples and analytical methods</b>	<b>59</b>
<b>III.5 Results</b>	<b>61</b>
<b>III.6 Discussion</b>	<b>68</b>
III.6.1 Boron sources in CVZ magmas	68
III.6.2 B-isotope fractionation, crustal contamination and the across-arc $\delta^{11}\text{B}$ variation	72
III.6.3 Coupled B, Sr and Nd mixing models	77
<b>III.7 Conclusions</b>	<b>81</b>

## **REFERENCES**

<b>APPENDIX</b>	<b>94</b>
<b>Appendix 1</b> (List of replicate $\text{Cs}_2\text{BO}_2^+$ -measurements of NIST SRM 951)	95
<b>Appendix 2</b> (List of individual boron isotope analyses of Andean arc volcanics)	97
<b>Appendix 3</b> (Sample list of investigated Andean arc volcanics)	99
<b>Appendix 4</b> (List of main and trace element concentrations)	100
<b>Appendix 5</b> (Danksagung)	<b>103</b>
<b>Appendix 6</b> (Curriculum vitae)	<b>104</b>

## ERWEITERTE ZUSAMMENFASSUNG

Geologische Prozesse an konvergenten Lithosphärenplattenränder haben großen Einfluß auf die stoffliche und strukturelle Entwicklung der kontinentalen Kruste. Insbesondere die Untersuchung der Stoffkreisläufe in Subduktionszonen bietet die Möglichkeit Aussagen über die Entwicklung der kontinentalen Kruste und der verschiedenen Mantelreservoirs zu machen, sowie die dynamischen Prozesse während der Subduktion und der einhergehenden prograden Metamorphose der ozeanischen Kruste zu charakterisieren. Traditionell wurden für diese Aufgabe die Isotopenverhältnisse der Elemente Strontium, Neodymium und Blei, sowie Verhältnisse fluidmobiler zu nicht-fluidmobiler Elemente eingesetzt. In der Diskussion über den Klimawandel sind in den letzten Jahren Themen wie z. B. der Einfluß des Stofftransfers über Subduktionszonen vom Ozean in den Mantel und zurück in die Biosphäre in den Brennpunkt der Geowissenschaften gerückt. Um die Auswirkungen der anthropogen herbeigeführten Veränderungen, wie z. B. die Erhöhung des CO<sub>2</sub>-Gehaltes der Atmosphäre, auf das Klima abzuschätzen, ist ein detaillierteres Wissen der generellen Stoffflüsse von der Biosphäre in die feste Erde und zurück notwendig, die sich seit dem Archaikum konzentriert an den Subduktionszonen konvergenter Lithosphärenplatten abspielen. Den Stoffflüssen leichter Elemente wird in jüngster Zeit besondere Bedeutung beigemessen, da Elemente wie Lithium, Beryllium und vor allem Bor aufgrund ihrer speziellen geochemischen Eigenschaften ein großes Anwendungspotential innerhalb der Geowissenschaften offensteht.

Im Rahmen dieser Arbeit wurden subduktionsbezogene „Arc“-Vulkanite aus der Zentralen Vulkanischen Zone der Anden (22° bis 27° S) im Hinblick auf eine mögliche Subduktionskomponente von der ozeanischen Nazca-Platte untersucht. Die Zentralen Anden stellen ein Extrembeispiel eines Ozean-Kontinent Subduktionssystems dar, das durch seine bis zu 70 km dicke kontinentale Kruste einzigartig ist. Weil die Mantelsignaturen der primären „Arc“-Magmen bei den meisten geochemischen Tracern durch Kontamination in der verdickten andinen Kruste teilweise oder vollständig überprägt sind, ist in dieser Arbeit das Element Bor und seine Isotopenzusammensetzung als Anzeiger für einen Stofftransfer von der ozeanischen Unterplatte in die andine Oberplatte angewandt worden. Grundlegende Studien der letzten Jahre haben gezeigt, dass Bor wegen seiner hohen Mobilität in wässrigen Lösungen und Schmelzen und seiner starken Inkompatibilität bei den meisten magmatischen Prozessen besonders geeignet ist, um den Stofftransfer in Subduktionszonen zu untersuchen. Insbesondere durch die charakteristische Borisotopensignatur der durch Meerwasseralteration an <sup>11</sup>B angereicherten ozeanischen Kruste, die sich von allen anderen an der

„Arc“-Magmengenese beteiligten (Haupt-) Reservoiren unterscheidet, ist es möglich einen Stofftransfer von der ozeanischen Unterplatte in die „Arc“-Magmen zu identifizieren. Isotopenverhältnisse radiogener Elemente, wie die von Strontium, Neodymium und Blei, und Haupt- und Spurenelementkonzentrationen haben in der Vergangenheit keinen eindeutigen Hinweis auf die Beteiligung von Material aus der subduzierten Nazca-Platte an der Zusammensetzung der andinen „Arc“-Vulkanite ergeben. Ein weiteres Ziel war es, einen Beitrag zum generellen Verständnis der in Subduktionszonen ablaufenden Transferprozesse zu leisten und eventuell das Verhalten der Borisotope, d. h. eine eventuelle Isotopenfraktionierung während der Subduktion, genauer zu charakterisieren. Durch die Kombination von Bor- mit Strontium- und Neodymiumisotopendaten wurden in einem Mischungsmodell die Anteile der involvierten Hauptreservoire am Aufbau der „Arc“-Vulkanite kalkuliert. Um dieses Vorhaben analytisch zu ermöglichen, war es zuerst notwendig die  $\text{Cs}_2\text{BO}_2^+$ -Graphit Methode, die als genaueste und am breitesten anwendbarste Methode zur Bestimmung der Borisotopie angesehen wird, am GeoForschungsZentrum Potsdam neu einzurichten. Ein Schwerpunkt lag dabei auf der Untersuchung von Referenzmaterialien. Die in der Vergangenheit am GeoForschungsZentrum Potsdam angewandte  $\text{BO}_2^-$  Methode erwies sich für dieses Projekt als wenig geeignet, um die Borisotopenzusammensetzung von magmatischen Gesteinen mit niedrigen Borkonzentrationen zu bestimmen.

Die vorliegende Arbeit gliedert sich in drei Teile. Teil 1 beschreibt die angewandten Verfahren und dokumentiert alle notwendigen Tests, Kalibrierungen und Weiterentwicklungen der nasschemischen und massenspektrometrischen Methoden. Die im Teil 2 präsentierten Borisotopen- und Borkonzentrationsdaten von Referenzmaterialien werden in Bezug auf ihre Richtigkeit und Genauigkeit diskutiert und sind in den nächsten Monaten als Artikel in *Geostandard Newsletters* vorgesehen. Die übergeordnete geochemische Fragestellung dieser Arbeit, die Anwendung von Bor als geochemischer Tracer im Subduktionssystem der Zentralen Anden, wird im Teil 3 präsentiert. Dieser Teil wurde als Artikel im September 2002 in *Geochemistry Geophysics Geosystems (G<sup>3</sup>)* eingereicht.

Die  $\text{Cs}_2\text{BO}_2^+$ -Graphit Methode wurde Anfang 2000 am GeoForschungsZentrum Potsdam aufgebaut. Die ersten, im Rahmen dieser Arbeit gewonnenen Ergebnisse wurden in dem Artikel von *Kasemann et al.* [2001] publiziert. Während des Aufbaus der  $\text{Cs}_2\text{BO}_2^+$ -Graphit Methode konnten mehrere Weiterentwicklungen der von *Nakamura et al.* [1992] und *Tonarini et al.* [1997] erstmals beschriebenen Verfahren etabliert werden. So ermöglicht die Umorganisation der sequentiellen Ionenchromatographie nach *Tonarini et al.* [1997]

die Verwendung des sehr effizienten Bor-spezifischen Anionentauscherharzes AMBERLITE 743 auch für Proben die mit Flußsäure aufgeschlossen werden. Durch die Auswechslung borhaltiger Luftfilter, die nach einer intensiven Testphase als Hauptquelle für den beobachteten hohen Boruntergrund in der Laborluft des Reinstraums des GeoForschungsZentrum Potsdam identifiziert wurden, konnte der Bor-Untergrundwert pro Probenaufbereitung um eine Größenordnung von ca. 200 ng Bor auf einen Wert von < 30 ng reduziert werden.

Für die Borsäure NIST SRM 951, die international als Referenz zur Kalkulation der  $\delta^{11}\text{B}$ -Werte verwendet wird, konnte aus 83 Einzelmessungen ein mittleres  $^{11}\text{B}/^{10}\text{B}$  Verhältnis von 4.05416 mit einer Reproduzierbarkeit dieses Mittelwertes von 0.04 ‰ ( $2\sigma_m$ ) bestimmt werden. Dieser Mittelwert zeigt eine Abweichung von 2.6 ‰ vom zertifizierten  $^{11}\text{B}/^{10}\text{B}$ -Verhältnis und liegt damit im typischen Bereich für die  $\text{Cs}_2\text{BO}_2^+$ -Graphit Methode. Für die zur Isotopenverdünnung genutzte, an  $^{10}\text{B}$  angereicherte, Borsäure NIST SRM 952 konnte ein  $^{11}\text{B}/^{10}\text{B}$ -Verhältnis von  $0.05413 \pm 0.00018$  ( $2\sigma_m$ ) bestimmt werden.

Weil bis heute nur wenige Referenzmaterialien auf ihre Borisotopenzusammensetzung untersucht wurden, sollten die bereits charakterisierten „Arc“-Magmatite JA-1, JB-3 und JR-2 vom Geological Survey of Japan zur Bewertung der Richtigkeit der hier bestimmten  $\delta^{11}\text{B}$ -Werte dienen. Die in dieser Studie bestimmten  $\delta^{11}\text{B}$ -Werte des JA-1 (+5.3 ‰), JB-3 (+5.9 ‰) and JR-2 (+2.9 ‰) überlappen im analytischen Fehler (externe Reproduzierbarkeit) mit den publizierten Werten und demonstrieren damit die Richtigkeit der präsentierten Daten und die Effizienz der angewandten analytischen Verfahren. Erstmals wurden für das sedimentäre Referenzmaterial TB (-12.6 ‰) vom Zentralen Geologischen Institut und für die MPI-DING Gläser GOR-128-G (+13.6 ‰), GOR-132-G (+7.1 ‰) und StHs6/80-G (+4.5 ‰)  $\delta^{11}\text{B}$ -Werte bestimmt. Durch wiederholte individuelle Präparationen einer Probe, einschließlich der beiden unterschiedlichen Aufschluss- und Präparationsmethoden, wurde eine „echte“ externe Reproduzierbarkeit von maximal 1 ‰ ( $1\sigma$ ) für silikatische Materialien mit niedrigen Borkonzentrationen zwischen 10 und 88  $\mu\text{g g}^{-1}$  B bestimmt. Dieser Maximalfehler ist angesichts der komplexen Probenpräparation und der geringen Borkonzentrationen der untersuchten Silikatproben für die meisten Anwendungen in der magmatischen Geochemie akzeptabel, da  $\delta^{11}\text{B}$ -Werte silikatischer Gesteine einen Bereich von ca. -20 bis plus 20 ‰ abdecken und somit je nach untersuchtem geologischen System erhebliche Variationen in der Borisotopenzusammensetzung vorliegen.

Proben, die sowohl mit unterschiedlichen massenspektrometrischen Methoden ( $\text{Cs}_2\text{BO}_2^+$ -Graphit und  $\text{BO}_2^-$  Methode) gemessen, als auch mit unterschiedlichen nasschemischen



Aufschluss- und Trennungsvorgänge bearbeitet wurden zeigen eine hohe Übereinstimmung der  $\delta^{11}\text{B}$ -Werte innerhalb der externen Reproduzierbarkeit. Das bedeutet, dass die angewandten Verfahren keinen systematischen Fehler aufweisen.

Die Borkonzentrationen der 10 bearbeiteten Referenzproben liegen zwischen 7 und 159  $\mu\text{g g}^{-1}$  B und überlappen innerhalb von 14 % mit Literaturdaten. Aufgrund wiederholter Borkonzentrationsbestimmung mehrerer individuell präparierter Teile einer Probe konnte eine externe Reproduzierbarkeit von < 10 % bestimmt werden.

Zur Untersuchung des Stofftransfers zwischen ozeanischer Unterplatte und andiner Oberplatte und der krustalen Kontamination der „Arc“-Magmen in der Zentralen Vulkanischen Zone wurden Bor-, Strontium, Neodymium- und Bleiisotopenverhältnisse sowie Haupt- und Spurenelementkonzentrationen an 21 quartären bis miozänen Lavenproben von 13 vulkanischen Zentren bestimmt. Die ausgewählten Proben stellen ein Profil von der vulkanischen Front im Westen bis in den „Back-arc“-Bereich im Osten über unterschiedlichen Tiefen der nach Osten abtauchenden eozänen Nazca-Platte dar. Dies ermöglicht die Untersuchung dynamischer Prozesse während der Subduktion und der einhergehenden Dehydratation der Unterplatte. Alle früheren Studien über die Borisotopenzusammensetzung von „Arc“-Vulkaniten haben sich mit Ozean-Ozean Subduktionszonen beschäftigt, während hier die erste systematische Untersuchung zur Borisotopenverteilung subduktionsbezogener Vulkanite in einer Kontinent-Ozean Subduktionszone durchgeführt wurde.

Aufgrund ihrer Haupt- und Spurenelementkonzentrationen handelt es sich bei den untersuchten Proben um mittel bis hoch an Kalium angereicherte basaltische Andesite bis Dazite, die ein für „Arc“-Vulkanite typisches Spurenelementmuster mit hohen Konzentrationen an lithophilen Elementen und niedrigen Nb-, P- und Ti-Konzentrationen zeigen. Die  $\delta^{11}\text{B}$ -Werte und Borkonzentrationen variieren über einen großen Bereich von -7 bis +4 ‰ und 6 bis 60  $\mu\text{g g}^{-1}$  B, wobei Proben mit positiven  $\delta^{11}\text{B}$ -Werten generell hohe Borkonzentrationen und Proben mit negativen  $\delta^{11}\text{B}$ -Werten generell niedrige Borkonzentrationen aufweisen. Im Vergleich zu Mittelozeanischen Rücken Basalten (MORB) haben die untersuchten andinen „Arc“-Vulkanite relativ radiogene  $^{87}\text{Sr}/^{86}\text{Sr}$ - (0.705981 – 0.708107) und  $^{207}\text{Pb}/^{204}\text{Pb}$ - (15.585 – 15.694) und nicht-radiogene  $^{143}\text{Nd}/^{144}\text{Nd}$ - (0.512249 – 0.512481) Isotopenverhältnisse.

Das auffälligste Merkmal bezüglich der Bordaten ist die systematische Variation der  $\delta^{11}\text{B}$ -Werte von +4 zu -7 ‰ über das andine „Arc“-Profil von Westen nach Osten. Eine solche „Across-arc“-Variation der  $\delta^{11}\text{B}$ -Werte wurde schon für verschiedene Ozean-Ozean

Suduktionszonen gefunden und konnte anhand dieser Arbeit erstmals in einer Kontinent-Ozean Subduktionzone nachgewiesen werden.

Die positiven  $\delta^{11}\text{B}$ -Werte der Vulkanite der vulkanischen Front zeigen eine Beteiligung einer  $^{11}\text{B}$ -reichen Komponente am Aufbau der andinen Vulkanite, die am wahrscheinlichsten aus Fluiden der alterierten ozeanischen Kruste der abtauchenden Nazca-Platte stammt. Diese Beobachtung macht einen alleinigen Ursprung der untersuchten Laven aus der kontinentalen Kruste und/oder dem Mantelkeil unwahrscheinlich und gibt erstmals einen deutlichen Hinweis auf einen Stofftransfer von der ozeanischen Nazca-Platte in die andine Oberplatte. Die Isotopenverhältnisse von Strontium, Neodymium und Blei zeigen je nach den Konzentrationen dieser Elemente in den involvierten Reservoirs (Nazca-Platte, Mantelkeil, andine Kruste) und ihrer Mobilität in Fluiden und Schmelzen unterschiedliche Signaturen. Die Bleiisotopenzusammensetzung ist von Blei aus der krustalen Kontamination dominiert und zeigt deshalb rein krustale Werte. Die Strontium- und Neodymiumisotopenverhältnisse zeigen im Gegensatz dazu eine Mischung zwischen einer Mantel- (alterierte ozeanische Kruste und/oder Mantelkeil) und einer Krustenquelle.

Der Trend zu systematisch negativeren  $\delta^{11}\text{B}$ -Werten und kleineren B/Nb-Verhältnissen von der vulkanischen Front zum „Back-arc“ wird als Resultat einer Borisotopenfraktionierung, einhergehend mit einer stetigen Abnahme der Fluidkomponente und einer relativ konstanten krustalen Kontamination, interpretiert. Der Einfluß von Bor aus dem Erdmantel scheint wegen der sehr geringen Konzentrationen von  $< 1 \mu\text{g g}^{-1}$  B in Mantelgesteinen eine untergeordnete Rolle zu spielen.

Die Borisotopenfraktionierung zwischen Mineral und Fluid während der Dehydratation der subduzierenden Unterplatte wurde mit einer Rayleigh-Fraktionierung und neuen experimentellen Daten zur Fraktionierung der Borisotope während der prograden Bildung von Schichtsilikaten (Smektit-Illit), die die Hauptträger von Bor in der alterierten ozeanischen Platte sind, modelliert. Die kalkulierte Isotopenfraktionierung entspricht dem theoretisch vermuteten Verlauf, mit  $\delta^{11}\text{B}$ -Werten des entwässernden Fluides von ca. +35 ‰ am Beginn der Subduktion und einer exponentiellen Abnahme des Fraktionierungsfaktors mit steigender Temperatur. Dieser Fraktionierungseffekt beruht auf der von der Koordination abhängigen Verteilung der Borisotope in Mineral und Fluid, wobei  $^{11}\text{B}$  bevorzugt in den trigonalen  $\text{B}(\text{OH})_3$ -Komplex im entwässernden Fluid geht und  $^{10}\text{B}$  dadurch im Slab-Restit der ozeanischen Platte angereichert wird.

Durch eine Kombination des Fraktionierungsmodells mit einem Temperaturmodell für die Subduktionszone der Zentralen Anden von *Springer* [1999] wurden die Tiefen der bearbeiteten Lokalitäten über der Wadati-Benioff Zone in die Temperatur am Übergang der Nazca-Platte zum Mantelkeil, dem „Slab“-Mantel Interface, übersetzt. Dadurch konnte die

Borisotopenzusammensetzung des Subduktionszonenfluides in der jeweiligen Tiefe modelliert werden. Sowohl die  $\delta^{11}\text{B}$ -Werte der Anden-Vulkanite als auch Literaturdaten eines „Fore-arc“-Fluides [Benton *et al.*, 2001] und von „Slab“-Restiten [Peacock and Hervig, 1999] stimmen sehr gut mit der modellierten Entwicklung der  $\delta^{11}\text{B}$ -Werte des Subduktionszonenfluides und der „Slab“-Restit Komponente überein. Diese Beobachtung gibt Anlaß zu der Vermutung, dass das Borbudget von „Arc“-Vulkaniten bis in den „Back-arc“-Bereich von Bor aus den Subduktionszonenfluiden der ozeanischen Platte dominiert wird, die nach Kerrick und Connolly [2001] in kalten bis intermediär temperierten Subduktionszonen, wie den Anden, über den gesamten „Sub-arc“-Bereich vorhanden sind.

Das Modell einer Mischung zwischen einer Subduktionskomponente, die über das gesamte „Arc“-Profil die mittlere Borisotopenzusammensetzung der subduzierten Platte aufweist, und einer Mantelkomponente, wie es in früheren Arbeiten als Erklärung für die systematische „Across-arc“-Variation der  $\delta^{11}\text{B}$ -Werte herangezogen wurde, erscheint unter Berücksichtigung des Prozesses der Borisotopenfraktionierung während der Subduktion fraglich.

Dynamische Mischungsmodelle zwischen Subduktionszonenfluid, Mantelkeil und andiner Kruste anhand von Bor-, Strontium- und Neodymiumisotopenverhältnissen, die sowohl die Borisotopenfraktionierung als auch die fortschreitende Dehydratation der Unterplatte berücksichtigen, zeigen, dass die Borisotopenzusammensetzung des hydratisierten Mantels bis in den „Back-arc“-Bereich durch Bor aus den Subduktionszonenfluiden der ozeanischen Platte bestimmt wird. Die primären „Arc“-Magmen aus dem hydratisierten Mantel werden nach diesem Modell während des Aufstiegs durch die andine Kruste mit durchschnittlich 15 bis 30 % krustalen Schmelzen kontaminiert.

Die Modellierungsrechnungen legen nahe, dass die Fraktionierung der Borisotope während der Dehydratation der Unterplatte ein genereller Prozess in Subduktionszonen ist und die  $\delta^{11}\text{B}$ -Werte von „Arc“-Vulkaniten entscheidend mitbestimmt. Demnach müssen  $\delta^{11}\text{B}$ -Werte von „Arc“-Vulkaniten nicht notwendigerweise Unterschiede in der primären Zusammensetzung der subduzierten ozeanischen Platte reflektieren, vielmehr dokumentieren sie den dynamischen Prozess der Borisotopenfraktionierung während der Subduktion.

Die modellierte Borisotopenfraktionierung hat aber nicht nur Auswirkungen auf die Zusammensetzung der „Arc“-Vulkanite, sondern hat ebenso Auswirkungen auf die „Slab“-Restit Komponente die tief in den Mantel subduziert wird. Die von Chaussidon und Marty [1995] gefundenen sehr negativen  $\delta^{11}\text{B}$ -Werte von ca. -10 ‰ für Ozean-Insel-Basalt-Magmen (OIB) reflektieren möglicherweise die Beteiligung einer, an  $^{10}\text{B}$  angereicherten, subduzierten „Slab“-Restit Komponente am Aufbau dieser Magmen.

# CHAPTER I

## Methodology of boron isotope and concentration analyses

### I.1 Introduction

The element boron has two stable isotopes,  $^{10}\text{B}$  and  $^{11}\text{B}$  with an average abundance of approximately 20 % and 80 % in terrestrial reservoirs, leading to an  $^{11}\text{B}/^{10}\text{B}$  ratio of about 4 in most natural materials. Based on favourable geochemical characteristics of boron – high solubility and mobility in aqueous solutions and incompatibility in most magmatic environments, the enormous relative mass difference of about 10 % of the two boron isotopes and the wide range of natural boron-isotope compositions of up to 7 % (Fig. 1) – this element has great potential as a geochemical tool to study various kinds of transfer and mixing processes in earth and planetary sciences [Palmer and Swihart, 1996].

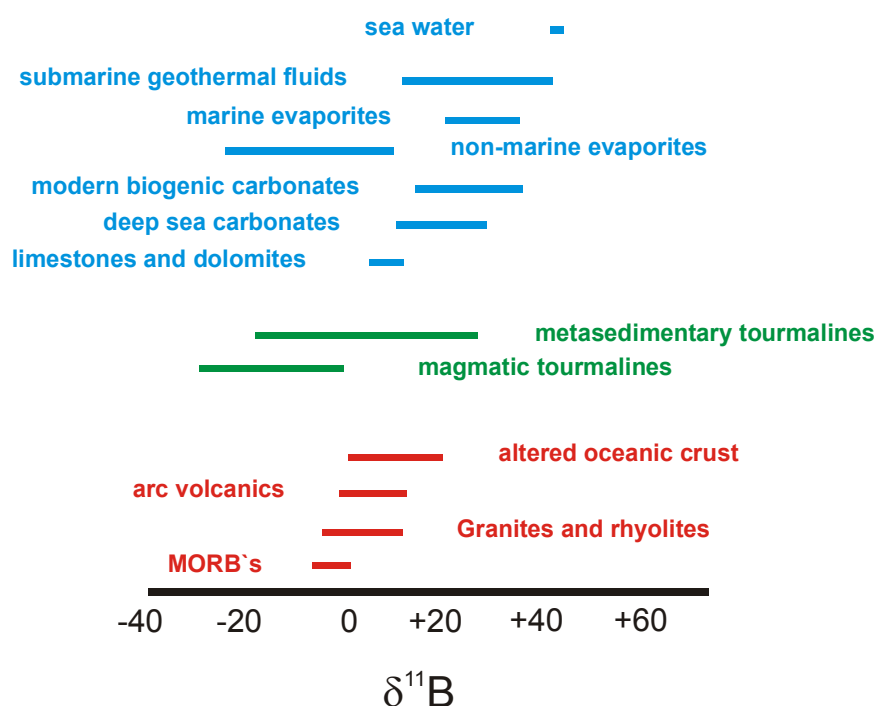


**Figure 1:** Comparison of  $\delta^{11}\text{B}$  values of volcanic rocks (red), tourmalines (green), carbonates (blue), evaporites (blue) and fluids (blue) (modified after Barth [1993]).

Boron isotope fractionation due to the equilibrium reaction of  $\text{H}_3\text{BO}_3$  (trigonal) +  $\text{OH}^- = \text{H}_4\text{BO}_4^-$  (tetrahedral) produces large differences in boron-isotope compositions in nature (Fig. 1), because  $^{11}\text{B}$  preferentially enters the trigonal  $\text{B}(\text{OH})_3$ -species ( $\text{BO}_3^{3-}$  in minerals) and  $^{10}\text{B}$  the tetrahedral  $\text{B}(\text{OH})_4^-$ -species ( $\text{BO}_4^{5-}$  in minerals). The distribution, depending on the co-ordination of boron isotopes, was first investigated by *Schwarcz et al.* [1969], who studied the boron-isotope fractionation during boron absorption onto clay minerals from seawater, and by *Kakihana et al.* [1977], who carried out theoretical fundamentals of boron-isotope fractionation using ion exchange resins.

In fluids, the ratio of  $\text{B}(\text{OH})_3$  to  $\text{B}(\text{OH})_4^-$  is a function of the pH value that mainly controls the distribution of  $^{11}\text{B}$  and  $^{10}\text{B}$  (Fig. 2 a). At low pH values  $\text{B}(\text{OH})_3$  is the dominant species and at high pH values the  $\text{B}(\text{OH})_4^-$  species.

The early fundamental study of *Oi et al.* [1989] demonstrated that the extent of boron-isotope fractionation is also strongly depending on temperature. A good fit to the data of *Oi et al.* [1989] shows an exponential decrease of the boron-isotope fractionation factor ( $\alpha$ ) between borate salts and co-existing solutions as a function of temperature (Fig. 2 b). Several recent studies confirm this behavior, mainly depending on temperature [e.g., *Williams et al.*, 2001a and b], and show that at 550° to 1100° C there is still a slight boron-isotope fractionation of up to about 3 ‰ between hydrous fluid and silicate melt [*Hervig et al.*, 2002]. It must be pointed out that this co-ordination controlled fractionation behavior of boron creates the opposite distributions between the heavy and the light isotope as shown by most other stable isotope systems (e.g., oxygen or sulfur), whose fractionation is simply mass dependent.

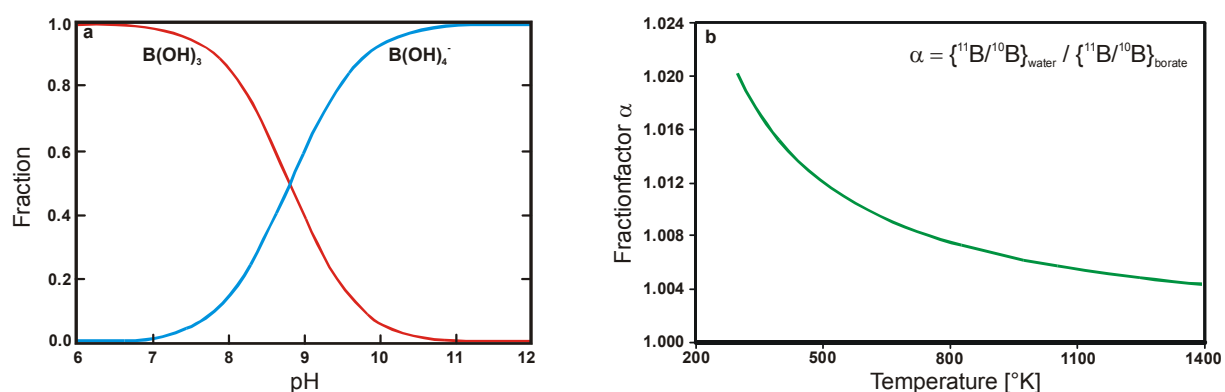


**Figure 2:** a) Distribution of boron-species  $\text{B}(\text{OH})_3$  and  $\text{B}(\text{OH})_4^-$  vs. pH in aqueous solutions after *Palmer and Swihart* [1996]; b) Fraction factor  $\alpha$  vs. temperature of  $^{11}\text{B}/^{10}\text{B}$  ratios in borate minerals and co-existing fluids ( $\alpha = \{^{11}\text{B}/^{10}\text{B}\}_{\text{water}} / \{^{11}\text{B}/^{10}\text{B}\}_{\text{borate}}$ ) demonstrated by a good fit ( $\alpha = 1 + 6 / T$  [*pers. com. Simon Peacock*]) to the data of *Oi et al.* [1989].

In the past the use of boron and its isotopes in earth sciences was mainly hindered by problems with separating boron from major matrix elements without influencing the isotopic composition. Additionally, the low analytical precision of the mass spectrometric techniques and imperfect dissolution and separation methods restricted the use of boron isotopes [e.g., *Ramakumar et al.*, 1985; *Gregoire*, 1987; *Vengosch et al.*, 1989].

Due to the technological progress in mass spectrometry during the past 15 years [see review by *Swihart*, 1996] interest has grown in bringing boron isotopes into geosciences. New applications for boron in environmental sciences, like paleo pH and CO<sub>2</sub> reconstruction [e.g., *Pearson and Palmer*, 2000; *Lemarchand et al.*, 2000], as well as studies of silicates within the material cycle of subduction zones (see references of CHAPTER III) have increased the number of publications enormously.

However, to obtain meaningful results it is imperative that sample preparation is performed properly and therefore a detailed analytical description of the methodology of boron concentration and isotope analyses is given below. To ensure about the accuracy of the obtained data, a variety of reference materials (NIST SRM 951 and 952, and silicate geological reference materials) were used to control the whole analytical procedure for boron loss and boron-isotope fractionation.

Boron-isotope compositions are generally reported as a  $\delta$  notation relative to the NIST boric acid standard SRM 951 [*Catanzaro et al.*, 1970; *NIST*, 1999]:

$$\delta^{11}\text{B} = \left[ \left\{ \frac{{}^{11}\text{B}/{}^{10}\text{B}_{\text{sample}}}{{}^{11}\text{B}/{}^{10}\text{B}_{\text{standard}}} \right\} - 1 \right] * 1000$$

Because the new implementation and modification of the Cs<sub>2</sub>BO<sub>2</sub><sup>+</sup>-graphite method (PTIMS) at the GeoForschungsZentrum Potsdam was a main part of this thesis, this method is explained in more detail relative to other used methods.

## I.2 Reagents and laboratory equipment

Water was purified to a conductivity of  $18.2 \text{ M}\Omega \text{ cm}^{-1}$  with an Academic Milli-Q purification system. This water was used for all preparation steps. Concentrated HCl (analytic grade) was purified by sub boiling point distillation using a two-bottle Teflon distiller in the presence of mannitol at  $65^\circ\text{C}$  [e.g., Nakamura *et al.*, 1992]. The two bottles (one feed- and one collecting bottle) are joined in a right angle and connected with a Teflon block. The feeding bottle contains  $\sim 750 \text{ ml}$   $7 \text{ M}$  HCl mixed with  $1.5 \text{ g}$  mannitol and was heated to not more than  $65^\circ \text{C}$  with a heating mat. The collecting bottle was placed in a basin of water to condense the evaporated HCl from the feeding bottle. The distillation typically takes four weeks to collect nearly  $650 \text{ ml}$  in the distillation reservoir. The prepared HCl usually has a concentration between  $6.6$  and  $6.8 \text{ M}$ .

Concentrated hydrofluoric acid (HF; ULTREX<sup>®</sup> Baker), perchloric acid ( $\text{HClO}_4$ ; Suprapur<sup>®</sup> MERCK) and ammonia solution (Suprapur<sup>®</sup> MERCK) were used in commercial high purity quality without further purification. The fusion decomposition was carried out using potassium carbonate ( $\text{K}_2\text{CO}_3$ ; pro analysi) from MERCK. Mannitol, a polyhydric alcohol ( $\text{CH}_2\text{OH}-(\text{CHOH})_4-\text{CH}_2\text{OH}$ ), serving as a boron complexing agent, was used as D(-)-Mannit from MERCK dissolved in water to obtain  $2 \%$  and  $0.2 \%$  mannitol solutions. Ion exchange chromatography was carried out using the boron-specific anion resin AMBERLITE 743 (20 - 50 mesh) from Fluka Chemie AG and the cation resin AG 50W-X8 (200 - 400 mesh) from Bio-Rad. Cesium, as cesium carbonate ( $99.995 \%$ ) from Aldrich Chemistry, was dissolved in water to obtain  $0.0925 \text{ M}$  and  $0.00925 \text{ M}$  Cs-solutions. NIST graphite was suspended in a  $30 \%$  ethanol –  $70 \%$  water mixture in order to obtain a suspension with  $40 \text{ mg}$  graphite  $\text{ml}^{-1}$ . NIST boric acids SRM 951 and SRM 952 [Catanzaro *et al.*, 1970; NIST, 1999] were used as standard and spike solutions for boron-isotope analyses. The crystalline boric acid material was dissolved in water to obtain a  $1000 \mu\text{g l}^{-1}$  boron solution for the NIST SRM 951 and a  $188 \mu\text{g l}^{-1}$  solution for the NIST SRM 952, respectively.

In general, precaution must be taken to use only Teflon-, polyethylen- (PE)- or quartz-ware during the entire sample preparation, because common laboratory glassware usually contains a few weight percent of boron that can be easily leached by acidic sample solutions. The Teflon- and PE-ware and the Savillex<sup>®</sup> beakers were cleaned prior to each use with  $6 \text{ M}$  HCl on a hot plate at  $< 100^\circ \text{C}$  for a minimum of three days. The equipment was then stored for a further three days in water, after three rinses with water to remove HCl from the first cleaning step.

### I.3 Boron concentration analyses

To extract boron from silicate rock samples the method of  $K_2CO_3$  fusion decomposition [Owens *et al.*, 1982] was chosen. First, 1.0 g of  $K_2CO_3$  was weighed into platinum crucibles to cover the bottom of the vessel. Then 0.5 g of finely powdered sample ( $< 35 \mu\text{m}$ ) were spread onto the first  $K_2CO_3$  layer followed by a second 1.0 g layer of  $K_2CO_3$  on top of the sample (sample :  $K_2CO_3$  = 1 : 4). The crucibles were closed with a platinum lid and transferred to a muffle furnace and fused for 30 minutes at  $950^\circ \text{C}$ . After cooling to room temperature, 10 ml of water was added to the crucibles to leach boron from the fusion cake for 12 hours in an oven at  $50^\circ \text{C}$ . The entire solution, including the insoluble phases (metal hydroxides and alkaline earth carbonates), was then transferred to Teflon cups and heated for three hours at  $105^\circ \text{C}$  in an oven. To separate the boron-containing solution from the insoluble phases, the sample was filtered through a cellulose laboratory filter. To avoid boron-loss, the filter cake was washed twice with water.  $HClO_4$  was then added to the supernatant to neutralise the alkaline solution, remove carbonate by degassing of carbon dioxide ( $CO_2$ ) and precipitate potassium as potassium perchlorate ( $KClO_4$ ) from the solution. The  $KClO_4$ -precipitates were then removed by a second filtration step performed as described above, collecting the supernatant in a calibrated 100 ml polypropylene-cylinder. To avoid boron-loss to the gas phase, mannitol was added to the solution to achieve a boron to mannitol ratio between 1 : 20 and 1 : 200. Finally, the polypropylene-cylinder was filled with water to a calibrated volume of 100 ml.

Separation of boron from major cations ( $Fe^{2+}$ ,  $K^+$ ,  $Ca^{2+}$ ,  $Mg^{2+}$ ,  $Na^+$ , ...) was achieved using ion exchange chromatography. Six ml of AG 50W-X8 (200 – 400 mesh) cation exchange resin was filled in 30 ml polypropylene columns and cleaned and conditioned three times with 20 ml 4 N HCl followed by 4 washes with 5 ml water each. Before sample loading, 100 ml Teflon cups were placed under the columns. A 20 ml split of the sample solution was loaded onto the columns. To remove all the boron from the columns the resin was washed twice with 6 ml water. The collected sample solution was weighed out ( $\rho = 1$ ) and depending on the estimated boron concentration introduced directly or after a further dilution step into the ICP-spectrometer.

Boron concentration analyses were carried out with a VARIAN Liberty 200 Inductively-Coupled-Plasma Optical-Emission-Spectrometer (ICP-OES) at emission line 249.773 nm. If the sample solution contained high iron concentrations, interference from a nearby iron emission line may possibly overlap and influence the boron signal. Therefore, the iron signal



was generally observed on emission line 238.204 nm. Calibration was typically made using a  $1 \mu\text{g g}^{-1}$  boron-standard solution diluted in 0.05 M HCl. To obtain precise and reproducible analytical results the boron concentrations in the sample solution should vary within the optimum concentration range between 0.1 and  $1 \mu\text{g g}^{-1}$ .

The internal precision of ICP-OES-measurements is typically better than 2 %. The external reproducibility of the whole procedure was determined with international silicate geological reference materials (see CHAPTER II) after individual dissolution and separation steps. Reproducibility is typically better than 5.1 %, but varies in a range from 10 to 2.8 % (1RSD = relative standard deviation). Accuracy was evaluated by a qualitative comparison with published data [Govindaraju, 1994; Imai et al., 1995; D'Orazio, 1999]. The majority of obtained mean boron concentrations show a good agreement with the published values and overlap typically within the maximum external uncertainty of 14 % (see CHAPTER II).

## I.4 Methods of boron isotope analyses

### I.4.1 Mass spectrometric methods

Today several mass spectrometric techniques are used to determine boron-isotope ratios. Thermal-Ionisation-Mass-Spectrometry (TIMS) is by far the most applied technique, but Multi-Collector Inductively-Coupled-Plasma Mass-Spectrometry (MC-ICP-MS) and Secondary-Ionisation-Mass-Spectrometry (SIMS) are also common techniques in earth sciences. In this study, positive TIMS (PTIMS) as well as negative TIMS (NTIMS) were used due to their advantages for particular types of sample material. A comparison of ionisation efficiency, boron loads and analytical precision between the  $\text{Cs}_2\text{BO}_2^+$ -graphite method and the  $\text{BO}_2^-$ -method is given in Table 1.

**Table 1:** Comparison of ionisation efficiency loaded boron and analytical precision among the  $\text{Cs}_2\text{BO}_2^+$ -graphite method and the  $\text{BO}_2^-$ -method.

Species	Ionization ( $10^{-12}$ A $\text{mg}^{-1}$ )	Boron loaded [ $\mu\text{g g}^{-1}$ ]	Precision $2\sigma$ [%]	References
$\text{Cs}_2\text{BO}_2^+$ -graphite	0.24 - 100	0.05 - 5	0.3	[1], [2], [3]
$\text{BO}_2^-$	300-10000	0.001 – 0.05	0.7 - 2	[4], [5]

**References:** [1] = Spivack and Edmond [1986]; [2] = Xiao et al. [1988]; [3] = Leeman et al. [1991]; [4] = Vengosch et al. [1989]; [5] = Hemming and Hanson [1994]

### I.4.1.1 Thermal ionisation mass spectrometry (TIMS)

#### I.4.1.1.1 PTIMS: The $\text{Cs}_2\text{BO}_2^+$ -graphite method

For PTIMS, the  $^{11}\text{B}/^{10}\text{B}$  ratio was determined by measuring the polyatomic ions  $\text{Cs}_2^{10}\text{BO}_2^+$  and  $\text{Cs}_2^{11}\text{BO}_2^+$  on masses 308 and 309, respectively, which ionise from a cesium-tetraborate ( $\text{Cs}_2\text{B}_4\text{O}_7$ ) deposit on a graphite-coated tantalum filament. The  $\text{Cs}_2\text{BO}_2^+$ -graphite method is preferred for silicate rock samples, but in general other types of samples, such as waters and carbonates can also be analysed with this method [e.g., *Lemarchand et al.*, 2000; *Gaillardet and Allégre*, 1995]. Analyses were performed on a Finigan MAT 262 TIMS equipped with a special "double" Faraday cup configuration by static multicollection. This Faraday cup has a fixed spacing for dicesium metaborate. Contrary to the typical used peak-jumping measuring mode (dynamic collection), simultaneous measurements of masses 308 and 309 yield to higher in-run precision (see comparison by *Deyhle* [2001]), also if the ion beam decays, or increases rapidly or is unstable.

In contrast to the NTIMS  $\text{BO}_2^-$ -method, during PTIMS measurements only negligible mass fractionation occurs due to the very high molecular masses. However, ionisation efficiency in relation to other mass spectrometric methods is poor (Table 1). In our laboratory 0.5  $\mu\text{g}$  boron was used in the standard procedure for natural silicate samples and for NIST SRM 951, whereas 200 ng boron for silicate samples and 100 ng boron for NIST SRM 951 are thought to be the minimum load to achieve reproducible results. *Deyhle* [2001] reported a minimum level of 100 ng boron for silicate samples and 50 ng boron for NIST SRM 951. The variable minimum amounts reported from various laboratories may be explained by different types of graphite used, which influences the signal intensity and stability of the  $\text{Cs}_2\text{BO}_2^+$  beam. *Xiao et al.* [2000] reported that the efficiency and capability of different types of graphite for the  $\text{Cs}_2\text{BO}_2^+$ -method is weakly influenced by the purity and size but significantly affected by the microstructure of graphite.

According to *Swihart* [1996], *Deyhle* [2001] and *Gonfiantini et al.* [in prep.] the  $\text{Cs}_2\text{BO}_2^+$ -graphite method produces the most precise results, especially for samples with complex matrices, such as silicate rocks.

#### I.4.1.1.2 NTIMS: The $\text{BO}_2^-$ method

The NTIMS  $\text{BO}_2^-$ -method has normally been used to analyse water samples, salts, carbonates, and boron-rich mineral phases, such as tourmaline. However, this method is generally unsuitable for magmatic rocks with low boron concentrations. Analyses of international reference materials (JB-2, JA-1 and JA-3) at the beginning of this project showed, that most of the NTIMS measurements of silicate rock samples fail to reproduce the published literature values (see NTIMS data reduction section I.7.2). In addition, only one complete study of  $\delta^{11}\text{B}$  values from silicate rocks and tourmalines carried out by NTIMS has been published to date [Kasemann *et al.*, 2000].

For the NTIMS method, the ion of interest is  $\text{BO}_2^-$  on masses 42 and 43. The ionisation efficiency of this method is on the order of 1000 times higher than that for the  $\text{Cs}_2\text{BO}_2^+$ -graphite method (Table 1). Therefore, a minimum of 1 ng boron is sufficient to achieve reliable signal intensities and in-run precision. Another advantage of this method is that, for waters and carbonates, almost no purification (filtration or one cation exchange chromatography step) is necessary, leading to a theoretically very small boron-procedural blank. Disadvantages are isobaric interferences on masses 42 and 43 with  $\text{CNO}^-$  molecules at the beginning of the measurements, most likely derived from the organic ion exchange resins and the mannitol [e.g., Hemming and Hanson, 1994]. Additionally, the high mass-dependent fractionation due to the low molecular masses (see section I.4.1 and I.7.2), results in an overall precision for NIST SRM 951 typically not better than 0.5 ‰ (2RSD) [see review by Swihart, 1996].

#### I.4.1.2 MC-ICP-MS and SIMS

To complete the list of mass spectrometric methods to determine boron-isotope ratios, the MC-ICP-MS and SIMS techniques should be mentioned.

The MC-ICP-MS technique has the greatest potential to establish relatively easy, fast and precise boron-isotope analyses for silicate rocks and mineral separates, because the sample material can be easily introduced in the mass spectrometer by aqueous solution and high ionization efficiency yield potential boron analyses in ppb levels [e.g., Rehkämper *et al.*, 2001; Lécuyer *et al.*, 2002]. However after our own test series with a VG Axiom MC-ICP-MS at the University of Freiberg we suggested that difficulties with boron-memory effects in the

tubing system, signal stability and long- to medium- term instrumental fractionation stability make this technique unsuitable for silicate samples at this time.

SIMS uses a focused primary  $O^-$  or  $Cs^+$  ion beam to ionise material in-situ from solid polished samples at the microvolume scale. This technique has been applied to materials such as tourmalines [e.g., *Trumbull and Chaussidon, 1999*], melt inclusions [e.g., *Rose et al., 2001*] and matrix glass in volcanic rocks [e.g., *Clift et al., 2001*]. However, the analytical precision is strongly dependent on the boron concentration of the analysed material which limits the application of this technique. Furthermore, matrix effects as a result of the primary ionisation beam are not yet fully understood [e.g., *Yamazaki, 1998*] and demonstrate the requirement for well characterised silicate reference materials (see CHAPTER II; [*Kasemann et al., 2001*]).

## **I.5 Sample preparation**

### **I.5.1 Dissolution methods**

Alkaline fusion, acid attack and pyrohydrolysis are the standard methods for the dissolution of silicate rock samples prior to boron isotope analyses reported in literature [see review by *Swihart, 1996*]. *Spivack and Edmond* [1986] developed a pyrohydrolysis method for silicate samples at 1400° C, in which boron was volatilised and later collected by a flow of water vapor. Large amounts of sample and reagents and a long duration of sample preparation make this method unsuitable for the quantity and the kind of samples studied in this project. Thus, the  $K_2CO_3$  fusion method, modified after *Owens et al.* [1982], and the HF dissolution method, modified after *Nakamura et al.* [1992], were used.

Carbonate fusion is preferred for boron concentration analyses using ICP-OES (see section I.3), whereas for boron isotope analyses both methods are used. The carbonate fusion method is characterised by an excellent extraction of boron, highly alkaline conditions, large amounts of reagents and a complex preparation procedure. These circumstances make this method suitable for rocks with resistant mineral phases (e.g., zircon) but may lead to an elevated boron-procedure blank [see review by *Swihart, 1996*].

Acid attack with HF is more simple than carbonate fusion and uses smaller amounts of reagents, but because the dissolution occurs at 70° C the decomposition of resistant mineral phases may not reach completion. Moreover, boron-isotope fractionation may occur during

sample preparation under acidic conditions, because boron can easily be lost as volatile components, such like  $\text{BCl}_3$  or  $\text{BF}_3$  [Ishikawa and Nakamura, 1990]. Therefore extraction and separation methods must be tested and recovery yields of boron should approach 100 % to exclude isotope fractionation effects. To avoid boron-loss, mannitol (see section I.3) was added to acidic solutions as a complexing agent. In a series of recovery and fractionation tests Ishikawa and Nakamura [1990] demonstrated that volatilisation and fractionation of boron in acidic solutions is negligible if mannitol is added to the sample to achieve a mannitol to boron molar ratio of more than 2 : 1. Due to the low temperature stability of mannitol [Ishikawa and Nakamura, 1990], acidic sample solutions should not be heated to be higher than 70° C.

### **I.5.1.1 Carbonate fusion**

The carbonate fusion procedure used is the same as reported for boron concentration analyses (see section I.3) up to the heating in the oven. The insoluble phases (metal hydroxides and alkaline earth carbonates) were then separated from the boron-bearing solution by centrifugation in 10 ml plastic tubes. The supernatant was transferred to 15 ml Savillex® Teflon beakers. The residual insoluble phase was centrifuged twice, each time after washing with 1 to 3 ml water to remove all boron from the insoluble phases. All wash fluid was added to the original supernatant.

The efficiency of boron extraction was tested by fusing the international reference material JB-3 (basalt) combined with a subsequent anion chromatography step (see section I.5.2.1.1). The amount of boron in the resulting solution was determined with ICP-OES. The achieved recovery was 98.7 %, relative to the recommended value of 18.0  $\mu\text{g g}^{-1}$  boron for JB-3 [Imai *et al.*, 1995]. This value demonstrates excellent recovery of boron using the fusion method with  $\text{K}_2\text{CO}_3$  and is in the same range as reported by Tonarini *et al.* [1997].

### **I.5.1.2 Acid attack**

Rock powders were dissolved with concentrated HF in 15 ml Savillex® Teflon beakers. Depending on the boron concentration of the sample, up to 200 mg of powdered sample was soaked with 0.2 ml 2 % mannitol solution (40 to 60  $\mu\text{g}$  mannitol per 1  $\mu\text{g}$  expected amount of boron). Because the reaction of silicates and most secondary mineral phases is vigorous 30 N HF was added very carefully to the sample powder (1.5 ml HF per 100 mg

sample). The beaker was then placed in an ultrasonic bath at 65° C for 3 hours. Leaving the beaker for another 36 hours in an oven at 65° C was normally sufficient to dissolve the sample completely, if no tourmaline or other resistant mineral phases are present. Complete dissolution was controlled by visual inspection. A centrifuge was used to separate the boron-containing solution from insoluble fluoride phases. The resulting solution was then dried at < 70° C to remove silicon as the volatile silicon tetrafluoride (SiF<sub>4</sub>). The loss of silicon reduced the amount of cations significantly prior to ion exchange chromatography, allowing a smaller column size due to the smaller total ion load on the first cation exchange chromatography step. The sample was then re-dissolved in 0.5 to 3.0 ml 6.6 N HCl. Usually some fluorides, a white precipitate, remained un-dissolved in the beaker, because of the low solubility of fluorides in HCl, in particular calcium and magnesium fluorides. The fluoride precipitates did not contain boron (see recovery test this section) and therefore were removed by centrifugation. Finally, the sample solution was evaporated to dryness at 65° C prior to the first cation chromatography step.

The HF dissolution method was tested for dissolution efficiency by dissolving the international reference material JA-3 (andesite) combined with a subsequent cation chromatography step (see section I.5.2.1.2). The amount of boron in the resulting solution was determined with ICP-OES. Relative to the recommended value of 24.8 µg g<sup>-1</sup> boron for JA-3 [Imai *et al.*, 1995] the achieved recovery was 108.6 %. This "excess" can be explained by the analytical uncertainty, for some samples up to 10 % (see section I.3 and CHAPTER II). Imai *et al.* [1995] report a standard deviation of 2.9 ppm based on six individual values of JA-3. However, the mean boron concentration of JA-3 obtained at the GeoForschungsZentrum Potsdam with the procedure described in section I.3 is 26.8 ± 1.0 µg g<sup>-1</sup> (CHAPTER II, Table 1) and demonstrates excellent agreement with the here determined boron concentration of 26.9 µg g<sup>-1</sup>, indicating good boron recovery using HF dissolution despite analytical uncertainties.

### **I.5.2 Boron separation by ion exchange chromatography**

TIMS-techniques require clean samples containing, ideally, only boron to achieve high signal intensities [Leeman *et al.*, 1991; Tonarini *et al.*, 1997] and to avoid isobaric interferences with organic molecules [Hemming and Hanson, 1994; Xiao and Wang, 1998].

Ion exchange chromatography was chosen instead of methyl-borate distillation for boron separation because of its easy implementation, high efficiency and low blank contribution. Ion exchange resins consist of a solid substrate (polymerised styrene) to which acidic or basic functional groups are attached allowing the reversible exchange of ions between the solid and the fluid phase. Boron-specific anion exchange resin AMBERLITE 743 (20 - 50 mesh) and cation exchange resin AG 50W-X8 (200-400 mesh) were selected to achieve an adequate purity of the sample. AMBERLITE 743 consists of a N-methyl-glucamine group fixed on a polystyrenic backbone, where at pH values  $> 7$ , boron is strongly absorbed in the  $B(OH)_4^-$  form (Fig. 2 a; [Kiss, 1988]). The AG 50W-X8 resin is a cross-linked polystyrene sulfonic acid resin that strongly adsorbs doubly charged positive cations at low acidity.

*Lemarchand et al.* [2002] demonstrated that boron losses during ion exchange chromatography may alter the "true"  $^{11}B/^{10}B$  ratio of a sample. The two boron isotopes show a slightly different elution behavior using AMBERLITE 743 and therefore nearly complete boron recovery must be achieved to avoid boron-isotope fractionation on the columns. For this reason the anion and cation chromatography steps were calibrated under the conditions and with reagents used during this study. To observe the boron-retention on the resin and boron-elution from the resin, 1 ml batches of the solution were passed through the columns during loading, washing and elution and were collected and measured for their boron concentrations with ICP-OES.

Both separation procedures, one after  $K_2CO_3$  fusion ("K<sub>2</sub>CO<sub>3</sub> chemistry") and one after HF attack ("HF chemistry") were modified after *Leeman et al.* [1991], *Nakamura et al.* [1992] and *Tonarini et al.* [1997]. In the standard procedure 3  $\mu$ g of sample boron was loaded on the anion columns (0.3 ml resin), because this amount of boron will not overload the capacity of the resin in the column. The theoretical boron capacity of the AMBERLITE 743 resin is 5.7 mg boron per ml of resin and given by Rohm and Haas®. Theoretically, the anion columns would not be overloaded with 0.003 mg sample boron, because 0.3 ml AMBERLITE 743 should have a capacity of 1.71 mg boron. However, the real boron capacity depends on the total ion load of the sample solution and is therefore difficult to calculate. In order to avoid blocking of the columns the solutions must be free of solid precipitates.

The procedures of ion exchange presented in section I.5.2.1 result from column calibrations. The elution curves of the individual steps are given at the end of each description in section I.5.2.1.1 (Fig. 3), I.5.2.1.2 (Fig. 4) and I.5.2.1.3 (Fig. 5).

### I.5.2.1 Ion exchange chromatography after alkaline fusion

#### I.5.2.1.1 Purification after $K_2CO_3$ fusion (first separation step)

For the first separation step Teflon columns (h =20 mm, r = 2 mm) were used and loaded with 0.3 ml AMBERLITE 743 resin. The columns were cleaned with two 5 ml batches of 6.6 N HCl followed by two 5 ml batches of water and conditioned with 2 ml 2 N  $NH_4OH$  followed by 3 ml water. The flow rate was adjusted to less than 0.25 ml per min, using Teflon frits of different porosity and thickness. One to 12 ml of alkaline sample solution (pH > 11), containing approximately 3  $\mu\text{g}$  boron, was then loaded onto the preconditioned columns. Under these conditions nearly 100 % of the boron is present as  $B(OH)_4^-$  (Fig. 2 a) and therefore is strongly absorbed by the AMBERLITE 743 resin.

Sequential washing steps using 2 ml of water, 2 ml 2 N  $NH_4OH$  and 3 ml of water removed the majority of matrix cations. Before starting elution, 15 ml Savillex® Teflon beakers containing 4  $\mu\text{moles}$  of mannitol per each  $\mu\text{mol}$  boron were prepared and placed under the columns. The boron fraction was finally eluted with 8 ml 2 N HCl. The first ml 2 N HCl was loaded on the columns in 0.1 ml batches followed by 7 batches of 1 ml. Extreme care was necessary to avoid  $CO_2$  gas bubbles generated from the reaction of calcium carbonate with HCl, because the bubbles can disturb or totally interrupt the vertical flow within the columns.

The behavior of boron and iron during the first anion chromatography step is shown in Figure 3. During sample loading and washing only trace amounts of boron and iron passed through the columns, whereby potassium (not shown) was effectively separated from boron. The elution curves indicate a boron recovery of about 95.4 % and demonstrate that double charged cations, such as iron, were not effectively separated from the boron fraction.

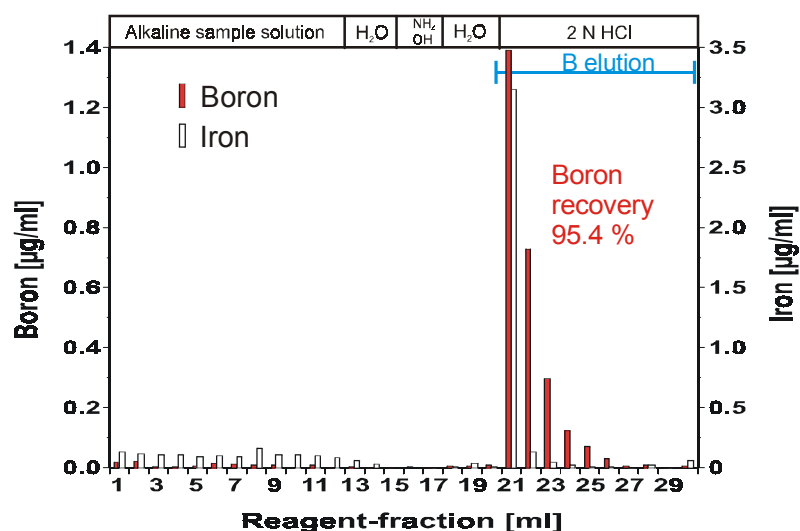


**Figure 3:**

Anion exchange chromatography procedure (first step) showing the different reagent types and the elution behavior of boron (red) and iron (white). The calculated boron recovery for this separation step was 95.4 %.



### I.5.2.1.2 Removal of major cations (second separation step)

To remove the major cations, 2.5 ml of AG 50W-X8 (200 – 400 mesh) was loaded on conical polypropylene columns (h = 40 mm, r = 8 mm).

First, the columns were cleaned with two 5 ml batches of 6.2 N HCl. Flow rates were limited to not higher than 0.5 ml per min. The columns were then conditioned with 5 ml 0.02 N HCl, loaded in 1 ml batches. The dried, chloride-form sample was re-dissolved in 1 to 5 ml 0.02 N HCl and loaded on the columns. Under low pH conditions, boron is mainly present as the  $B(OH)_3$ -species (Fig. 2 a) and passes rapidly through the columns, while the main cations were absorbed on the resin and remain in the columns (Fig. 4). The boron fraction was collected immediately in a 15 ml Savillex® Teflon beakers after loading the sample and was completely removed from the columns with another batch of 5 ml 0.02 N HCl, loaded in 1 ml batches (Fig. 4). Weak HCl solution (0.02 N) was used instead of water to avoid a long boron elution-tail.

In general, the second separation step is not critical for boron loss and the elution curve indicates a boron recovery of nearly 100 %.

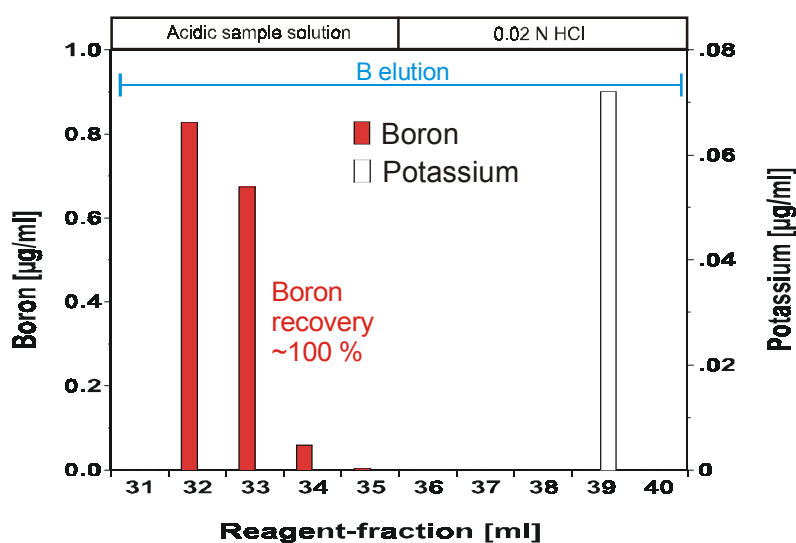


**Figure 4:**

Cation exchange chromatography procedure (second step) showing the different reagent types and the elution behavior of boron (red) and potassium (white). The calculated boron recovery for this separation step was nearly 100 %.

### I.5.2.1.3 Purification of boron (third separation step)

The sample solution obtained after the second separation step was adjusted to alkaline pH (> 11 pH) by addition of 2 N  $\text{NH}_4\text{OH}$  to convert all boron to  $\text{B}(\text{OH})_4^-$ . To avoid boron loss during sample loading and washing it was imperative to maintain a pH value of > 11, because at lower pH values boron is also present in significant amounts as  $\text{B}(\text{OH})_3$  (Fig. 2 a), which is not absorbed by the resin, and may result in fractionation of boron isotopes [cf. *Lemarchand et al.*, 2002].

The separation scheme was the same as described in section I.5.2.1.1. Because the total ion load of the sample solution was low at this stage of the purification procedure, the elution of boron was well defined compared to the first chromatography step, and boron recovery exceeded 99 % (Fig. 5).

Before drying, Cs-solution (0.0925 M or 0.00925 M) was added to the sample solution to achieve a B/Cs molar ratio of two. The sample solution was then reduced to a volume of 15 to 10  $\mu\text{l}$  and a portion of this solution, containing  $\sim 500$  ng boron, was directly loaded on the filament as described in section I.6.

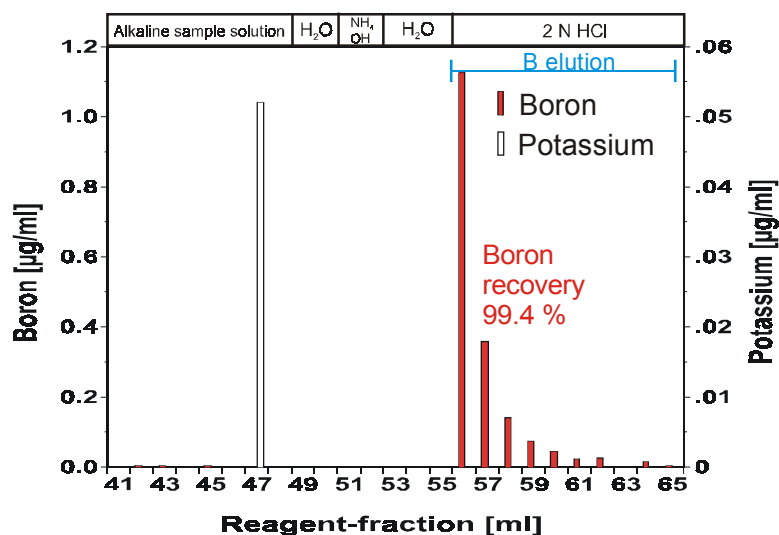


**Figure 5:**

Anion chromatography procedure (third step) showing the different reagent types and the elution behavior of boron (red) and potassium (white). The calculated boron recovery for this separation step was 99.4 %.

### I.5.2.2 Ion exchange chromatography after HF attack

To use the very efficient boron specific AMBERLITE 743 resin for boron separation after HF attack a re-organisation of the separation procedure described in section I.5.2.1 was carried out. In order to start under acidic conditions an additional fourth cation chromatography step was performed in advance of the three separation steps described in section I.5.2.1. Cation exchange chromatography was chosen, because it is not critical for boron loss. In addition an overloading of the cation columns, due to high total ion loads of the starting solution, would not result in boron loss and would only effect the efficiency of the cation retention on the resin.

After the HF attack (see section I.5.1.2), the dried sample was re-dissolved in 1 to 5 ml 0.02 N HCl and passed through the cation columns as described in section I.5.2.1.2. The sample solution was then converted to alkaline conditions by addition of  $\text{NH}_4\text{OH}$  ( $> 11$  pH). Often Fe-, Mg-, and Ca-hydroxides formed after the  $\text{NH}_4\text{OH}$ -addition. These precipitates were removed by centrifugation prior to loading the alkaline solution on the anion chromatography step (see sections I.5.2.1.1). The sample solution obtained from this anion chromatography was evaporated to dryness at  $65^\circ\text{C}$ . Then it was re-dissolved in 1 to 2 ml 0.02 N HCl and passed through a second cation chromatography (see section I.5.2.1.2). Finally, the anion chromatography step was performed a second time after adjusting the solution to alkaline conditions to achieve a suitable sample quality for mass spectrometry. The resulting solution was then handled as described in section I.5.2.1.3.

## I.6 Loading techniques for TIMS

For the  $\text{Cs}_2\text{BO}_2^+$ -graphite method, samples were loaded on single tantalum filaments. Filaments were degassed in a vacuum heating bench ( $< 2 * 10^{-6}$  Torr) for 40 min at 2.5 A and 40 min at 4.2 A. A graphite–ethanol-water suspension ( $40\text{ mg graphite ml}^{-1}$ ) was used as an emitter to obtain maximum ionisation efficiency.

The samples were loaded in two different ways:

For the “graphite first“ technique, the filament was coated with  $1\ \mu\text{l}$  graphite slurry and heated at 0.7 A. Before reaching complete dryness, 1 to  $4\ \mu\text{l}$  sample solution containing typically  $\sim 500$  ng boron was loaded onto the graphite layer. After the sample was completely dry the current was raised to 1.8 A for 20 seconds. Conditioning the sample at 1.8 A stabilised

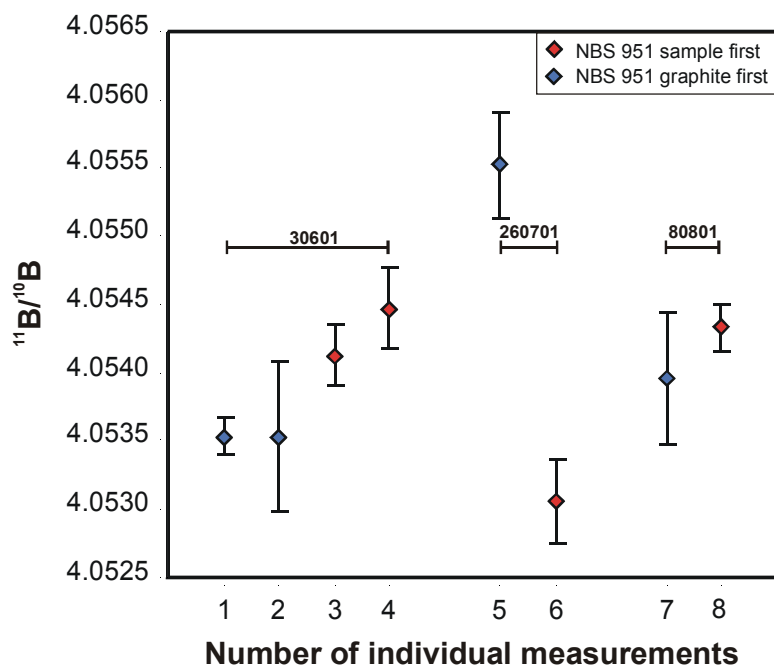
the ion current at the beginning of TIMS-analysis. *Deyhle* [2001] reported raising  $^{11}\text{B}/^{10}\text{B}$  ratios during the first block of measurement before reaching a stable signal. This can be explained with an inhomogeneous sample cake probably due to low temperatures used to dry the samples on the filaments, which can result in a slight mass dependent fractionation between the ions  $\text{Cs}_2^{10}\text{BO}_2^+$  and  $\text{Cs}_2^{11}\text{BO}_2^+$ . Conditioning the sample for 20 seconds at 1.8 A, as developed in this project, results in a more homogeneous sample cake and prevent this fractionation at the beginning of the measurement. Additionally, no shift in the overall  $^{11}\text{B}/^{10}\text{B}$  ratio of NIST SRM 951 and reference materials was observed as a result of this high current.

The second way to load a sample was modified after *Deyhle* [2001]. The sample solution (1 to 4  $\mu\text{l}$ ) was loaded first on the tantalum filament and heated nearly to dryness at 0.7 A. Then, 1  $\mu\text{l}$  graphite slurry was coated carefully over the slightly wet sample layer and dried completely at 0.7 A. Finally, the sample was conditioned for 20 seconds at 1.8 A as described above.

For NIST SRM 951 the “sample first“ technique resulted in a more stable  $\text{Cs}_2\text{BO}_2^+$ -signal and a better in-run precision relative to the reverse technique (Table 2 and Fig. 6) and was therefore preferred during this study. Natural samples, especially silicate rock samples, rarely behave like a standard. Sometimes the first and sometimes the second technique resulted in more precise measurements. This unsystematic behaviour may be explained by complex matrices and minor differences in each loading procedure, as the result of the “human factor“.

**Table 2:** Comparison between different loading techniques: column “sample“ gives the loading technique and the position (Pos.) on the sample wheel; column “date“ gives the date of measurement; column “ $^{11}\text{B}/^{10}\text{B}$ “ gives the measured ratio; column “1SD“ gives the 1SD in-run precision; column “2SD mean“ gives the  $2\text{SD}_{\text{mean}}$  in-run precision based on the blocks.

Sample	Date	$^{11}\text{B}/^{10}\text{B}$	1 SD	$2\text{SD}_{\text{mean}}$
NBS 951 “graphit first“ (Pos.1)	30601	4.05353	0.00013	0.00013
NBS 951 “graphit first“ (Pos.2)	30601	4.05353	0.00055	0.00055
NBS 951 “sample first“ (Pos.3)	30601	4.05413	0.00048	0.00022
NBS 951 “sample first“ (Pos.4)	30601	4.05447	0.00034	0.00030
NBS 951 “graphit first“ (Pos.12)	260701	4.05552	0.00085	0.00039
NBS 951 “sample first“ (Pos.13)	260701	4.05306	0.00037	0.00030
NBS 951 “graphit first“ (Pos.12)	80801	4.05396	0.00049	0.00049
NBS 951 “sample first“ (Pos.13)	80801	4.05433	0.00038	0.00018

**Figure 6:**

Comparison between different loading techniques ("graphite first" or "sample first"): Red diamonds indicate the "graphite first" and blue diamonds the "sample first" technique; error bars show the 2SD mean in-run precision of the NIST SRM 951 measurements. Numbers indicate the date of the measurements.

Loading for NTIMS was modified after the procedure reported by *Kasemann et al.* [2001]. A single degassed rhenium filament (40 min at 2.5 A and 40 min at 4.2 A) was coated with 0.5  $\mu\text{l}$  boron-free seawater serving as an emitter and heated at 0.7 A to dryness. Afterwards, a volume of 1 to 4  $\mu\text{l}$  sample solution containing typically 25 to 50 ng boron was loaded on the seawater salt-layer. The sample was evaporated to dryness at 0.7 A. The current was then raised slowly to 1.2 A and held there for 30 seconds to condition and homogenise the sample cake.

## I.7 Mass spectrometry and data reduction

### I.7.1 PTIMS measuring procedure and data reduction

$\text{Cs}_2\text{BO}_2^+$ -measurements were carried out on a static multi-collector Finnigan MAT 262 mass spectrometer equipped with a double Faraday collector configuration having a fixed spacing for masses 308 and 309. This special Faraday collector makes simultaneous collection of both  $\text{Cs}_2\text{BO}_2^+$ -species possible (static multicollection), leading to a better in-run precision relative to the usually performed dynamic peak-jumping collection method.

The following procedure was slightly modified after *Nakano and Nakamura* [1998].

Samples were introduced in the mass spectrometer and the system was evacuated until the vacuum reached  $2 \cdot 10^{-7}$  Torr. The filament current was then automatically raised slowly to 1.1 A at a rate of  $50 \text{ mA min}^{-1}$  with a closed valve to the ion source. The valve was then opened and the filament current was raised manually at a rate of 20 to  $25 \text{ mA min}^{-1}$ . Between 1.2 and 1.4 A the  $\text{Cs}^+$ -signal on mass 133 normally started to appear and was used to focus the ion beam. When the  $\text{Cs}^+$ -signal reached  $1 \cdot 10^{-12}$  A the magnetic field strength was changed to mass 309 ( $\text{Cs}_2^{11}\text{BO}_2^+$ ). The filament current was further raised at a rate of 10 to 15 mA with permanent focusing until the ion current of  $\text{Cs}_2^{11}\text{BO}_2^+$  reached 1 to  $2 \cdot 10^{-13}$  A. Before each measurement the positions and shape of the peaks (308 Faraday cup 10 and 309 Faraday collector 9) were checked with a mass- (Fig. 7 a) and a peak-scan procedure (Fig. 7 b).

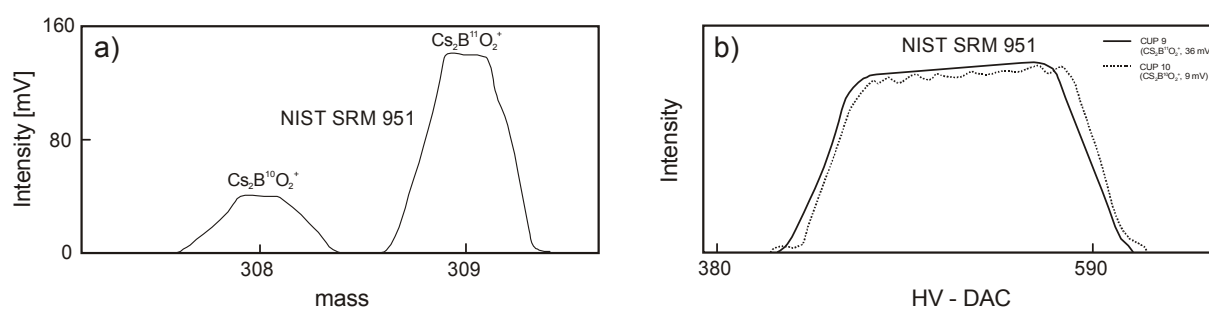


**Figure 7:** Mass-scan (a) and peak-scan (b) prior to a  $\text{Cs}_2\text{BO}_2^+$ -measurement of NIST SRM 951. a) Typical mass scan over masses 308 and 309 (bad peak shape is due to low signal intensity). b) Typical peak scan on a rising  $\text{Cs}_2\text{BO}_2^+$ -signal; peaks are slightly shifted due to mechanical configuration of the double Faraday collector (shifted tops of the peaks are due to raising signal intensities during the scanning).

Data collection was typically started between ion beam intensities of  $1 \cdot 10^{-12}$  and  $5 \cdot 10^{-12}$  A on mass 309 on a permanently declining signal. The ratio of  $\text{Cs}_2^{11}\text{BO}_2^+$  to  $\text{Cs}_2^{10}\text{BO}_2^+$  was measured in blocks of 20 individual scans each with an integration time of 4 seconds. All scans were checked with a 2SD error criteria for outliers, based on the block averages.

Because the  $\text{Cs}_2\text{BO}_2^+$ -signal commonly declines rapidly and the ion beam is only intense enough during a limited time no baseline was measured between the blocks. Data were corrected for baseline effects, using the last baseline calibration value, performed at the beginning of each working day. A comparison of NIST SRM 951 data corrected with concurrently measured baseline values between each block and of baseline values from the beginning of the working day showed no recognisable differences.

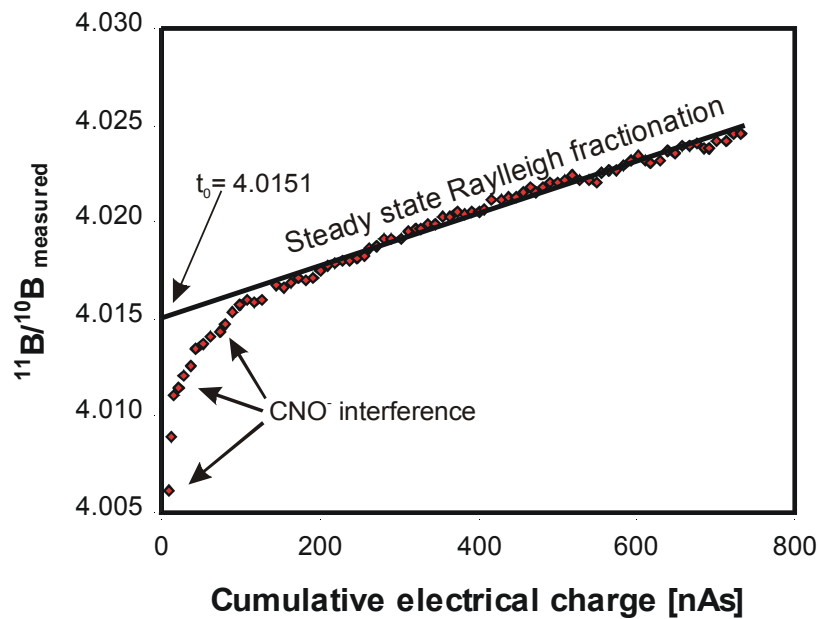
$^{11}\text{B}/^{10}\text{B}$  ratios were automatically corrected for oxygen  $^{17}\text{O}$  isotope interference subtracting  $-0.00079$  to achieve correct  $^{11}\text{B}/^{10}\text{B}$  ratios [Spivack and Edmond, 1986].

Interlaboratory comparison of data was done by a normalization ( $\delta^{11}\text{B}$  notation) of the measured sample ratio to the mean of concurrently (sample wheel) measured NIST SRM 951 ratios (Appendix 1). This method eliminates the impact of an instrumental offset relative to the certified value of *Catanzaro et al.* [1970], assuming the same instrumental fractionation for the NIST SRM 951 and for a concurrently measured sample. The bias of the long term average of NIST SRM 951 for PTIMS in the laboratory of the GeoForschungsZentrum Potsdam relative to the certified value of *Catanzaro et al.* [1970] ( $4.04362 \pm 0.00069$ ) was 2.7 ‰, which is near the high end of reported values from other PTIMS laboratories [Leeman et al., 1989; Nakamura et al., 1992; Tonarini et al., 1997; Deyhle, 2001].

### 1.7.2 NTIMS measuring procedure and data reduction

For detection of  $\text{BO}_2^-$  ions a multicollector VG SECTOR 54-30 mass spectrometer operated in the negative mode. After samples were introduced into the mass spectrometer the system was pumped to a vacuum better than  $1 \cdot 10^{-7}$  Torr. The filament temperature was then automatically increased to  $850^\circ\text{C}$  at a rate of  $120 \text{ mA min}^{-1}$  and then manually raised to about  $900^\circ\text{C}$  where the  $^{11}\text{BO}_2^-$  signal normally started to appear. The signal was focused several times and heated until the ion beam on mass 43 reaches  $1 \cdot 10^{-11} \text{ A}$  ( $\sim 950^\circ\text{C}$ ). At this stage of the procedure the  $\text{BO}_2^-$ -signal typically increased. Data acquisition was started in the range of  $1.0$  to  $2.0 \cdot 10^{-11} \text{ A}$  on mass 43 and comprised typically 82 blocks of 12 scans each.

Nearly all analyses carried out with seawater as an emitter substance showed a significant interfering  $\text{CNO}^-$  signal mainly on mass 42 [Hemming and Hanson, 1994] at the beginning of each measurement (Fig. 8). During the first hour of the measurement the interfering  $\text{CNO}^-$ -signal normally disappeared and the  $^{11}\text{B}/^{10}\text{B}$  ratio developed with the assumed Rayleigh-type steady state fractionation. Organic interference and mass depended fractionation were corrected with a linear regression of the late,  $\text{CNO}^-$  free, scans to  $t_0$  (starting time of the measurement) in order to obtain the  $^{11}\text{B}/^{10}\text{B}$  ratio at the time when the first fraction of sample evaporated. Therefore block averages were plotted against the cumulative electrical charge (Fig. 8).

**Figure 8:**

$^{11}\text{B}/^{10}\text{B}$  vs. cumulative electrical charge: Evolution of  $^{11}\text{B}/^{10}\text{B}$  ratio during NTIMS  $\text{BO}_2^-$ -measurement of NIST SRM 951; regression line to  $t_0$  of the linear data array give the "true"  $^{11}\text{B}/^{10}\text{B}$  ratio of the sample without  $\text{CNO}^-$  interference at the beginning of the measurement.

Interlaboratory comparison of data was done by a normalisation ( $\delta^{11}\text{B}$  notation) of measured sample ratios to concurrently analysed NIST SRM 951 ratios from the same sample wheel. Boron-isotope data carried out in this project using NTIMS were not corrected for  $^{17}\text{O}$  oxygen isobaric interference.

Experimentally obtained bias of NIST SRM 951 measured at the GeoForschungsZentrum Potsdam with NTIMS was  $-6.9\text{‰}$  relative to the certified ratio of *Catanzaro et al.* [1970]. This value is in good agreement with other NTIMS laboratories which report values of NIST SRM 951 in the same range [*Zeininger and Heumann, 1983; Vengosh et al., 1989; Klötzli, 1992; Hemming and Hanson, 1994*].



## I.8 Analytical boron blank

Contamination of samples with blank-boron during chemical preparation is a serious problem and has to be observed and tested, because boron components are extremely mobile and volatile and boron is a very common element in industrial products and especially in laboratory equipment.

Blank-boron can be inherited during sample preparation from the reagents used, the laboratory equipment and the ambient air. In the first two years of this project the total procedure-blank of the "K<sub>2</sub>CO<sub>3</sub> chemistry" (see section I.5.2.1) was relatively high (about 200 ng boron see *Kasemann et al.* [2001]). At that time, the high blank level was explained by having poor reagent blanks and the K<sub>2</sub>CO<sub>3</sub> was thought to be the main boron blank source. But after intensive testing from May to August 2001, the ambient air was found to be the main contaminant.

Boron silicate glass pocket-filters installed in the air-management system of the clean laboratory of the GeoForschungsZentrum Potsdam introduced an excessive boron flux into the laboratory environment. This was tested by exposing small volumes of ultra-pure water (1 or 2 ml) over different time periods to the ambient air of the clean laboratory (results see section I.8.2). After this clear and convincing finding, the boron-containing filters were changed and replaced by pocket-filters made of polyethylen and polystyrol in August 2001. This change of the filter medium resulted in a drop of the boron procedure-blank of about one order of magnitude (see section I.8.5).

### I.8.1 NIST SRM 952 as the spike material

To determine the boron-blank contribution during sample preparation the method of isotope-dilution mass-spectrometry (ID-MS) was used. Knowing the isotopic composition and concentration of a spike component, which is enriched in at least one isotope of the element of interest, the concentration of the element of interest can be calculated by the determination of the isotopic composition of a sample/spike mixture.

Commercial boric acid NIST SRM 952 [*Catanzaro et al.*, 1970; *NIST*, 1999], enriched in <sup>10</sup>B, was used as the spike material.

Boron blanks were calculated after the equation given below:

$$B[\text{pg}] = \left( M^{11}\text{B} * \frac{M^{10}\text{B}}{^{11/10}\text{blank}} \right) * \text{spike}[\text{mg}] * \text{molarity spike}[\text{pmol} / \text{mg}] * \left( \frac{^{11/10}\text{mixture} - ^{11/10}\text{spike}}{1 - \frac{1}{^{11/10}\text{blank}} * ^{11/10}\text{mixture}} \right)$$

NIST SRM 952 were measured three times and yielded a mean  $^{11}\text{B}/^{10}\text{B}$  ratio of  $0.05413 \pm 0.00016$  (1SD; Table 3). This ratio is in reasonable agreement with the published ratio of 0.05348 from *Nakamura et al.* [1992] determined by the same method.

**Table 3:** Comparison of replicate measurements of boron spike solution NIST SRM 952 with the  $\text{Cs}_2\text{BO}_2^+$ -graphite method (PTIMS) from this study and from *Nakamura et al.* [1992] and with the  $\text{Na}_2\text{BO}_2^+$  method from *Catanzaro et al.* [1970] and *NIST* [1999].

Sample	Reference	Boron [ $\mu\text{g}$ ]	$^{11}\text{B}/^{10}\text{B}$	2SD <sub>mean</sub>
<u><i>Cs<sub>2</sub>BO<sub>2</sub><sup>+</sup>-graphite method:</i></u>				
NIST SRM 952 I	This study	0.5	0.05397	0.000002
NIST SRM 952 II	This study	1.5	0.05435	0.000118
NIST SRM 952 III	This study	3.0	<u>0.05406</u>	0.000014
	<b>This study</b>	<b>Average</b>	<b>0.05413</b>	
		<b>1 SD</b>	<b>0.00016</b>	
NIST SRM 952 I	Nakamura	1.0	0.05352	0.00004
NIST SRM 952 II	et al. [1992]	1.0	<u>0.05343</u>	0.00008
		Average	0.05348	
		1 SD	0.00006	
<u><i>Na<sub>2</sub>BO<sub>2</sub><sup>+</sup> method:</i></u>				
NIST SRM 952	Catanzaro et al. [1970] NIST [1999]	Certified ratio	0.05319	

The large difference between our  $^{11}\text{B}/^{10}\text{B}$  ratio of 0.05413 and the certified ratio of 0.05319 [*Catanzaro et al.*, 1970; *NIST*, 1999] may be due to the different mass spectrometric methods applied. The  $\text{Cs}_2\text{BO}_2^+$ -graphite method produces significantly higher  $^{11}\text{B}/^{10}\text{B}$  ratios (see Table 2 in CHAPTER II) than the  $\text{Na}_2\text{BO}_2^+$  method for NIST SRM 951, which was used from the National Institute of Standards and Technology for the certification of both boric acid materials. A possible explanation also includes contamination of the NIST SRM 952 by air-derived boron (discussed below in I.8.2), because only a little contamination by boron with a natural composition ( $^{11}\text{B}/^{10}\text{B}$  ratio of  $\sim 4$ ) is sufficient to increase the spike  $^{11}\text{B}/^{10}\text{B}$  composition considerably.

### I.8.2 Air-derived boron-blank

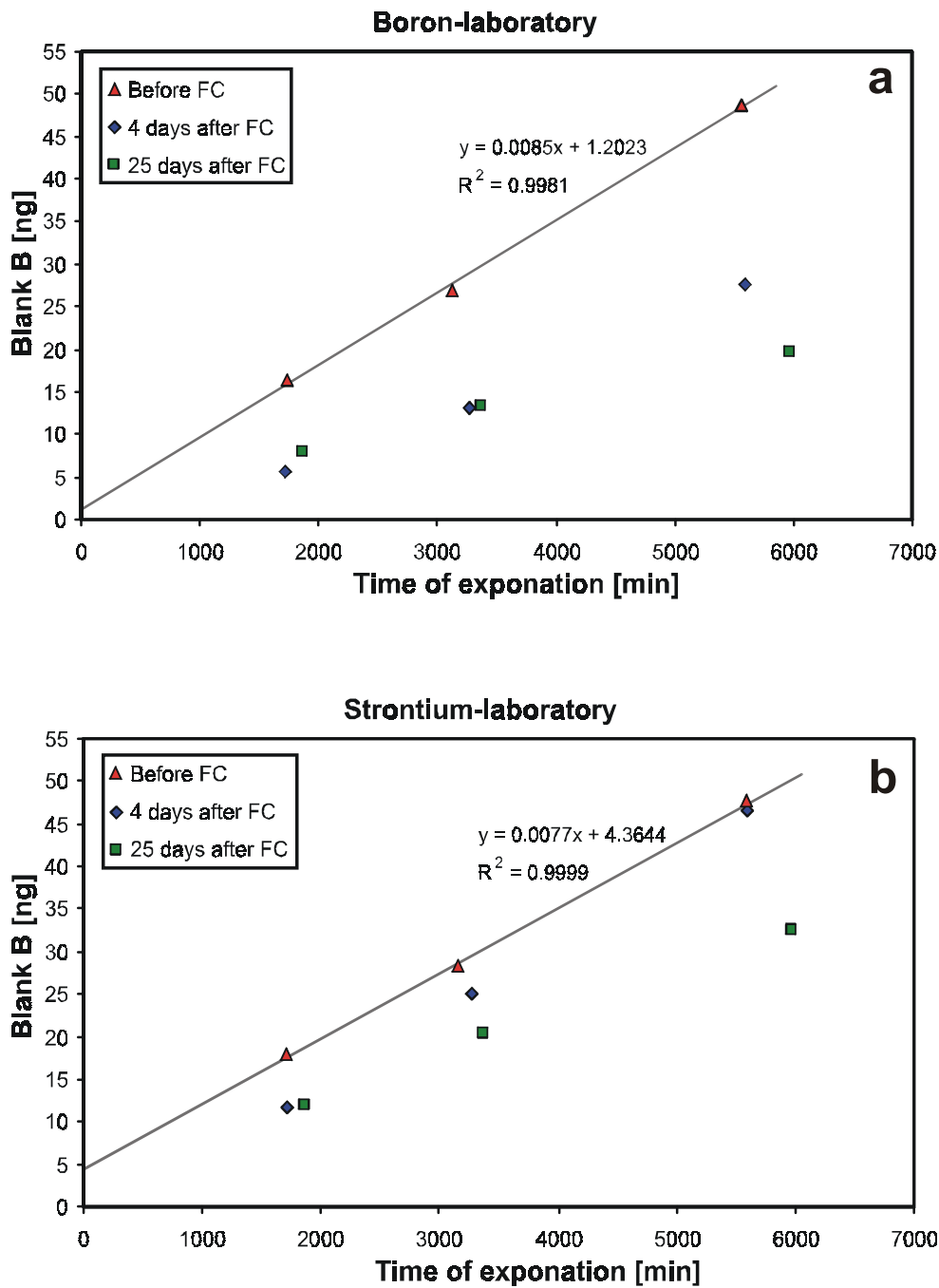
The boron contamination derived from the ambient laboratory air was investigated by exposing a series of open 15 ml Savillex® beakers filled with 2 ml water, 20 to 40 mg spike solution (NIST SRM 952) and 10 to 20 µl 0.02 % mannitol solution on the working platforms of two clean laboratory rooms during different time intervals. The accumulated amount of boron was calculated using ID-MS, after measuring the blank-spike mixture with the NTIMS  $\text{BO}_2^-$ -method.

The experiments were repeated three times, one prior to the filter change, one four days after and one 25 days after the filter change. The results of these experiments clearly indicated an extensive air-derived contamination of boron with time and showed a nearly linear accumulation rate between 0.0085 (boron laboratory) and 0.0077 (strontium laboratory) ng boron  $\text{min}^{-1}$  before the filter change and of 0.0028 (boron laboratory) and 0.0050 (strontium laboratory) ng boron  $\text{min}^{-1}$  after the filter change for a Savillex® beaker (Figs. 9 a and b). In the boron laboratory the boron blank decreased to less than 50 % 25 days after the filter change relative to the initial value. These linear patterns of boron accumulation as a function of time ( $R^2 > 0.989$  for all experiments) in the Savillex® beakers cannot be derived from the blank boron added from the reagents used, because the reagent-blank component does not change with time. The relatively slow decrease of the air-derived boron-blank component after the replacement of the boron-containing filters, especially in the strontium laboratory (Fig. 9 b), may have been due to a memory effect, because boron introduced by the old filters was possibly accumulated, re-mobilised and removed from the laboratory very slowly.

The source for this high boron flux in the laboratory air was identified as boron silicate glass pocket-filter (Camfil® MDA-S-GW-1166 x 566/566 x 66 +01PU). In the clean laboratory of the GeoForschungsZentrum Potsdam, these filters cleaned the incoming air from outside as well as the recycled air from the clean laboratory. For production and fire protection reasons the filters contain about 30 %  $\text{B}_2\text{O}_3$  (*pers. com. Mr. Kretschmann, Camfil®*). In Potsdam we determined a boron concentration of 11.8 % (38.0 %  $\text{B}_2\text{O}_3$ ) for the Camfil® boron silicate glass material of the pocket-filters, which is slightly higher than the concentration given by Camfil®. Boron isotope composition for this material was also determined from the same sample solution and yielded  $\delta^{11}\text{B}$  values of 0.4 and 2.1, respectively. Because these  $\delta^{11}\text{B}$  values are very near to zero on the  $\delta$  scale and a maximum

of 12.8 % different from the analysed samples (see CHAPTERS II and III), even a relatively high boron blank would not shift the  $\delta^{11}\text{B}$  value of the samples much (see section I.8.6).

**Figure 9:** Exposing experiments to investigate the air-derived boron-blank contamination in the clean laboratory of the GeoForschungsZentrum Potsdam: Figures a) boron laboratory and b) strontium laboratory show the boron accumulation in open Savillex<sup>®</sup> beakers as a function of time before and 4 and 25 days after the filter change (FC).



In August 2001 the boron silicate glass pocket-filters were removed and replaced with pocket-filters made of polyethylene and polystyrol (Camfil® Cam.FLO A, UF, P (Taschenfilter mit synthetischen Medium) and CITYCARP). The new synthetic carbonhydroxite filter material contains very low boron concentrations between 0.8 to 1.1  $\mu\text{g g}^{-1}$  boron (own analyses) and is suitable for clean laboratories in which boron analyses are carried out.

The process by which boron was removed from the boron-bearing filters and transferred to the clean laboratory air and into the samples is thought to be leaching due to the acid humidity. A transfer by particles is not likely because HEPA filters (Camfil®) placed under the ceiling of every clean laboratory room have a very small mesh size and in general the particle flux in a clean laboratory of category 100 (100 particles  $> 0.5 \mu\text{m}$  per  $\text{m}^3$ ), like at the GeoForschungsZentrum Potsdam, is low.

In summary, boron silicate glass pocket-filters are the most serious boron-blank source for clean laboratory environments in which boron is used and analysed in trace amounts, for example in the microwafer industry and analytical (geo-) sciences, because this product is the preferred material for most clean laboratories due to its high filtering efficiency and relatively low costs.

### **I.8.3 Reagent blanks**

Reagent blanks for the main materials used ( $\text{H}_2\text{O}$ ,  $\text{HCl}$ ,  $\text{HF}$ ,  $\text{NH}_4\text{OH}$  and  $\text{K}_2\text{CO}_3$ ) were determined, but are not meaningful due to a high air-derived blank amount, since all measurements were performed prior to the replacement of boron silicate glass pocket-filters (see section I.8.2). However, a procedure blank level of  $< 30 \text{ ng}$  boron achieved after the filter change (see section I.8.5) clearly shows the minor importance of boron introduced by the reagents relative to the air-derived boron prior to filter change.

The most critical contaminant of all reagents is expected to be the  $\text{K}_2\text{CO}_3$  used for fluxed fusion. All liquid reagents should have very low boron concentrations, because only high purity grade was used (see section I.2). The maximum boron concentration of the  $\text{K}_2\text{CO}_3$  used for this study can be calculated with the limiting assumption that the total boron of the  $\sim 20 \text{ ng}$  procedure blank after "K<sub>2</sub>CO<sub>3</sub> chemistry" (see section I.5.2.1) is derived from the  $\text{K}_2\text{CO}_3$ . Using this approach the maximum boron concentration of the  $\text{K}_2\text{CO}_3$  is  $0.1 \mu\text{g g}^{-1}$  and shows that the  $\text{K}_2\text{CO}_3$  is of a acceptable quality.

#### I.8.4 PTIMS loading blank

The PTIMS loading blank was investigated using a tantalum filament loaded only with 1  $\mu\text{l}$  graphite slurry and 0.5  $\mu\text{l}$  Cs-solution and 0.5  $\mu\text{l}$  mannitol-solution. Figure 10 shows a mass-scan in the mass-range between 307 and 310 at 1700 mA on the RPQ-counter. The observed intensity of < 1000 counts on mass 309 ( $\text{Cs}_2^{11}\text{BO}_2^+$ ; Fig. 10) is insignificantly small relative to the overall procedure blank, which is built up mainly by boron derived from the ambient air and chemical reagents.

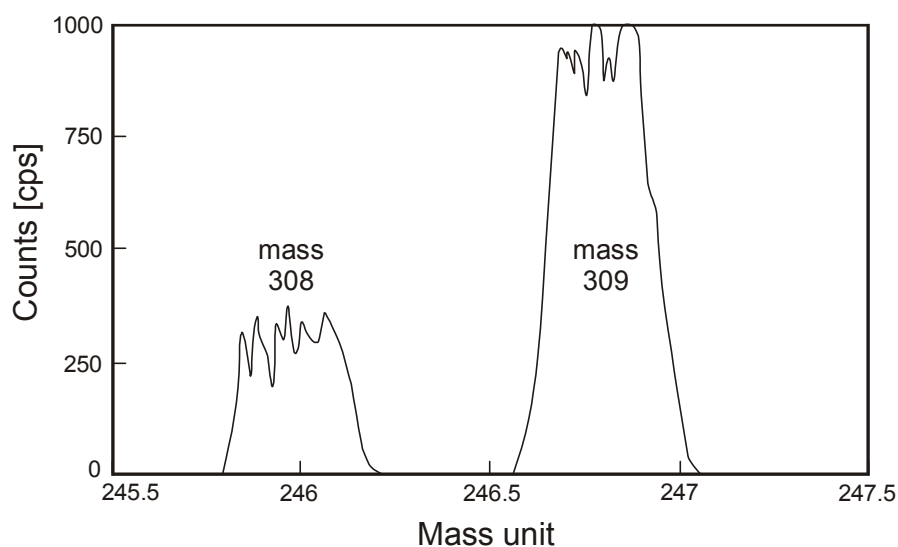


**Figure 10:**

Mass scan on the RPQ-counter (counts vs. mass unit) of a “blank“ tantalum filament loaded only with 1  $\mu\text{l}$  graphite slurry, 0.5  $\mu\text{l}$  0.00925 M Cs-solution and 0.5  $\mu\text{l}$  0.2 % mannitol-solution.

#### I.8.5 PTIMS procedure blanks

Procedure blanks were directly determined by ID-MS after complete dissolution and separation procedures (see section I.5.2) using the  $\text{Cs}_2\text{BO}_2^+$ -graphite method. Altogether, eight procedure blanks were determined, two for the procedure after HF dissolution (“HF chemistry”) and six for the procedure after alkaline fusion (“ $\text{K}_2\text{CO}_3$  chemistry”). Three of these blanks date prior to the replacement of the boron silicate glass pocket-filters in August 2001 and five after their replacement (Table 4; Fig. 11).

Before the filter change, the overall procedure blank for the “ $\text{K}_2\text{CO}_3$  chemistry”, spiked after the whole chemical procedure, showed very reproducible values of 98.7 and 98.9 ng boron, respectively. Another procedure blank spiked before starting the ion exchange chromatography indicated a maximum blank level of 122.5 ng for the whole “ $\text{K}_2\text{CO}_3$  chemistry” before the filter change.

**Table 4:** List of boron procedure blanks determined prior to and two and five months after the filter change (FC) in August 2001.

Method after $K_2CO_3$ or HF	Date	Spike <u>before</u> or <u>after</u> chemistry	Calculated procedure blank level [ng boron]
<i><u>Before FC:</u></i>			
$K_2CO_3$ (I)	June 2001	before	98.7
$K_2CO_3$ (II)	June 2001	before	98.9
$K_2CO_3$ (III)	June 2001	after	122.5
<i><u>2 months after FC:</u></i>			
$K_2CO_3$ (IV)	October 2001	before	22.4
HF (I)	October 2001	before	59.5
<i><u>5 months after FC:</u></i>			
$K_2CO_3$ (V)	January 2002	before	17.4
$K_2CO_3$ (VI)	January 2002	before	15.9
HF (II)	January 2002	before	30.2

Twice, two and five months after the filter change, the procedure blanks were determined again. Two months after the change the procedure blank of the  $K_2CO_3$ -method decreased to ~25 % of the initial value and after five months to a blank level significantly under 20 ng boron.

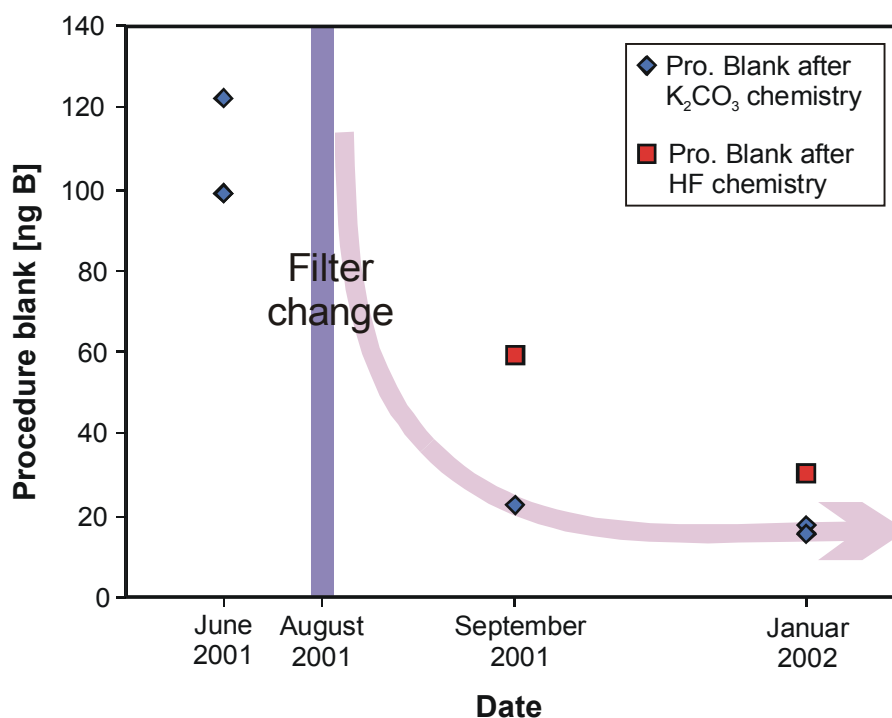


**Figure 11:** Boron procedure-blank evolution prior to and after the replacement of the boron silicate glass pocket-filters; x axis is only scaled after filter change. Arrow indicates the exponential decrease of the procedure-blank after filter replacement.

The decrease of boron procedure blanks shows an exponential curvature, with a major decrease in the first two months and a minor decrease from the second to the fifth month. Procedure blanks for "HF chemistry" were higher than those determined for the "K<sub>2</sub>CO<sub>3</sub> chemistry", but shows also a decrease after the filter change, from 59.5 ng after three months to 30.2 ng boron after five months. The exponential decrease of the overall procedure blanks after the filter change clearly demonstrates that boron derived from the ambient was and may still be the main reason for the relatively high boron-blank level in the past and the < 30 ng boron blank measured at the end of this study.

The achieved boron-blank levels after the filter change of about 30 ng for samples processed through the "HF chemistry" and < 20 ng boron for samples processed through the "K<sub>2</sub>CO<sub>3</sub> chemistry" are higher than those reported from *Tonarini et al.* [1997] (11.6 ng B) and *Nakamura et al.* [1992] (3 to 4 ng B). However, the level achieved is about one order of magnitude lower than that reported by *Kasemann et al.* [2001] for the clean laboratory of the GeoForschungsZentrum Potsdam in the year 2000.

### **I.8.6 Overall boron-blank effect on the "true" $\delta^{11}\text{B}$ value of a sample**

In Figure 12 the blank effect on the "true"  $\delta^{11}\text{B}$  value of a sample is shown. Because 3  $\mu\text{g}$  sample boron is normally used for the ion exchange chromatography procedure, a blank of about 200 ng boron [see *Kasemann et al.*, 2001] would result in an isotopic shift of about 0.4 ‰ from the "true" sample value (Fig. 12 yellow field), if the boron isotope composition of the blank is 20 ‰ different from the sample value. Note that the main boron blank source in the clean laboratory of the GeoForschungsZentrum Potsdam, the boron bearing pocket-filters, had an  $\delta^{11}\text{B}$  value of about +1 (see section I.8.2), which is not very different from most investigated samples (-7.2 to +13.6, see CHAPTERS II and III). Therefore curves of 10 ‰ difference (Fig. 12) between the composition of the blank boron and a sample are a more realistic condition, indicate a maximum deviation from the true  $\delta^{11}\text{B}$  value of about 0.17 ‰ caused by the high boron blank in the laboratory of the GeoForschungsZentrum Potsdam prior to the filter change.



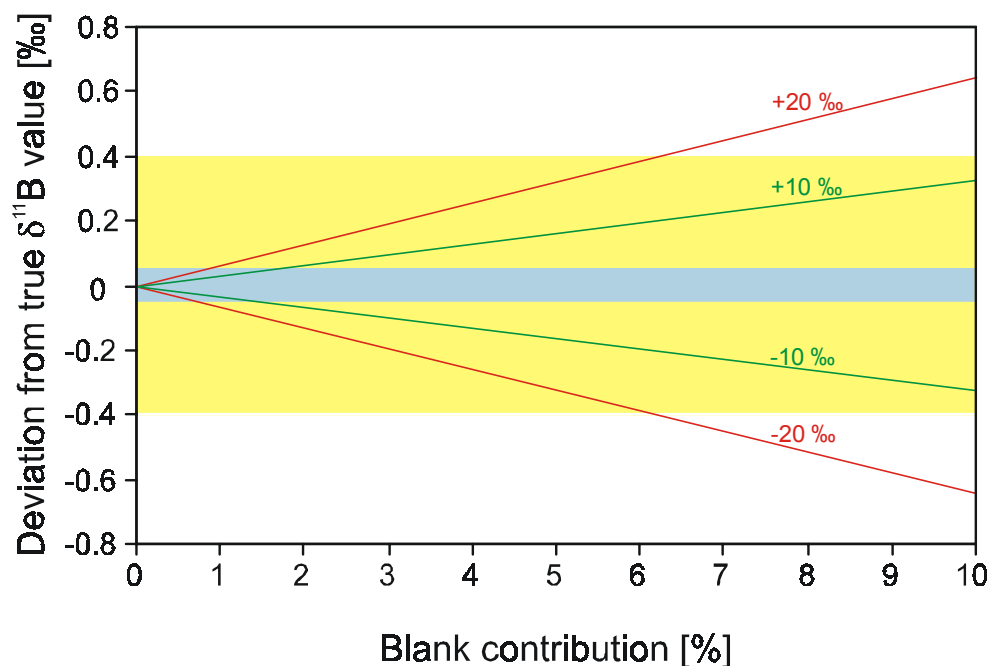


**Figure 12:** Effect of boron-blank on "true"  $\delta^{11}\text{B}$  value (Figure modified after *Tonarini et al.* [1997]): Curves show hypothetical blanks of  $\delta^{11}\text{B}$  ranging from  $-20$  to  $+20$  ‰ (red) and  $-10$  to  $+10$  ‰ (green). The yellow field indicate the maximum deviation prior to filter change and the blue field after filter change.

In summary, the blank prior to the filter change was relatively high, but a maximum shift of  $0.4$  ‰ is within the estimated overall analytical uncertainty of  $0.6$  to  $1.0$  ‰ (1SD; see CHAPTERS II and III). After the filter change the blank effect of  $< 30$  ng boron was negligible (blue field) relative to the commonly used  $3$   $\mu\text{g}$  boron for ion exchange chromatography, because it would have shifted the real sample  $\delta^{11}\text{B}$  value only  $0.05$  ‰, if the  $\delta^{11}\text{B}$  value of the blank was  $10$  ‰ different from the sample.

### I.9 Summary of new methodological developments

In the course of this study the  $\text{Cs}_2\text{BO}_2^+$ -graphite method for the determination of the boron isotope composition of silicate materials was installed at the GeoForschungsZentrum Potsdam. During installation of the new method all necessary tests and calibrations were carried out successfully.

Compared to the generally used procedures of *Nakamura et al.* [1992] and *Tonarini et al.* [1997] three major changes were made:

- The most important finding was the re-organisation of ion exchange chromatography steps after a HF dissolution using the very efficient boron specific AMBERLITE 743 resin. To start with an acidic sample solution, an additional cation chromatography step was introduced in advance of the exchange procedure described in *Tonarini et al.* [1997], because a cation chromatography is easy to perform and not crucial for boron loss.
- To avoid an unstable  $\text{Cs}_2\text{BO}_2^+$ -beam at the beginning of the TIMS-measurements an additional heating (sample conditioning) at 1.8 A for 20 seconds of the sample cake has been identified to stabilise the  $\text{Cs}_2\text{BO}_2^+$ -beam.
- To save data acquisition time on the commonly rapidly declining  $\text{Cs}_2\text{BO}_2^+$ -signal no baseline calibration was measured between the single blocks and the baseline correction was done with a baseline value from the beginning of the analytical session. A comparison of NIST SRM 951 data corrected with concurrently measured baseline values between each block and with baseline values from the beginning of the analytical session show no recognisable difference.

A major contribution to the successfully installation of the  $\text{Cs}_2\text{BO}_2^+$ -graphite method was the identification of the main boron blank source in the clean laboratory of the GeoForschungsZentrum Potsdam. Extensive reagent testing and finally a series of exposure experiments indicated an air derived boron contamination. As the source for the high boron flux in the laboratory air boron silicate glass pocket-filters (ca. 30 %  $\text{B}_2\text{O}_3$ ) were identified, from which boron is thought to have been leached and transferred to the samples by the acidic laboratory humidity. Replacement of the boron silicate glass pocket-filters by synthetic polyethylene and polystyrol pocket-filters decreased the boron procedure-blank one order of magnitude. A boron procedure blank of < 30 ng allows now the determination of low boron bearing silicate rocks like mantle materials.

The whole preparation procedure was tested with known reference materials. The obtained  $^{11}\text{B}/^{10}\text{B}$  ratios and  $\delta^{11}\text{B}$  values and analytical precision of NIST SRM 951 and 952 and silicate reference materials compare well with published data and demonstrate good precision and accuracy.

## CHAPTER II

### **Boron isotopic composition and concentration of ten geological reference materials**

To be submitted to: *Geostandard Newsletters*

#### **II Abstract**

We present boron (B) isotope and concentration data from geological silicate reference materials covering a wide spectrum of B-isotope compositions and B concentrations. B-isotope compositions were determined by Thermal Ionisation Mass Spectrometry ( $\text{Cs}_2\text{BO}_2^+$ -graphite and  $\text{BO}_2^-$  method) and B concentrations by Inductively-Coupled-Plasma Optical-Emission-Spectrometry (ICP-OES). The obtained  $\delta^{11}\text{B}$  values range from  $-12.6$  to  $+13.6$  and are reproducible within  $0.7$  ‰ (1RSD) on the basis of individually prepared sample aliquots. The  $\delta^{11}\text{B}$  values of JA-1 ( $+5.3$  ‰), JB-3 ( $+5.9$  ‰) and JR-2 ( $+2.9$  ‰) overlap within analytical uncertainty the published data. We also report the first  $\delta^{11}\text{B}$  values for the TB ( $-12.6$  ‰) and the MPI-DING glasses GOR-128-G ( $+13.6$  ‰), GOR-132-G ( $+7.1$  ‰) and StHs6/80-G ( $-4.5$  ‰). The  $\delta^{11}\text{B}$  values obtained by the  $\text{Cs}_2\text{BO}_2^+$ -graphite and the  $\text{BO}_2^-$  method as well as the majority of  $\delta^{11}\text{B}$  values obtained using different sample preparation methods agree within analytical uncertainty. We therefore conclude that these analytical methods introduce no systematic error on the calculated  $\delta^{11}\text{B}$  values. The obtained B concentrations range from  $7$  to  $159$   $\mu\text{g g}^{-1}$ . Based on replicate analyses from individually prepared sample aliquots an overall external reproducibility of better than  $10$  % was determined. Our B concentrations are in agreement to within  $14$  % of the published values.

#### **II.1 Introduction**

Based on the geochemical characteristics of B, mainly its high solubility and mobility in aqueous solutions and incompatibility in most magmatic environments, B-isotopes have great potential as a geochemical tool for the study of various kinds of mixing and transfer processes in earth and planetary sciences [see review by *Palmer and Swihart, 1996*].

In the past, the use of B and its isotopes was mainly hindered by problems associated with the extraction and separation of B from other matrix elements without affecting the isotopic composition. In addition, the low precision of the mass spectrometric techniques and problems related to dissolution and separation limited the application of B-isotopes [see review by *Swihart*, 1996]. Because of technological progress, especially in the field of mass spectrometry, interest has grown in the last 15 years to establish B-isotopes as a tracer in geoscience.

At present, only a few silicate geochemical reference materials are already characterised in terms of their B-composition and a real interlaboratory comparison of B-isotope compositions is only possible with the JB-2 (island-arc tholeiitic basalt; [*Nakamura et al.*, 1992; *Tonarini et al.*, 1997, *Deyhle*, 2001, *Kasemann et al.*, 2001]) and four recently introduced reference materials of the International Atomic Energy Agency (IAEA; [*Tonarini et al.*, in prep; *Gonfiantini et al.*, in prep.]). In addition to the natural rock samples mentioned above, the synthetic glasses NIST 610 and 612, mainly used in microanalytics, are already characterised in terms of their B composition by *Kasemann et al.* [2001].

The aim of this study is to characterise geological silicate reference materials in terms of both B-isotope composition and B concentration. We have analysed seven powdered silicate rocks used as reference materials for bulk wet chemistry techniques and three silicate geological reference glasses used for in-situ microanalysis. In addition, we report data for the long term variation of NIST SRM 951 boric acid standard used to normalise measured  $^{11}\text{B}/^{10}\text{B}$  ratios to the  $\delta^{11}\text{B}$  notation.

The data are discussed in terms of their analytical precision and are compared to published data. According to the two different wet chemical procedures and mass spectrometric methods applied we evaluate the impact of dissolution, separation and mass spectrometric methods on the calculated  $\delta^{11}\text{B}$  values. All results presented here were carried out at the GeoForschungsZentrum Potsdam (GFZ Potsdam).

B-isotope ratios are reported as  $\delta^{11}\text{B}$  values, i. e. normalised to the mean of concurrently measured NIST SRM 951 standards:

$$\delta^{11}\text{B} = \left[ \frac{\{^{11}\text{B}/^{10}\text{B}\}_{\text{sample}}}{\{^{11}\text{B}/^{10}\text{B}\}_{\text{NIST SRM 951}}} - 1 \right] * 1000.$$

## II.2 Samples

The Geological Survey of Japan (GSJ) and the Zentrale Geologische Institut (ZGI) have produced a variety of powdered whole rock reference materials for the geochemical community. Four reference rocks ranging from basaltic/gabbroitic to rhyolitic (JGb-1, JB-3, JA-3, JR-1, JR-2; Table 1) from the GSJ and two sedimentary reference rocks (TB and TS; Table 1) from the ZGI, were selected, because these materials cover a wide range of bulk compositions and potentially also a wide range of  $\delta^{11}\text{B}$  values and B concentrations.

In order to provide B concentration and isotope data for the calibration of in-situ microanalytical techniques such as Secondary-Ionization-MassSpectrometry (SIMS) or Laser-Ablation Inductively-Coupled-Plasma Mass-Spectrometry (LA-ICP-MS), we also selected three MPI-DING reference glasses (GOR-128-G, GOR-132-G and StHs6/80-G; Table 1). Informations about the preparation, composition and homogeneity of these glasses have been published by *Jochum et al.* [2000].

NIST certified boric acid SRM 951 [*Catanzaro et al.*, 1970; *NIST*, 1999] was used as a standard to control both the instrument dependent fractionation and complete analytical procedure and to translate the measured  $^{11}\text{B}/^{10}\text{B}$  ratios into the  $\delta^{11}\text{B}$  notation. NIST SRM 952, enriched in  $^{10}\text{B}$ , was used as a tracer to determine the B-blank concentration by isotope dilution. Both materials are sold by the National Institute of Standards and Technology (NIST; <http://www.nist.gov>).

It is important to point out that all used reference materials are to date well distributed and still available. The magmatite samples were sold by the GSJ (<http://www.aist.go.jp/RIODB/geostand/>). The Breitländer GmbH offers the ZGI samples (<http://www.breitlander.de>). The MPI-DING glasses are available from the Max-Planck Institute für Chemie, Mainz ([kpj@mpch-mainz.mpg.de](mailto:kpj@mpch-mainz.mpg.de) or [stoll@mpch-mainz.mpg.de](mailto:stoll@mpch-mainz.mpg.de)).

## II.3 Analytical methods

### II.3.1 Boron concentration analyses

B concentration analyses were carried out on a VARIAN Liberty 200 ICP-OES using the emission line at 249.773 nm. Before analyses, the samples were fluxed with  $K_2CO_3$  and B was chemically separated by cation exchange chromatography using AG 50W-X8 resin as described in *Kasemann et al.* [2001]. Calibration was typically made using a  $1 \mu\text{g ml}^{-1}$  B standard solution in 0.05 M HCl. To guarantee precise and reproducible analytical results the B concentrations in the sample solution were kept between 0.1 and  $1 \mu\text{g g}^{-1}$ .

### II.3.2 Boron isotope analyses

#### II.3.2.1 PTIMS: The $Cs_2BO_2^+$ -graphite method

Boron was extracted from silicate samples by alkaline fusion with  $K_2CO_3$  [*Tonarini et al.*, 1997] or alternatively by HF attack in the presence of mannitol [*Nakamura et al.*, 1992]. In both cases an aliquote sample solution comprising typically  $3 \mu\text{g B}$  was separated by sequential ion exchange chromatography.

Separation of B after alkaline fusion ("K<sub>2</sub>CO<sub>3</sub> chemistry") was carried out using the three step ion exchange chromatography of *Tonarini et al.* [1997]. Boron separation after HF attack ("HF chemistry") was carried out after a newly reorganised four step ion exchange chromatography procedure (see CHAPTER I), using an additional fourth cation chromatography step in advance to the three separation steps described by *Tonarini et al.* [1997].

The sample solution was loaded on a degassed tantalum filament coated with a graphite/ethanol slurry and heated at 0.7 A. Before reaching complete dryness,  $0.5 \mu\text{g B}$  dissolved in 2 N HCl and mixed with cesium-carbonate solution (1 mol B : 2 mol cesium) and mannitol ( $1 \mu\text{g B} : 40 \mu\text{g mannitol}$ ) was loaded onto the graphite layer. When the sample was completely dry the current was raised to 1.8 A for 20 seconds.

Boron isotope measurements were carried out on a Finnigan MAT 262 mass spectrometer equipped with a special double Faraday cup having a fixed spacing for the dicesium metaborate complexes by static multicollection [*Nakano and Nakamura*, 1998]. The isotopic composition of B was then measured on masses 308 ( $Cs_2^{10}BO_2^+$ ) and 309 ( $Cs_2^{11}BO_2^+$ ) with filament currents between 1.3 and 2.0 A ( $< 900^\circ \text{C}$ ) and ion beam intensities between  $1 * 10^{-12}$

and  $1 \times 10^{-11}$  A on mass 309. It has to be pointed out that necessary filament currents for samples proceeded through the "HF chemistry" are significant higher than for samples processed through the " $\text{K}_2\text{CO}_3$  chemistry".

Measurements typically consist of at least 3 blocks of twenty scans each whereby all scans are automatically corrected for oxygen isotope  $^{17}\text{O}$  interference subtracting 0.00079 from the measured  $^{11}\text{B}/^{10}\text{B}$  ratios [Spivack and Edmond, 1986].

### II.3.2.2 NTIMS: The $\text{BO}_2^-$ method

Measurements of  $\text{BO}_2^-$  ions at masses 42 and 43 were performed on a multicollector VG SECTOR 54-30 mass spectrometer by dynamic multicollection. Silicate samples were prepared as described for B concentration analysis. Typically 25 to 50 ng sample B were loaded on a rhenium filament coated with a salt-layer of B-free seawater, evaporated to dryness at 0.7 A and then heated for 30 seconds at 1.2 A. A manual for the TIMS-measurement procedure and the following data reduction is in detail described in CHAPTER I and by Kasemann *et al.* [2001].

### II.3.3 Boron blank

Procedure blanks for B after " $\text{K}_2\text{CO}_3$  and HF chemistry" were determined by isotope dilution using NIST SRM 952 as a tracer. During the course of the study the B-procedure blank decreased from about 200 ng B to less than 30 ng B. This makes up 6.5 % and 1.0 %, respectively of the 3  $\mu\text{g}$  B typically used for ion exchange chromatography.

Assuming the isotopic composition of the blank was 20 ‰ different of the respective sample composition, a 200 ng B-blank would have caused a  $\delta^{11}\text{B}$  shift of about 0.4 ‰, whereas the effect of a 30 ng B-blank is negligible. Note that a 0.4 ‰ shift is within the estimated overall analytical uncertainty (see section II.4).

## II.4 Results and discussion

### II.4.1 Boron concentrations

The results of replicate B concentration analyses of individually prepared sample aliquots are listed in Table 1. The obtained B concentrations of the ten reference materials range from 7 to 159  $\mu\text{g g}^{-1}$  B. The internal precision of ICP-OES measurements is in general better than 3 % and in most cases significantly better than 2 %. The external reproducibility of the whole wet chemical procedure determined by individually prepared sample aliquots typically varies between 3 and 5 % (1RSD; Table 1), with the exception of JB-3 (N = 3).

Accuracy was evaluated by comparison to B concentrations recommended for the GSJ and ZGI reference materials (Govindaraju, 1994; Imai *et al.*, 1995). Except for JGb-1 (N=1) and JR-1, all mean B concentrations determined on rock powders overlap to within 10 % of the literature data (Table 1). For JGb-1 only one single measurement was carried out and is therefore statistically not meaningful. The reported B concentration for JR-1 from Imai *et al.* [1995] appears problematic on the basis of its large error (1RSD = 29 %). However, Govindaraju [1994] and D'Orazio [1999] report B concentrations of 133 and 129  $\mu\text{g g}^{-1}$  for JR-1, respectively, which are in excellent agreement with our determined mean value of 134  $\mu\text{g g}^{-1}$ .

**Table 1:** Boron concentrations in ten silicate rock reference materials. 1SD (standard deviation); error refers to the external reproducibility determined by analyses of individually prepared sample aliquots (N).

Sample	Rock type	Material	Boron [ $\mu\text{g g}^{-1}$ ] ( $\pm$ 1SD)	1 RSD [%]	Range [ $\mu\text{g g}^{-1}$ ]	N	Literature ( $\pm$ 1SD)
JGb-1	gabbro	powder	7.0			1	4.0 ( $\pm$ 1.4)*
JB-3	basalt	powder	20.0 ( $\pm$ 2.0)	9.9	18 - 21	3	18.0 ( $\pm$ 3.1)*
JA-3	andesite	powder	26.8 ( $\pm$ 1.0)	3.9	25 - 28	15	24.8 ( $\pm$ 2.9)*
JR-1	rhyolite	powder	134.1 ( $\pm$ 3.7)	2.8	127 - 140	13	117 ( $\pm$ 34)*
JR-2	rhyolite	powder	158.6 ( $\pm$ 5.7)	3.6	149 - 169	12	145 ( $\pm$ 8.6)*
TB	clay shale	powder	88.1 ( $\pm$ 4.5)	5.1	74 - 93	34	90**
TS	black shale	powder	68.1 ( $\pm$ 2.9)	4.3	62 - 74	17	74**
GOR-128-G	komatiite	glass	22.7			1	21.8***
GOR-132-G	komatiite	glass	15.6			1	17.8***
StHs6/80-G	andesite	glass	11.6			1	12.5***

\* Imai *et al.* [1995]; \*\* Govindaraju [1994]; \*\*\* Jochum *et al.* [2000]

Our results of MPI-DING glasses GOR-128-G, GOR-132-G and StHs6/80-G, the first determined by a bulk wet chemical procedure, overlap within 14 % the published B concentrations determined by SIMS [Jochum *et al.*, 2000].



## II.4.2 Boron isotopic compositions

### II.4.2.1 NIST SRM 951

Eighty-three analyses of NIST SRM 951 carried out with the  $\text{Cs}_2\text{BO}_2^+$ -graphite method over a period of 26 months yielding a mean  $^{11}\text{B}/^{10}\text{B}$  ratio of 4.05416 and replicate within 0.38 ‰ (2RSD; Fig. 1; Appendix 1). In-run precision for individual NIST SRM 951 analyses vary between 0.03 and 0.3 ‰ (error-bars in Fig. 1 are 2RSD mean in-precision, calculated from the mean  $^{11}\text{B}/^{10}\text{B}$  ratios of the blocks). The long term variation of NIST SRM 951 shows a sin-curve like variation with time (Fig. 1), nevertheless, except for one analyses, all results plot well within the 2SD range and demonstrate a reproducibility of 0.04 ‰ 2RSD mean of the mean  $^{11}\text{B}/^{10}\text{B}$  ratio.

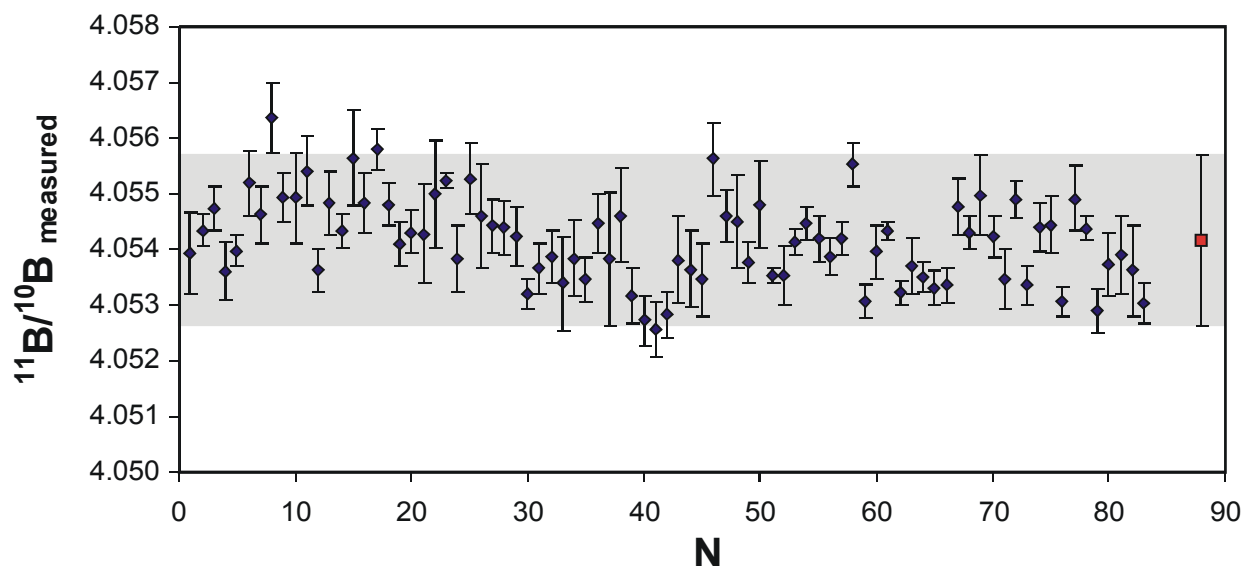


**Figure 1:** Long term (26 months) variation of NIST SRM 951: Blue diamonds show 83 individual analyses with 2RSD mean errors (in-run precision) based on block averages. The mean  $^{11}\text{B}/^{10}\text{B}$  ratio is indicate by the red square together with the 2SD range indicated by the shaded area.

A comparison of various NIST SRM 951 data measured with the  $\text{Cs}_2\text{BO}_2^+$ -graphite method shows comparable data quality for the majority of published studies and no correlation with the collection mode of the two boron complexes (static or dynamic; Table 2). Exceptionally are the data from *Lemarchand et al.* [2002], who carried out an optimised procedure for both B separation and mass spectrometry, obtaining a precision one order of magnitude better. The reproducible bias of the long term mean value for NIST SRM 951 determined by the  $\text{Cs}_2\text{BO}_2^+$ -graphite method in our laboratory relative to the certified value of 4.04362

determined by the  $\text{Na}_2\text{BO}_2^+$  method [Catanzaro *et al.*, 1970; NIST, 1999] is 2.7 ‰ and falls at the high end of reported values of other  $\text{Cs}_2\text{BO}_2^+$ -graphite studies (Table 2).

Twelve separate analyses of NIST SRM 951 carried out by the  $\text{BO}_2^-$  method yielded a mean  $^{11}\text{B}/^{10}\text{B}$  ratio of 4.01556 and replicate within 1.06 ‰ (2RSD; Table 2). This  $^{11}\text{B}/^{10}\text{B}$  ratio has a difference of 6.9 ‰ relative to the certified value and shows the characteristic offset to lower  $^{11}\text{B}/^{10}\text{B}$  ratios for NIST SRM 951 determined by NTIMS.

**Table 2:** Comparison of absolute  $^{11}\text{B}/^{10}\text{B}$  ratios determined by different mass spectrometric methods and different laboratories.

Reference	Data collection	Boron load [µg]	N	$^{11}\text{B}/^{10}\text{B}$ mean	2SD	2RSD [‰]
<i>Cs<sub>2</sub>BO<sub>2</sub><sup>+</sup>-graphite method:</i>						
Nakamura <i>et al.</i> [1992]	Dynamic	0.1 – 1.0	15	4.05121	0.00141	0.35
Tonarini <i>et al.</i> [1997]	Dynamic	0.2 – 0.6	11	4.05061	0.00078	0.19
Nakano and Nakamura [1998]	Static	1.0	18	4.05294	0.00200	0.49
Deyhle [2001]	Static	1.0	7	4.05224	0.00083	0.20
Lemarchand <i>et al.</i> [2002]	Dynamic	0.25	22	4.05288	0.00019	0.05
<b>This study</b>	Static	0.5	83	4.05416	0.00154	0.38
<i>BO<sub>2</sub><sup>-</sup> method:</i>						
Hemming and Hanson [1994]	Dynamic	0.001 – 0.02	10	4.00136	0.00253	0.63
<b>This study</b>	Dynamic	0.025	12	4.01556	0.00426	1.06
<i>Na<sub>2</sub>BO<sub>2</sub><sup>+</sup> method:</i>						
NIST [1999]	Dynamic			4.04362	0.00138	0.34

#### II.4.2.2 Influences of the chemical separation

Boron may, theoretically, undergo isotopic fractionation during sample preparation due to B loss during ion exchange chromatography or sample decomposition and evaporation under acid conditions [e.g., Lemarchand *et al.*, 2002; Ishikawa and Nakamura, 1990]. We tested our ion chromatography procedure by processing 3 µg B from NIST SRM 951 through one anion chromatography step and three times through the entire procedure of sample preparation after "K<sub>2</sub>CO<sub>3</sub> chemistry" (Table 3).

NIST SRM 951 passed through only one anion chromatography step gave a nearly identical  $^{11}\text{B}/^{10}\text{B}$  ratio compared with the unprocessed NIST SRM 951 from the same sample wheel. The  $\delta^{11}\text{B}$  values of four analyses of the NIST SRM 951 III solution from the same

chemistry scatter over a range of 0.84 ‰ relative to the mean value of unprocessed NIST SRM 951 and replicate within 0.28 ‰ (1RSD). The mean  $^{11}\text{B}/^{10}\text{B}$  ratio of the four individually processed NIST SRM 951 standards is 4.05324 with an uncertainty of 0.59 ‰ (1RSD; Table 3). The systematically higher analytical uncertainties (1SD) of unprocessed NIST SRM 951 (0.19 ‰), over processed NIST SRM 951 from the same chemistry (0.26 ‰), to processed NIST SRM 951 of individually chemistries (0.59 ‰) show that sample preparation in general has a detrimental effect on both the precision and the accuracy of the final  $\delta^{11}\text{B}$  values.

**Table 3:** Influence of ion exchange chromatography on B-isotope composition of NIST SRM 951: 2SD mean errors were calculated on the basis of the block averages;  $\delta^{11}\text{B}$  of processed NIST SRM 951 were normalised to the mean  $^{11}\text{B}/^{10}\text{B}$  ratio of concurrently analysed NIST SRM 951 (Appendix 1).

Sample	$^{11}\text{B}/^{10}\text{B}$	2 SD	NIST SRM 951	$\delta^{11}\text{B}$
	measured	mean	unprocessed	
NBS 951 I (Amberlite)	4.05450	0.00081	4.05473	-0.06
NBS 951 II ( <i>full <math>\text{K}_2\text{CO}_3</math> chemistry</i> )	4.05004	0.00113	4.05422	-1.03
<i>NBS 951 III.1 (full <math>\text{K}_2\text{CO}_3</math> chemistry)</i>	<i>4.05442</i>	<i>0.00150</i>	4.05423	<i>0.05</i>
<i>NBS 951 III.2 (full <math>\text{K}_2\text{CO}_3</math> chemistry)</i>	<i>4.05293</i>	<i>0.00076</i>	4.05347	<i>-0.13</i>
<i>NBS 951 III.3 (full <math>\text{K}_2\text{CO}_3</math> chemistry)</i>	<i>4.05170</i>	<i>0.00091</i>	4.05490	<i>-0.79</i>
<i>NBS 951 III.4 (full <math>\text{K}_2\text{CO}_3</math> chemistry)</i>	<i>4.05267</i>	<i>0.00026</i>	4.05335	<i>-0.17</i>
Average of NBS III	4.05293			-0.26
External reproducibility 1SD	0.00113			
External reproducibility 1SD [‰]	0.28			
NBS 951 IV ( <i>full <math>\text{K}_2\text{CO}_3</math> chemistry</i> )	4.05548	0.00171	4.05466	<i>0.20</i>
Average NBS I - IV	4.05324			-0.36
External reproducibility 1SD	0.00237			
External reproducibility 1SD [‰]	0.59			

The mean  $^{11}\text{B}/^{10}\text{B}$  ratio of all NIST SRM 951 aliquots processed through chemistry is about -0.36 ‰ lower than for NIST SRM 951 aliquots without chemistry (Table 3 and Table 2). Surprisingly, nearly the same offset of between -0.25 and -0.40 ‰ was reported by *Tonarini et al.* [1997] and *Deyhle* [2001] and therefore seems to be a characteristic feature for the  $\text{Cs}_2\text{BO}_2^+$ -graphite method after " $\text{K}_2\text{CO}_3$  chemistry", most likely caused by a slight B-isotope fractionation during ion exchange chromatography [e.g., *Lemarchand et al.*, 2002] or possibly by isobaric interferences of  $\text{Cs}_2\text{NO}^+$  molecules derived from organic material during  $\text{Cs}_2\text{BO}_2^+$  TIMS-measurements [*Xiao and Wang*, 1998].

### II.4.2.3 Silicate reference materials

All  $^{11}\text{B}/^{10}\text{B}$  ratios determined by the  $\text{Cs}_2\text{BO}_2^+$ -graphite method, along with the concurrently determined values for the NIST SRM 951 and normalised  $\delta^{11}\text{B}$  values and their in-run precision and external reproducibility are presented in Table 4.

The finally calculated mean  $\delta^{11}\text{B}$  values for the investigated reference materials are the mean of one or more individually prepared sample aliquots (Table 4 column  $\delta^{11}\text{B}$  mean), whereby the  $\delta^{11}\text{B}$  value of one individually prepared sample aliquots is the mean of one or more measurements on one chemically processed sample (Table 4 column  $\delta^{11}\text{B}$  run).

The  $\delta^{11}\text{B}$  values of the investigated reference materials fall in the range between -12.6 and +13.6 ‰ known for terrestrial silicate rocks (Table 4 and 5, see Fig. 1 in CHAPTER I). The lower end is defined by a  $\delta^{11}\text{B}$  value of -12.6 ‰ (-12.4 ‰ PTIMS; -12.7 ‰ NTIMS) of the clay shale TB and shows most likely the incorporation of  $^{10}\text{B}$  by clay minerals during sedimentation and diagenesis.

The arc volcanic rocks JA-1 (+5.3 ‰), JB-3 (+5.8 ‰), JR-2 (+2.9 ‰) are from the Izu-arc and show slightly positive  $\delta^{11}\text{B}$  values very typical for arc settings in general (see Fig. 12 in CHAPTER III). For the MPI-DING glasses we assume that the isotopic composition of the artificial glasses reflects the primary composition of the starting material, because as *Kasemann et al.* [2001] have demonstrated, a rapid high temperature melting process does not cause significant B-isotope fractionation. The andesitic ash glass StHs6/80-G from Mount St. Helens (continental arc setting) shows a mantle like  $\delta^{11}\text{B}$  value of -4.5 ‰, which may reflect a dominant mantle source, crustal contamination or B-isotope fractionation during subduction. Both komatiite glasses from Gorgona island (GOR-128-G +13.6 ‰ and GOR-132-G +7.1 ‰) mark the upper range of  $\delta^{11}\text{B}$  values. This is surprising, as in general, mantle derived rocks show negative  $\delta^{11}\text{B}$  values. A possible explanation includes seawater alteration, because both samples are known to have erupted in a submarine environment.

**Table 4:** Compilation of all measured  $^{11}\text{B}/^{10}\text{B}$  ratios, the concurrently determined value for the NIST SRM 951 (NIST 951<sub>(unpro.)</sub>) and normalised  $\delta^{11}\text{B}$  values along with the in-run precision (calculated on the basis of the block averages) and external reproducibility (1SD) of the  $\delta^{11}\text{B}$  values.

Sample	Chemistry	$^{11}\text{B}/^{10}\text{B}$	Measured		$\delta^{11}\text{B}$ mean		1SD [‰]		
			2RSD mean	NIST 951 <sub>(unpro.)</sub>	run	mean			
<b>GSI:</b>									
<b>JB-3</b>	K <sub>2</sub> CO <sub>3</sub>	4.07717	0.00029	4.05335	5.88				
PTIMS	HF	4.07926	0.00052	4.05335	6.39	6.13	0.37		
		4.07756	0.00026	4.05362	5.91				
		4.07605	0.00043	4.05422	5.38				
		4.07483	0.00137	4.05295	5.40	5.56	0.30		
					<b>Mean JB-3</b>	<b>5.85</b>	<b>0.40</b>		
<b>JA-1</b>	K <sub>2</sub> CO <sub>3</sub>	4.07572	0.00122	4.05376	5.42				
PTIMS		4.07477	0.00131	4.05376	5.18	5.30	0.17		
							<b>Mean JA-1</b>	<b>5.30</b>	<b>0.17</b>
<b>JR-2</b>	K <sub>2</sub> CO <sub>3</sub>	4.06522	0.00038	4.05373	2.83	2.83			
PTIMS	HF1	4.06537	0.00119	4.05366	2.89	2.89			
		HF 2	4.06824	0.00075	4.05429	3.44			
			4.06504	0.00117	4.05414	2.69	3.07	0.53	
							<b>Mean JR-2</b>	<b>2.93</b>	<b>0.12</b>
<b>ZGI:</b>									
<b>TB</b>	K <sub>2</sub> CO <sub>3</sub>	4.00525	0.00142	4.05361	-11.93				
PTIMS	HF	4.00552	0.00157	4.05458	-12.10	-12.01	0.12		
		4.00177	0.00124	4.05355	-12.77	-12.77			
							<b>Mean PTIMS TB</b>	<b>-12.39</b>	<b>0.54</b>
<b>TB</b>	K <sub>2</sub> CO <sub>3</sub> 1	3.96752		4.01592	-12.05	-12.05			
NTIMS	K <sub>2</sub> CO <sub>3</sub> 2	3.96302		4.01541	-13.05				
		3.96025		4.01533	-13.72	-13.38	0.47		
							<b>Mean NTIMS TB</b>	<b>-12.72</b>	<b>0.94</b>
					<b>Mean (PTIMS and NTIMS) TB</b>	<b>-12.56</b>	<b>0.65</b>		
<b>MPI-DING:</b>									
<b>GOR-128-G</b>	K <sub>2</sub> CO <sub>3</sub>	4.10916	0.00090	4.05335	13.77				
PTIMS	HF	4.10838	0.00128	4.05476	13.22				
		4.10915	0.00071	4.05464	13.44	13.48	0.27		
		4.10895	0.00157	4.05371	13.63	13.63			
							<b>Mean GOR-128-G</b>	<b>13.55</b>	<b>0.11</b>
<b>GOR-132-G</b>	K <sub>2</sub> CO <sub>3</sub>	4.08369	0.00098	4.05335	7.49				
PTIMS		4.08427	0.00049	4.05476	7.28				
		4.08125	0.00101	4.05464	6.56	7.11	0.48		
							<b>Mean GOR-132-G</b>	<b>7.11</b>	<b>0.48</b>
<b>StHs6/80-G</b>	K <sub>2</sub> CO <sub>3</sub>	4.03618	0.00054	4.05476	-4.58				
PTIMS		4.03700	0.00072	4.05476	-4.38	-4.48	0.14		
							<b>Mean StHs6/80-G</b>	<b>-4.48</b>	<b>0.14</b>

All reported PTIMS data show an in-run precision typically better than 0.00157 2RSD mean (0.38 ‰) calculated over the number of blocks, which is in the same range as for unprocessed NIST SRM 951 (Figure 2; Appendix 1). Repeated  $\text{Cs}_2\text{BO}_2^+$ -measurements of several aliquots of an isotopically homogeneous samples of one chemical preparation replicate within 0.53 ‰ for PTIMS (1SD; Table 4). The overall external uncertainty including several individual chemical preparations with both procedures (“ $\text{K}_2\text{CO}_3$  chemistry and HF chemistry”) is calculated to be smaller than 0.54 ‰ (1SD; Table 4) and ranges from 0.11 to 0.54 ‰ (Table 4). This demonstrates, that replicate measurements of several aliquots of one sample preparation leads to the same uncertainty as is calculated from the mean values of individual preparations. Therefore, we conclude that sample loading and TIMS-measurements represent significant limitations on the overall precision of  $\text{Cs}_2\text{BO}_2^+$ -measurements of silicate materials in this study.

Compared to our results, *Tonarini et al.* [2001] and *Gonfiantini et al.* [in prep.] reported an external reproducibility between 0.07 - 0.52 ‰ and 0.12 - 0.74 ‰ (1RSD), respectively, calculated from two or more individual sample preparations. However, the intercomparison study of *Gonfiantini et al.* [in prep.] indicates a remarkable difference between the mean  $\delta^{11}\text{B}$  values carried out by different laboratories of up to 3.8 ‰, which demonstrates the general analytical limit of this method for silicate materials. This offset is most likely due to a relative shift of the zero scale and/or B-isotope fractionation during sample preparation.

In addition to the  $\delta^{11}\text{B}$  values obtained mainly by the  $\text{Cs}_2\text{BO}_2^+$ -graphite method, we obtained a  $\delta^{11}\text{B}$  value determined by the  $\text{BO}_2^-$  method for TB (Table 4). The reproducibility of  $\delta^{11}\text{B}$  values within measurements of an individual preparation and within mean  $\delta^{11}\text{B}$  values of several preparations are slightly higher than those of the  $\text{Cs}_2\text{BO}_2^+$ -graphite method. However, the mean  $\delta^{11}\text{B}$  value of -12.7 ‰ of the TB obtained by NTIMS overlap well within the analytical uncertainty with the PTIMS value of -12.4 ‰ and in principle demonstrates that no systematic offset between different mass spectrometry methods exists [e.g., *Kasemann et al.*, 2001; *Gonfiantini et al.*, in prep.].

In order to evaluate the possible influence of the different sample preparation procedures (“ $\text{K}_2\text{CO}_3$  chemistry and HF chemistry”) we additionally use the dataset of CHAPTER III (Appendix 2) carried out exactly following the same sample preparation procedures reported here.

Figure 2 compares mean  $\delta^{11}\text{B}$  values obtained after “ $\text{K}_2\text{CO}_3$  chemistry” with mean  $\delta^{11}\text{B}$  values obtained after “HF chemistry”.

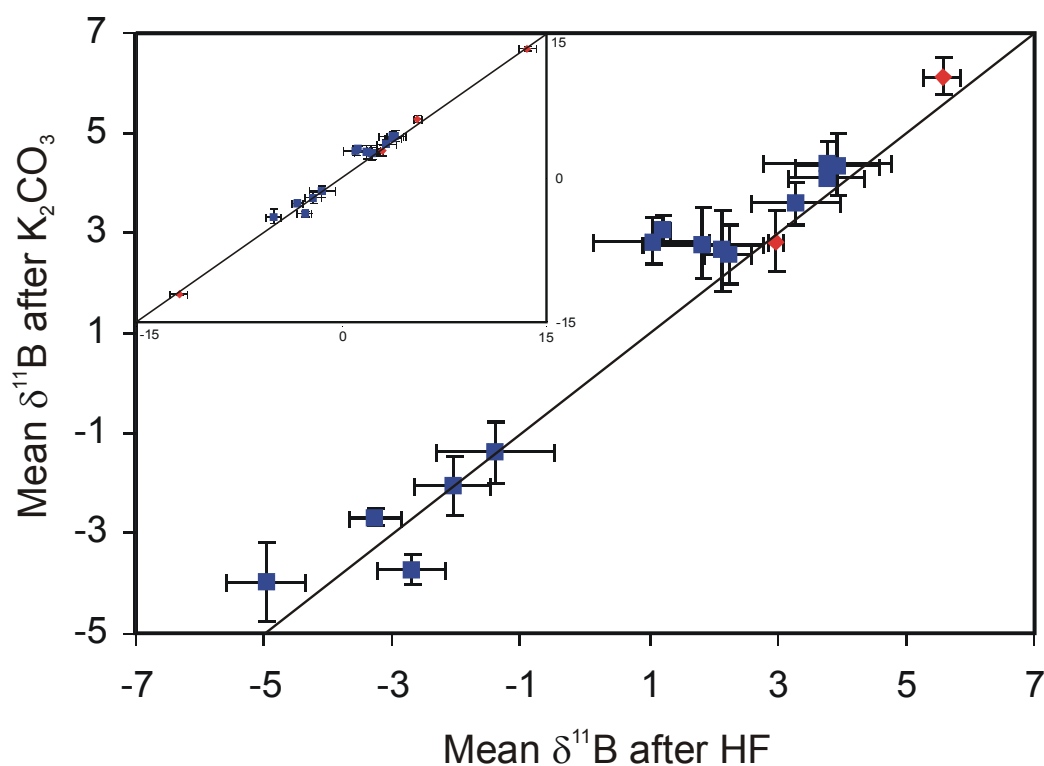


**Figure 2:** Comparison of  $\delta^{11}\text{B}$  values obtained after “ $\text{K}_2\text{CO}_3$  or HF chemistry”; red squares indicate data from this study and blue squares from CHAPTER III; error bars indicate the calculated 1SD external reproducibility of the mean  $\delta^{11}\text{B}$  values (Table 4; Appendix 2).

Eleven of 18 samples plot within their calculated individual external reproducibility (1SD; Table 4; Appendix 2) on the 1 : 1 correlation line. However, the HF data show a small but visible systematic offset towards lower  $\delta^{11}\text{B}$  values relative to the  $\text{K}_2\text{CO}_3$  data. We suggest that the reason for this offset could be mass dependent fractionation of  $\text{Cs}_2^{10}\text{BO}_2^+$  and  $\text{Cs}_2^{11}\text{BO}_2^+$  on the filament as a result of relatively high ionisation currents, which are in general higher for samples treated with HF than is the case for those treated with  $\text{K}_2\text{CO}_3$ . Nevertheless, this offset is minor, because with the exception of only three samples all other  $\delta^{11}\text{B}$  values overlap within a maximum analytical uncertainty of 1 ‰ (see section III.4 in CHAPTER III) with the 1 : 1 correlation line.

## II.5 Conclusions and recommended values

The B-isotope compositions and B concentrations presented here contribute towards establishing well characterised reference materials for geochemical bulk and in-situ analysis. Table 5 presents our final B concentrations  $\delta^{11}\text{B}$  values and compares them with published data.

**Table 5:** Comparison of our recommended B concentrations and  $\delta^{11}\text{B}$  values with published data. Note  $\delta^{11}\text{B}$  of TB is the mean of the PTIMS and NTIMS data.

Sample	B [ $\mu\text{g g}^{-1}$ ] ( $\pm 1\text{SD}$ )	B [ $\mu\text{g g}^{-1}$ ] Literature	$\delta^{11}\text{B}$ mean	1 RSD [%]	$\delta^{11}\text{B}$ runs Range	$\delta^{11}\text{B}$ Literature
<b>JB-3</b>	20.0 ( $\pm 2.0$ )	18.0 ( $\pm 3.1$ ) <sup>a</sup>	5.85	0.40	5.38 - 6.39	6.5 - 6.7 ( $\pm 0.2$ ) <sup>d</sup>
<b>JA-1</b>			5.30	0.17	5.18 - 5.42	5.4 ( $\pm 0.20$ ) <sup>e</sup>
<b>JA-3</b>	26.8 ( $\pm 1.0$ )	24.8 ( $\pm 2.9$ ) <sup>a</sup>				
<b>JR-1</b>	134.1 ( $\pm 3.7$ )	117 ( $\pm 34$ ) <sup>a</sup>				
<b>JR-2</b>	158.6 ( $\pm 5.7$ )	145 ( $\pm 8.6$ ) <sup>a</sup>	2.93	0.12	2.69 - 3.44	2.9 ( $\pm 0.48$ ) <sup>f</sup>
<b>TB</b>	88.1 ( $\pm 4.5$ )	90 <sup>b</sup>	-12.56	0.65	-12.01 - -13.72	
<b>TS</b>	68.1 ( $\pm 2.9$ )	74 <sup>b</sup>				
<b>GOR-128-G</b>	22.7	21.8 <sup>c</sup>	13.55	0.11	13.22 - 13.77	
<b>GOR-132-G</b>	15.6	17.8	7.11	0.48	6.56 - 7.49	
<b>StHs6/80-G</b>	11.6	12.5	-4.48	0.14	-4.38 - -4.58	

<sup>a</sup> Imai et al. [1995]; <sup>b</sup> Gonvindaraju [1994]; <sup>c</sup> Jochum et al. [2000]

<sup>d</sup> Ishikawa and Nakamura [1994]; Ishikawa et al. [1997], [1999], [2001];

<sup>e</sup> Ishikawa and Nakamura [1994]; <sup>f</sup> Kasemann et al. [2001]

The obtained B concentrations range from 7 to 159  $\mu\text{g g}^{-1}$  (Table 5). The majority of the mean values are reproducible within 5 % (1RSD) and overlap within 14 % published values.

The obtained mean  $\delta^{11}\text{B}$  values cover a range of -12.6 to 13.6 ‰. Replicate analyses of individually proceeded silicate materials yield an overall external reproducibility of the whole analytical procedure of better than 0.7 ‰ (1RSD). This is an acceptable value for most applications in earth sciences with respect to the wide range of  $\delta^{11}\text{B}$  values in terrestrial rocks. The  $\delta^{11}\text{B}$  values of JA-1 (+5.3 ‰) and JR-2 (+2.9 ‰) are in excellent agreement with the data published from Ishikawa and Nakamura [1994] and Kasemann et al., [2001], respectively (Table 5). Our  $\delta^{11}\text{B}$  value of JB-3 (+5.8 ‰), however, shows slight difference of 0.65 ‰ to published values [Ishikawa and Nakamura, 1994; Ishikawa et al., 1997, 1999, 2001], nevertheless both mean values overlap within the maximum analytical uncertainty of 0.7 ‰. First  $\delta^{11}\text{B}$  values were obtained for TB (-12.6 ‰) and the MPI-DING glasses GOR-128-G (+13.6 ‰), GOR-132-G (+7.1 ‰) and StHs6/80-G (-4.5 ‰).



Because  $\delta^{11}\text{B}$  values obtained by two different mass spectrometric and sample preparation methods overlap within their analytical uncertainties, we conclude that these different methods introduces no systematic bias into the calculated  $\delta^{11}\text{B}$  values.

In summary, the good agreement of our GSJ data with published data along with the agreement of  $\delta^{11}\text{B}$  values obtained by both mass spectrometric methods reflects the good accuracy of the data presented here and confirms the accuracy of  $\delta^{11}\text{B}$  values for the MPI-DING glasses and the TB, which were first characterised in terms of their B-isotope composition.

## CHAPTER III

### **Slab-derived boron isotope signatures in arc volcanic rocks from the Central Andes and evidence for boron isotope fractionation during progressive slab dehydration**

Submitted to: *Geochemistry Geophysics Geosystems (G<sup>3</sup>)* (under review)

#### **III Abstract**

Late Miocene to Quaternary volcanic rocks from the frontal arc to the back-arc region of the Central Volcanic Zone in the Andes show a wide range of  $\delta^{11}\text{B}$  values (+4 to -7 ‰) and boron concentrations (6 to 60 ppm). Positive  $\delta^{11}\text{B}$  values of samples from the volcanic front indicate involvement of a  $^{11}\text{B}$ -enriched slab component, most likely derived from altered oceanic crust, despite the thick Andean continental lithosphere, and rule out a pure crust-mantle origin for these lavas. The  $\delta^{11}\text{B}$  values and B concentrations in the lavas decrease systematically with increasing depth of the Wadati-Benioff Zone. This across-arc variation in  $\delta^{11}\text{B}$  values and decreasing B/Nb ratios from the arc to the back-arc samples are attributed to the combined effects of B-isotope fractionation during progressive dehydration in the slab and a steady decrease in slab-fluid flux towards the back arc, coupled with a relatively constant degree of crustal contamination as indicated by similar Sr, Nd and Pb isotope ratios in all samples.

Modelling of fluid-mineral B-isotope fractionation as a function of temperature fits the across-arc variation in  $\delta^{11}\text{B}$  and we conclude that the B-isotope composition of arc volcanics is dominated by changing  $\delta^{11}\text{B}$  composition of B-rich slab-fluids during progressive dehydration. Crustal contamination becomes more important towards the back-arc due to the decrease in slab-derived fluid flux. Because of this isotope fractionation effect, high  $\delta^{11}\text{B}$  signatures in volcanic arcs need not necessarily reflect differences in the initial composition of the subducting slab.

Three-component mixing calculations for slab-derived fluid, the mantle wedge and the continental crust based on B, Sr and Nd isotope data indicate that the slab-fluid component dominates the B composition of the fertile mantle and that the primary arc magmas were contaminated by an average addition of 15 to 30 % crustal material.

### III.1 Introduction

The creation and recycling of oceanic lithosphere is one of the main exchange processes between the mantle and crust, and the formation of volcanic arcs in subduction settings is an important part of this system. During the past two decades several studies have shown that B can be an excellent tracer for mass transfer in subduction settings due to its mobility in aqueous fluids and its incompatible behavior in most magmatic processes [e.g., *Morris et al.*, 1990; *Bebout et al.*, 1999]. Also, the upper altered oceanic crust (AOC) shows a characteristic B-isotope composition which differs from the other major source reservoirs involved in magma genesis at arcs (subducted sediments, mantle peridotite and continental crust).

Previous studies of B-isotopes in arc magmas have dealt with ocean island settings where the complicating factor of continental crust contamination of primary magmas is avoided. This paper presents an application of B-isotope geochemistry to the study of continental arc volcanism in the Central Andes, where the continental lithosphere is particularly thick and where crustal contamination is a well-established feature of the magmas. The aim is to characterise the processes controlling the B-isotope signatures of continental arc volcanic rocks and, in combination with radiogenic isotopes (Sr, Nd, Pb), to model the contributions of the endmember reservoirs involved.

### III.2 Geological setting

The study area centers on the Neogene volcanic arc in the southern part of the Central Volcanic Zone (CVZ, 22° - 27° S) at the western margin of the Altiplano-Puna Plateau (Fig. 1). Subduction of the Nazca Plate under the South American continent has been active in this region since the Jurassic and has produced a series of successively younger volcanic arcs extending from the Jurassic arc at the coast to the Neogene and Quaternary arc in the Western Cordillera [*Coira et al.*, 1982; *Scheuber et al.*, 1994]. At present, Eocene oceanic crust (50 Ma) is being subducted beneath the margin. The Wadati-Benioff Zone (WBZ) images the Nazca plate to depths between 200 and 600 km [*Cahill and Isacks*, 1992; *The ANCORP Working Group*, 1999]. In the southern Central Andes, the dip of the down-going plate increases from about 15° near the coast to 20° - 25° in 60 - 100 km depths beneath the volcanic arc and then steepens further to 30° - 35° at greater depths (Figs. 1 and 2).

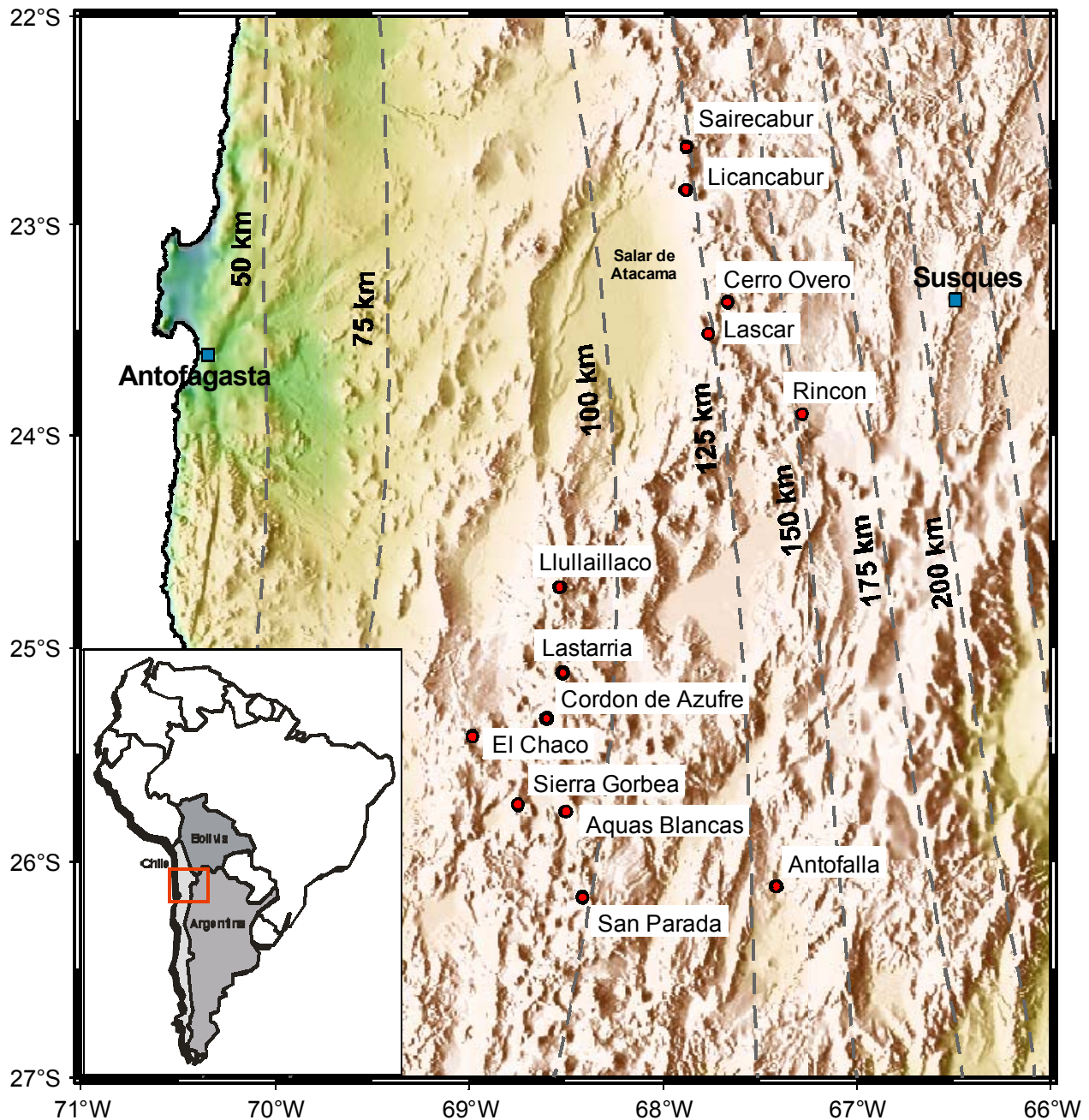


**Figure 1:** Topographic map of the study area (green: low elevations, brown: high) showing the locations of volcanoes studied (circles) and depth contours to the Wadati-Benioff Zone (from Cahill and Isacks, [1992]). Inset shows regional location of the study area.

The Central Andes orogen contains the world's second-largest continental plateau after Tibet and a 60 - 80 km thick continental crust. Tectonic shortening is the main process leading to the thickened crust, and the main phase of thickening was in the middle-Miocene [Allmendinger *et al.*, 1997]. Another factor suggested for uplift of the Altiplano-Puna plateau is the thermal effect of thinning or detachment of lithospheric mantle in the back arc [Kay *et al.*, 1994; Allmendinger *et al.*, 1997; Yuan *et al.*, 2002]. The Pre-Mesozoic basement of the

Central Andes was consolidated in the Paleozoic and is dominated by felsic metasedimentary rocks and granites derived from them [Coira *et al.*, 1982; Lucassen *et al.*, 2000]. Good coverage of geochemical and radiogenic isotope data from the basement rocks in our study area is available from Lucassen *et al.* [1999; 2000; 2001], and B-concentrations and B-isotope ratios of the metamorphic and igneous basement are discussed by Kasemann *et al.* [2000].

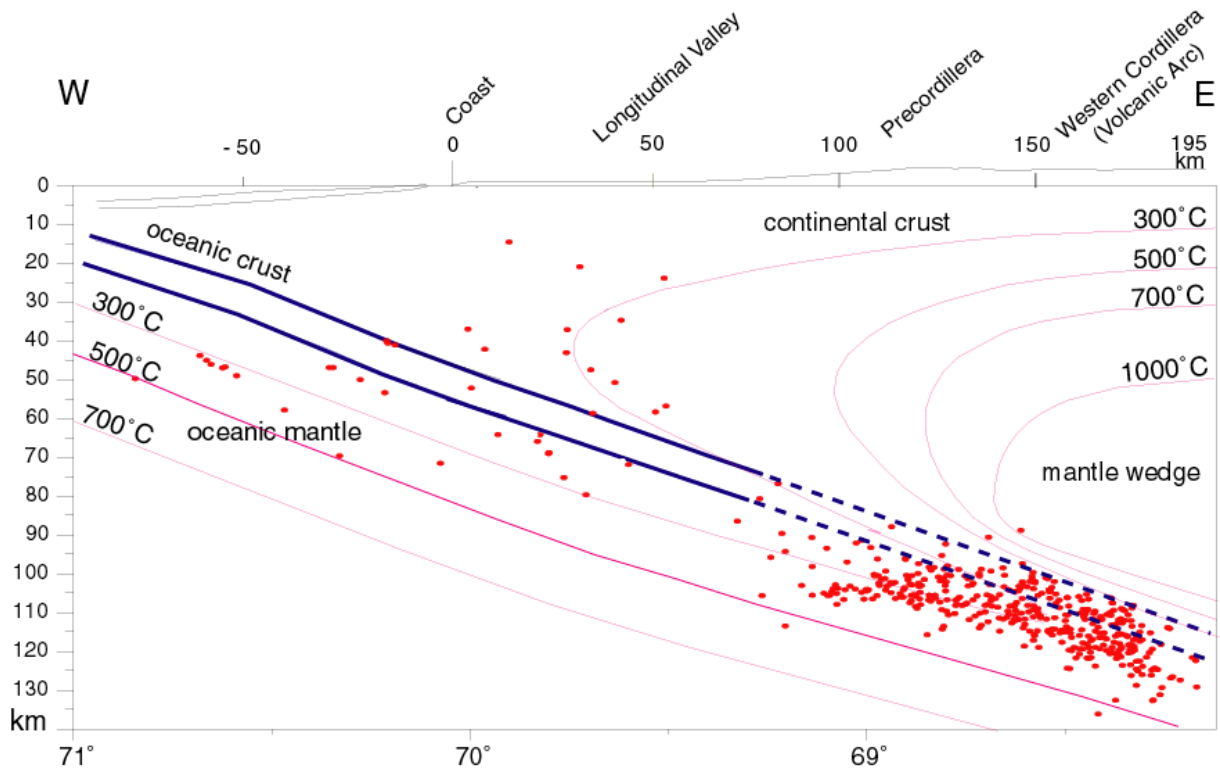


**Figure 2:** Interpretative cross section of the Central Andes subduction zone at 21° S after *The ANCORP Working Group* [1999] with temperature model of *Springer* [1999] and distribution of earth quake epicenters (red dots).

Subduction related volcanism in the southern CVZ was active from the early Miocene to the Quaternary and involved three main associations: composite stratovolcanoes of andesitic to dacitic composition that make up the frontal arc in the western Cordillera, large-volume rhyodacitic ignimbrites erupted from caldera complexes in and behind the arc, and small basaltic centers in the back arc region [Coira *et al.*, 1982; Allmendinger *et al.*, 1997]. Studies of the Quaternary stratovolcanoes in the CVZ have documented a high degree of crustal contamination in the andesites [*e.g.*, Davidson *et al.*, 1990; 1991; Feeley and Davidson, 1994] and it has also been shown that the degree of crustal contamination in arc andesites increased with time from the early Miocene to the Quaternary [Walker *et al.*, 1991; Kay *et al.*, 1994; Trumbull *et al.*, 1999]. Estimates of the proportion of crustal material in the CVZ andesites

range between 12 and 30 % [Kay *et al.*, 1994; Aitchison and Forrest, 1994; Trumbull *et al.*, 1999; Bourdon *et al.*, 2000].

The thickness of detrital trench sediments has been very low in this section of the Andes since at least the last 7 Ma because of the arid climate and internal drainage of the Altiplano-Puna plateau, and therefore detrital sediment subduction is not likely to have an important influence on the composition of CVZ arc magmas [*cf.* Bourdon *et al.*, 2000]. Subduction erosion of the continental forearc is thought to play an important role in the Central Andes and this could potentially introduce crustal material into the subduction zone [Stern, 1991; Kay and Abruzzi, 1996] although it is not clear that this material will reach sub-arc depths. Adam and Reuther [2000] suggested that much of the eroded material underplates the margin in 20 to 30 km depths, and is the reason for uplift in the Coastal Cordillera.

### III.3 Boron behavior in subduction zone processes

It is generally accepted that primary arc magmas at most subduction settings are generated by partial melting of the asthenospheric mantle wedge whose solidus temperature is reduced by influx of hydrous fluids released from the subducted slab [e.g., Gill, 1981; Tatsumi and Eggins, 1995]. Slab-derived fluids are also important for transporting fluid-mobile elements into the mantle wedge, and are thought to be responsible for the "subduction component" that distinguishes most arc magmas from MORB and other mantle-derived magmas [e.g., Hawkesworth *et al.*, 1993; Pearce and Peate, 1995]. In detail, the processes affecting the generation and composition of arc magmas depend on convergence parameters and the thermal structure of the subduction zone. Peacock [1996] presented thermal models of subduction zones for different convergence parameters and ages of the lower plate, and showed that temperatures at the slab-mantle interface can vary between 300° and 1250° C. For most settings, however, temperatures are insufficient to cause melting in the down-going slab. The Central Andean subduction zone in particular is expected to be rather cold because of the Eocene age of the subducting Nazca plate, the relatively rapid convergence rate and the low subduction angle of about 20° - 30°. A geophysical model for the Central Andes subduction zone by The ANCORP Working Group [1999] predicted temperatures of about 400° C at the slab-mantle interface below the volcanic front (Fig. 2). Therefore, we can expect that hydrous fluids are responsible for transport of slab-derived components into the mantle

under the CVZ and B is one of the elements most effectively and readily mobilised by this process.

An important issue relating to the release of B and other fluid-mobile elements from the subducting slab is whether dehydration is a continuous process governed by sliding reactions or is more punctuated due to breakdown of hydrous phases in narrow p - T intervals. *Kerrick and Connolly* [2001] calculated the metamorphic reactions of subducting average oceanic metabasalt with an initial content of 2.5 wt. % H<sub>2</sub>O. They showed that the devolatilization behavior is strongly dependent on the thermal structure of subduction zones. For the low to intermediate temperature conditions of the Central Andes setting, metabasalt can be expected to dehydrate progressively over the interval of subduction depth covered by our study (88 to 152 km below the arc), and therefore slab-derived B should be added to the mantle wedge under the entire area sampled.

Most existing studies of B systematics in island arcs report much higher B concentrations in the volcanic rocks than in MORB and high ratios of B over fluid-immobile elements (e.g. B/Nb), which suggest that slab-derived B is responsible for the B enrichment. Positive  $\delta^{11}\text{B}$  values from the Izu- [*Ishikawa and Nakamura, 1994*], the Kurile- [*Ishikawa and Tera, 1997*], the Lesser Antilles- [*Smith et al., 1997*], the Mariana- [*Ishikawa and Tera, 1999*] and Kamchatka arc [*Ishikawa et al., 2001*] were interpreted to reflect the influence of  $^{11}\text{B}$ -enriched altered oceanic crust in the slab-fluid. Furthermore, systematic across-arc variations of  $\delta^{11}\text{B}$  were discovered for the Izu-, Kurile- and Kamchatka arcs, and these were attributed to a changing proportion of slab-derived B from progressive slab dehydration relative to a constant mantle contribution [*Ishikawa and Nakamura, 1994; Ishikawa and Tera, 1997; Ishikawa et al., 2001*].

A main point of discussion in this paper will be that dehydration reactions in the slab can also cause significant fractionation of B-isotopes between aqueous fluids and residual minerals, particularly at low to medium temperatures. In principle, fractionation occurs because of differences in B-coordination, with  $^{11}\text{B}$  preferentially entering the trigonal B-complexes in the expelled fluid and  $^{10}\text{B}$  being enriched in the restite [*cf. Peacock and Hervig, 1999*]. Experimental investigations [*Oi et al., 1989; Williams et al., 2001 a and b*] and the B-isotope compositions of subduction-zone metamorphic rocks [*Peacock and Hervig, 1999*] suggest that the fractionation effect may be significant. Once the slab-derived B enters silicate melt, no significant further change in its isotopic composition is expected because of the high temperatures involved [*Ishikawa and Tera, 1997*]. New experimental determinations of B-isotope partitioning between hydrous fluid and silicate melt at 550° to 1100° C by

*Hervig et al.* [2002] showed B-isotope fractionation of up to about 3 ‰. Thus for igneous processes in the mantle wedge or within the crust, fractionation effects on the B-isotope composition are small and the isotopic composition of slab-derived B can be expected to survive incorporation into arc magmas.

#### III.4 Samples and analytical methods

The samples analysed in this study represent 13 volcanic centers located between 22° and 27° S over a total across-arc distance of about 180 km from west to east, which corresponds to a range of depths to the subducted slab of 88 to 152 km (Table 1, Fig. 1). There are two depth clusters of sampled volcanoes above the WBZ, one at ~93 km and the other at ~128 km and one sample from 152 km. Geological and geochronological informations on the individual centers are given in earlier works [*de Silva and Francis*, 1991; *Naranjo and Cornejo*, 1992; *Matthews et al.*, 1994; *Trumbull et al.*, 1999]. Nine of the volcanoes sampled are Quaternary in age, three are from between 5 and 8 Ma. Except for the 16 Ma old El Chaco lava, all magmas erupted after the mid-Miocene phase of crustal thickening and plateau uplift and under conditions of subduction similar to the present setting. Most samples have previously been well-characterized petrographically and geochemically [*Trumbull et al.*, 1999] and they can be considered to be representative for the typical range of CVZ arc magmas. Chemical compositions are reported in Table 1 and isotope ratios in Table 2. A more complete data set with additional main and trace element data is available in Appendix 3.

The B concentrations were determined by inductively coupled plasma optical emission spectrometry (ICP-OES) on a Varian Liberty 200 using a procedure described by *Kasemann et al.* [2001]. The long term reproducibility of the total procedure is generally better than 6 % and for reference basalt JB-2 measured over three years the reproducibility was 5.4 % (RSD) [*Kasemann et al.*, 2001]. Accuracy was tested against international reference materials (JB-2, JR-2) and was generally better than 10 % [*Kasemann et al.*, 2001].

B-isotope analyses were made on a Finnigan MAT 262 mass spectrometer equipped with a special double Faraday collector [*e.g.*, *Nakano and Nakamura*, 1998] using the  $\text{Cs}_2\text{BO}_2^+$ -graphite method modified after *Nakamura et al.* [1992] and *Tonarini et al.* [1997]. Eighty-three separate analyses of NIST 951 made over a period of 26 months yielded a mean  $^{11}\text{B}/^{10}\text{B}$  ratio of 4.05416, reproducible within 0.19 ‰ (RSD). External reproducibility of samples was



determined by replicate analyses of each sample using two different dissolution and separation procedures (after HF attack and K<sub>2</sub>CO<sub>3</sub> fusion) and was typically better than 0.7 ‰ (RSD), excluding sample LAST-RW3. We assume a maximum overall analytical uncertainty between 0.7 and 1.0 ‰ based on the repeated preparations of all samples, similar to the estimate of 0.8 ‰ (RSD) by *Kasemann et al.* [2001]. The procedural blank decreased during the course of the study from about 200 ng B to less than 30 ng B, which is between 6.5 % and 1 % relative to the 3 µg B typically used for ion exchange chromatography. The blank effect of 30 ng B is negligible, whereas 200 ng B causes a δ<sup>11</sup>B shift of about 0.4 ‰ if the δ<sup>11</sup>B value of the blank is 20 ‰ different from the sample. Note that a 0.4 ‰ shift is within the estimated overall analytical uncertainty. B-isotope ratios are reported as δ<sup>11</sup>B values relative to the concurrently measured NIST 951 standard ( $\delta^{11}\text{B} = [\{^{11}\text{B}/^{10}\text{B}\}_{\text{sample}} / \{^{11}\text{B}/^{10}\text{B}\}_{\text{standard}} - 1] * 1000$ ). The accuracy of the whole procedure for silicate rocks was checked by repeated analysis of individually prepared sample aliquots of basaltic reference material JB-2. The δ<sup>11</sup>B value of 7.14 ‰ for JB-2 (± 0.77 ‰ RSD; PTIMS) reported in *Kasemann et al.* [2001] and obtained in the course of this study is in excellent agreement with published values of 7.08 ‰ [*Nakamura et al.*, 1992], 7.23 ‰ [*Tonarini et al.*, 1997] and 6.85 ‰ [*Deyhle*, 2001].

The Sr, Nd and Pb isotopic analyses followed standard cation and anion resin ion exchange techniques described in *Romer et al.* [2001]. Strontium isotope composition was measured on a VG SECTOR 54-30 mass spectrometer and Nd and Pb isotope analyses were made with a Finnigan MAT 262 mass spectrometer. Concurrently measured international standards yielded mean values for SRM 987 (<sup>87</sup>Sr/<sup>86</sup>Sr) and La Jolla (<sup>143</sup>Nd/<sup>144</sup>Nd) of 0.710267 ± 25 (2σ external reproducibility, n = 24) and 0.511849 ± 9 (2σ external reproducibility, n = 22), respectively. The Pb isotope ratios were corrected for instrumental mass fractionation with a factor of 1 ‰ per mass unit using NBS 981 as reference. External reproducibility of NBS 981 was better than 1 ‰ during the course of the study.

Analysis of major elements were made by X-ray fluorescence on a Siemens ASR303AS spectrometer after fusion of sample powders with lithium tetraborate. Trace element analyses (Li, V, Cr, Co, Ni, Cu, Ga, Rb, Sr, Zr, Nb, Sb, Cs, Hf, Ta, W, Tl, Pb, Bi, Th and U) were performed by ICP-MS on a VG Plasma Quad PQ+ spectrometer following sample dissolution in HF-HNO<sub>3</sub> acid mixture [*Jochum et al.*, 2000]. Rare earth elements, Y and Sc were measured on a ICP-OES Varian Liberty 200 after a Na<sub>2</sub>O<sub>2</sub>-sinter dissolution [*Zuleger and Erzinger*, 1988].

### III.5 Results

The element compositions and isotope ratios determined in this study are listed in Tables 1 and 2. Our samples represent calc-alkaline medium- to high-K basaltic andesites to dacites (Fig. 3 a) whose compositions are typical for most Quaternary volcanic centers from the CVZ [e.g., *Davidson et al*, 1991]. Trace element concentrations normalized to primitive mantle (Fig. 3 b) show typical arc-related patterns [e.g., *Gill*, 1981; *Hawkesworth et al.*, 1993] with high values of large ion lithophile elements (Cs, Rb and Pb; in some samples U and Th) and low Nb, P and Ti concentrations. It is beyond the scope of this paper to discuss features of the major and trace element geochemistry of these samples in detail. Instead, we focus on B concentrations and isotope composition, and on those elements or isotope ratios relevant to interpretation of the B data.

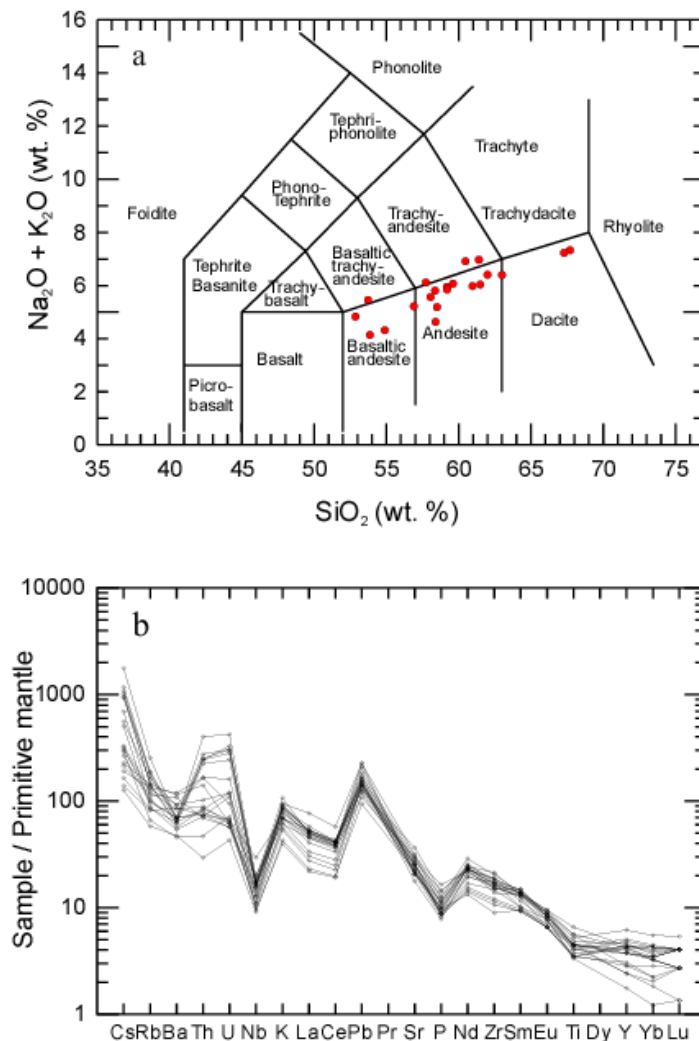


**Figure 3:** Whole-rock composition of samples investigated in (a) total alkalis vs. silica classification diagram and (b) primitive mantle-normalized trace element diagram (normalized values after Sun and McDonough, 1989).

**Table 1:** Elemental analyses for arc-volcanics of the CVZ in the Andes

Sample	Locality	SiO <sub>2</sub> [%]	K <sub>2</sub> O [%]	Na <sub>2</sub> O [%]	B [ppm]	Sr [ppm]	Nb [ppm]	Nd [ppm]	Pb [ppm]
CDA-2-21	Cordon de Azufre	58.4 <sup>a</sup>	2.40 <sup>a</sup>	3.41 <sup>a</sup>	54	492 <sup>a</sup>	11.6 <sup>a</sup>	32 <sup>a</sup>	10.8 <sup>a</sup>
CDA 1-4	Cordon de Azufre	58.1 <sup>a</sup>	2.32 <sup>a</sup>	3.25 <sup>a</sup>	49	539 <sup>a</sup>	11.1 <sup>a</sup>	31 <sup>a</sup>	9.0 <sup>a</sup>
LLUL-KH3	Llullaillacu	67.7	2.76	4.57	24	635	7.8	31	13.0
LLUL-RW-1	Llullaillacu	67.3	2.86	4.37	22	635	8.6		10.4
LAST-KH2	Lastarria	59.6	2.55	3.52	54	532	12.0	35	11.2
132-LAST RW 3	Lastarria	61.0 <sup>a</sup>	2.61 <sup>a</sup>	3.37 <sup>a</sup>	60	531 <sup>a</sup>	13.9 <sup>a</sup>	33 <sup>a</sup>	10.3 <sup>a</sup>
LIC-5/17	Licancabur	59.2	2.53	3.42	18	440	12.3	31	14.8
SAIR-2-3	Sairecapur	62.0	2.78	3.63	20	441	12.0	32	16.0
LASC-2-13	Lascar	58.4	1.62	3.01		432	7.2	20	10.1
LASC-2-15A	Lascar	58.5	1.69	3.50	14	464	9.0	21	11.0
OVER-2-10B	Cerro Overo	53.9	1.20	2.94	11	477	6.8	19	8.5
179-OVER-1-02	Cerro Overo	54.9 <sup>b</sup>	1.29 <sup>b</sup>	3.03 <sup>b</sup>	14	467 <sup>b</sup>	6.5 <sup>b</sup>	18 <sup>b</sup>	6.7 <sup>b</sup>
AN 01M	Salar de Antofalla	53.7	2.10	3.36	18	584	21.1	31	10.0
RIN 1	Ricon	52.9	1.84	2.99	10	628	14.2	30	7.7
CACO-94-1	El Chaco	61.5	2.15	3.89	32	557	10.0	26	12.0
TC-2-3	El Chaco	59.2 <sup>a</sup>	1.90 <sup>a</sup>	3.95 <sup>a</sup>	41	523 <sup>a</sup>	7.8 <sup>a</sup>	23 <sup>a</sup>	9.7 <sup>a</sup>
SAL-ZU-96H-7	Sierra Gorbea	56.9 <sup>a</sup>	2.10 <sup>a</sup>	3.12 <sup>a</sup>	53	439 <sup>a</sup>	12.0 <sup>a</sup>	27 <sup>a</sup>	10.0 <sup>a</sup>
SAL-ZU-96H-14	Sierra Gorbea	63.0 <sup>a</sup>	3.23 <sup>a</sup>	3.17 <sup>a</sup>	51	374 <sup>a</sup>	12.7 <sup>a</sup>	29 <sup>a</sup>	11.0 <sup>a</sup>
LAU-94-1	San Parada	60.5	2.61	4.30	18	594	9.0	33	12.0
AQUA-2-19	Aguas Blancas	57.7 <sup>a</sup>	2.06 <sup>a</sup>	4.05 <sup>a</sup>	13	775 <sup>a</sup>	11.1 <sup>a</sup>	33 <sup>a</sup>	9.0 <sup>a</sup>
AQUA-94-29A	Aguas Blancas	61.4	2.86	4.11	6	668	11.0	39	16.0

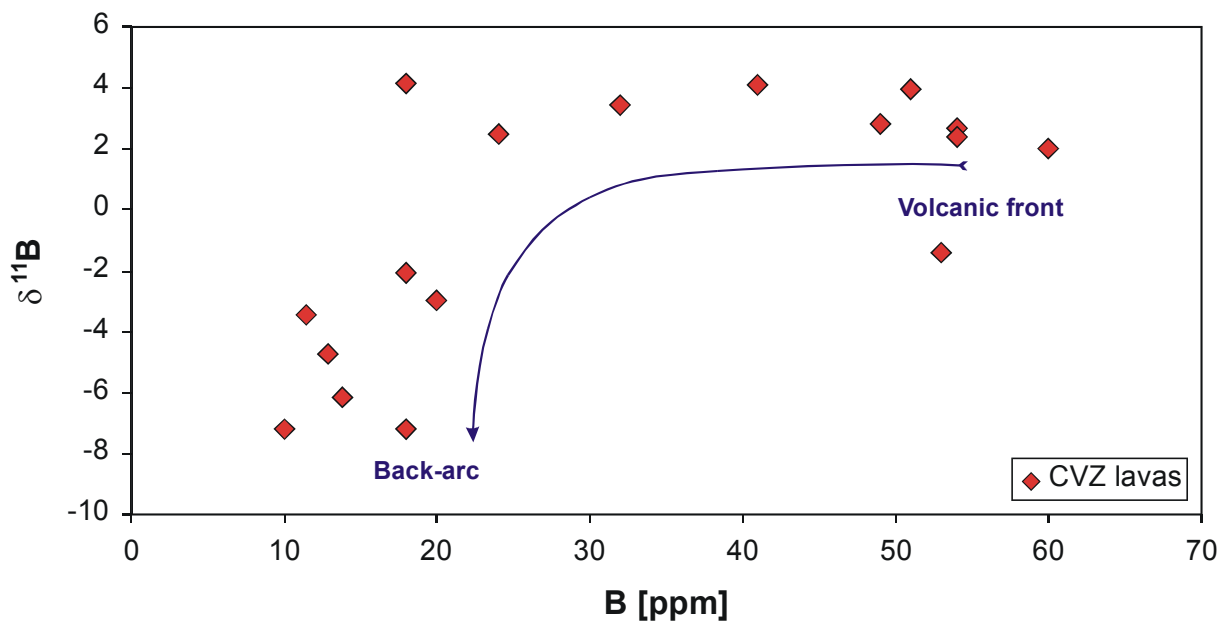
<sup>a</sup> Data from Trumbull et al. [1999]; <sup>b</sup> Data from Wittenbrink [1997]

Table 2: Isotope analyses for the arc-volcanics of the CVZ in the Andes

Sample	Depth WBZ	$\delta^{11}\text{B}$ ( $\pm 1\sigma$ )	$^{87}\text{Sr}/^{86}\text{Sr}$	$^{143}\text{Nd}/^{144}\text{Nd}$	$\epsilon_{\text{Nd}}$	$^{206}\text{Pb}/^{204}\text{Pb}$	$^{207}\text{Pb}/^{204}\text{Pb}$	$^{208}\text{Pb}/^{204}\text{Pb}$
CDA-2-21	93	2.7 ( $\pm 0.5$ )	0.706481	0.512429	-4.1	18.863	15.655	38.863
CDA 1-4	93	2.8 ( $\pm 0.5$ )	0.706514 <sup>a</sup>	0.512443 <sup>a</sup>	-3.8 <sup>a</sup>	18.807 <sup>a</sup>	15.628 <sup>a</sup>	38.748 <sup>a</sup>
LLUL-KH3	94	2.5 ( $\pm 0.7$ )	0.706653	0.512434	-4.0	18.759	15.650	38.787
LLUL-RW-1	94		0.706639	0.512424	-4.2	18.738	15.627	38.712
LAST-KH2	95	2.4 ( $\pm 0.2$ )	0.706915	0.512442	-3.8	18.813	15.585	38.632
132-LAST RW 3	95	2.0 ( $\pm 0.9$ )	0.706927 <sup>a</sup>	0.512450 <sup>a</sup>	-3.7 <sup>a</sup>	18.837 <sup>a</sup>	15.632 <sup>a</sup>	38.784 <sup>a</sup>
LIC-5/177	123	-2.1 ( $\pm 0.1$ )	0.707807	0.512284	-6.9	18.860	15.694	38.941
SAIR-2-3	123	-3.0 ( $\pm 0.4$ )	0.708107	0.512249	-7.6	18.870	15.684	38.931
LASC-2-13	127		0.706337	0.512423	-4.2	18.819	15.654	38.795
LASC-2-15A	127	-6.1 ( $\pm 0.1$ )	0.706438	0.512416	-4.3	18.817	15.657	38.803
OVER-2-10B	131	-3.5 ( $\pm 0.7$ )	0.706189	0.512463	-3.4	18.776	15.648	38.784
179-OVER-1-02	131		0.706240 <sup>b</sup>	0.512477 <sup>b</sup>	-3.1 <sup>b</sup>	18.788	15.663	38.838
AN 01M	132	-7.2 ( $\pm 0.2$ )	0.706269	0.512509	-2.5	18.781	15.612	38.663
RIN 1	152	-7.2 ( $\pm 0.1$ )	0.705981	0.512464	-3.4	18.887	15.665	39.054
CACO-94-1	88	3.4 ( $\pm 0.2$ )	0.706070	0.512481	-2.9	18.758	15.648	38.794
TC-2-3	88	4.1 ( $\pm 0.5$ )	0.706030 <sup>a</sup>	0.512471 <sup>a</sup>	-3.1 <sup>a</sup>	18.701 <sup>a</sup>	15.630 <sup>a</sup>	38.699 <sup>a</sup>
SAL-ZU-96H-7	92	-1.4 ( $\pm 0.1$ )	0.707020 <sup>a</sup>	0.512424 <sup>a</sup>	-4.1 <sup>a</sup>	18.810 <sup>a</sup>	15.634 <sup>a</sup>	38.762 <sup>a</sup>
SAL-ZU-96H-14	92	3.9 ( $\pm 0.2$ )	0.707250 <sup>a</sup>	0.512421 <sup>a</sup>	-4.1 <sup>a</sup>	18.803 <sup>a</sup>	15.635 <sup>a</sup>	38.752 <sup>a</sup>
LAU-94-1	92	4.2 ( $\pm 0.3$ )	0.706489	0.512428	-4.0	18.738	15.649	38.834
AQUA-2-19	96	-4.7 ( $\pm 0.3$ )	0.706420 <sup>a</sup>	0.512390 <sup>a</sup>	-4.7 <sup>a</sup>	18.746 <sup>a</sup>	15.623 <sup>a</sup>	38.699 <sup>a</sup>
AQUA-94-29A	96		0.707440	0.512389	-4.8	18.857	15.651	38.920

<sup>a</sup> Data from Trumbull et al. [1999]; <sup>b</sup> Data from Wittenbrink [1997]

The range of B concentrations in the samples is 6 to 60 ppm and their  $\delta^{11}\text{B}$  values vary between +4 and -7 ‰. There is a systematic relationship between B concentrations and  $\delta^{11}\text{B}$  ratios (Fig. 4) in that the samples with B contents greater than 25 ppm generally have higher  $\delta^{11}\text{B}$  values (> +2 ‰; except SALZU-96H-7) than those with lower B contents (< -2 ‰; except LAU-94-1). Correlations between the concentrations of B and other elements in the rocks are generally poor. To test for homogeneity of  $\delta^{11}\text{B}$  values in the volcanic centers, we analysed samples from two separate lava flows in four of the localities (Table 2) and for three of these examples, the  $\delta^{11}\text{B}$  values from separate flows replicate within 0.7 ‰ whereas the two lavas sampled from the 5 Ma old Sierra Gorbea locality differ by 5.3 ‰. The reason for this variation is not clear but repeated analyses rule out analytical error. The two samples differ in  $\text{SiO}_2$  content and may represent different stages of fractionation but according to *Ishikawa and Tera* [1997] fractionation should not affect the  $\delta^{11}\text{B}$  values much. Different degrees of crustal contamination in the two samples is unlikely since this should also affect their radiogenic isotope ratios and trace element signatures but these vary only slightly (Tables 1 and 2).



**Figure 4:** Boron concentrations and  $\delta^{11}\text{B}$  values of the investigated Andean arc-volcanic rocks. Arrow highlights the relationship between  $\delta^{11}\text{B}$  values and boron concentrations depending to the depth of the Wadati-Benioff Zone.

The most significant feature of the B-isotope data is the close correlation of  $\delta^{11}\text{B}$  values with depth to the WBZ. The highest  $\delta^{11}\text{B}$  values are from the western volcanic front at WBZ

depths of 88 - 96 km (interpolated from depth contours of *Cahill and Isacks* [1992]) and  $\delta^{11}\text{B}$  values decrease systematically toward the back-arc where the WBZ depths reach 152 km (Fig. 5). Only two samples plot below the trend in Figure 5 (SAL-ZU-96H-7 and AQUA-2-19). Sample SAL-ZU-96H-7 is one of the two lava samples from the Sierra Gorbea locality which show an unexplained 5.3 ‰ difference in  $\delta^{11}\text{B}$  values. Note that the other Sierra Gorbea sample plots on the trend. Sample AQUA-2-19 is from the 8 Ma Aquas Blancas center. *Trumbull et al.* [1999] already pointed out the unusual composition of andesites from the Aquas Blancas center compared with other volcanoes of similar age and location (e.g., extremely high La/Yb ratios).

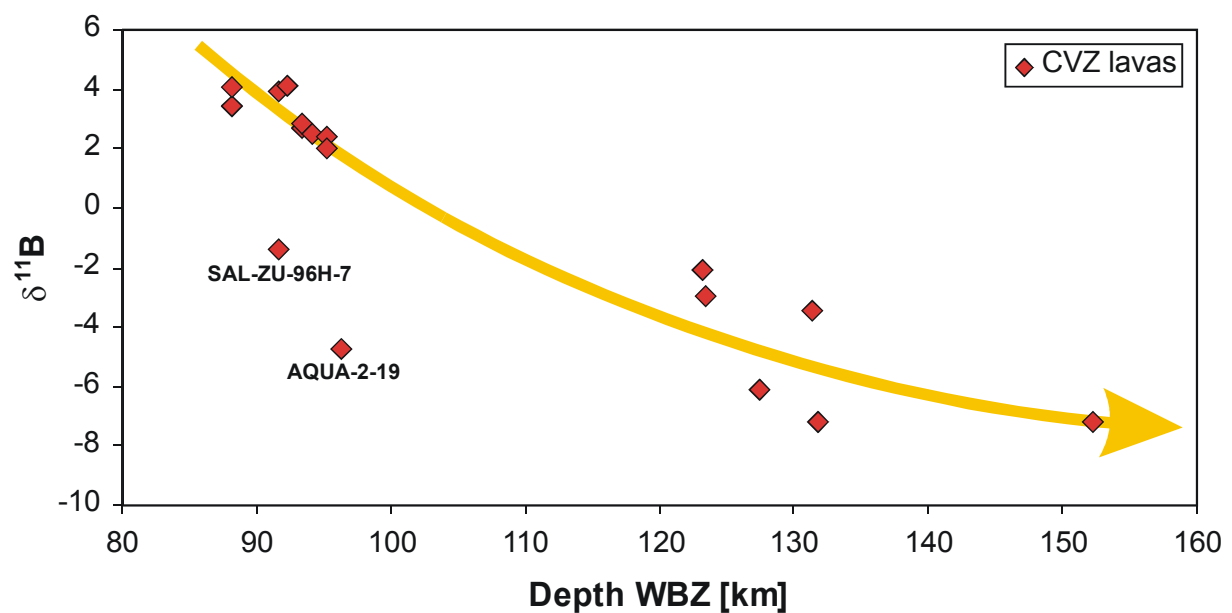


**Figure 5:** Variation of  $\delta^{11}\text{B}$  values of the investigated volcanic rocks with depth to the Wadati-Benioff Zone from *Cahill and Isacks* [1992]. Arrow highlights the  $\delta^{11}\text{B}$  across-arc variation.

The studied volcanic centers also cover a substantial N - S distance along the arc (Fig. 1). The along-arc variation in B-isotope composition, comparing volcanoes along a constant depth contour to the WBZ, is small relative to the across-arc difference. The variation for samples from the volcanic front (WBZ depths around 93 km) is about 2 ‰ excluding the two anomalous samples SAL-ZU-96H-7 and AQUA-2-19. Centers located farther east, at WBZ depths around 128 km, show about 5 ‰ variation N - S.

Commonly used indices for slab-derived elements in arc magmas are the ratio of fluid-mobile to immobile incompatible trace elements such as B/Nb or Pb/Nb. In our study, the B/Nb ratios are higher than the N-MORB value (0.14 after *Hofmann* [1988] and *Chaussidon and Marty* [1995]) as expected for arc settings (Fig. 6 a), and samples from the western volcanic front at shallow WBZ depth have higher B/Nb ratios than samples from farther east (again, with the exception of the Aquas Blancas samples). The Pb/Nb ratios are also higher than N-MORB values, but show no systematic changes across the arc and scatter between values of 0.5 and 1.7 (Fig. 6 b), which may reflect the dominance of crustal Pb in the samples as suggested by their Pb isotope ratios.

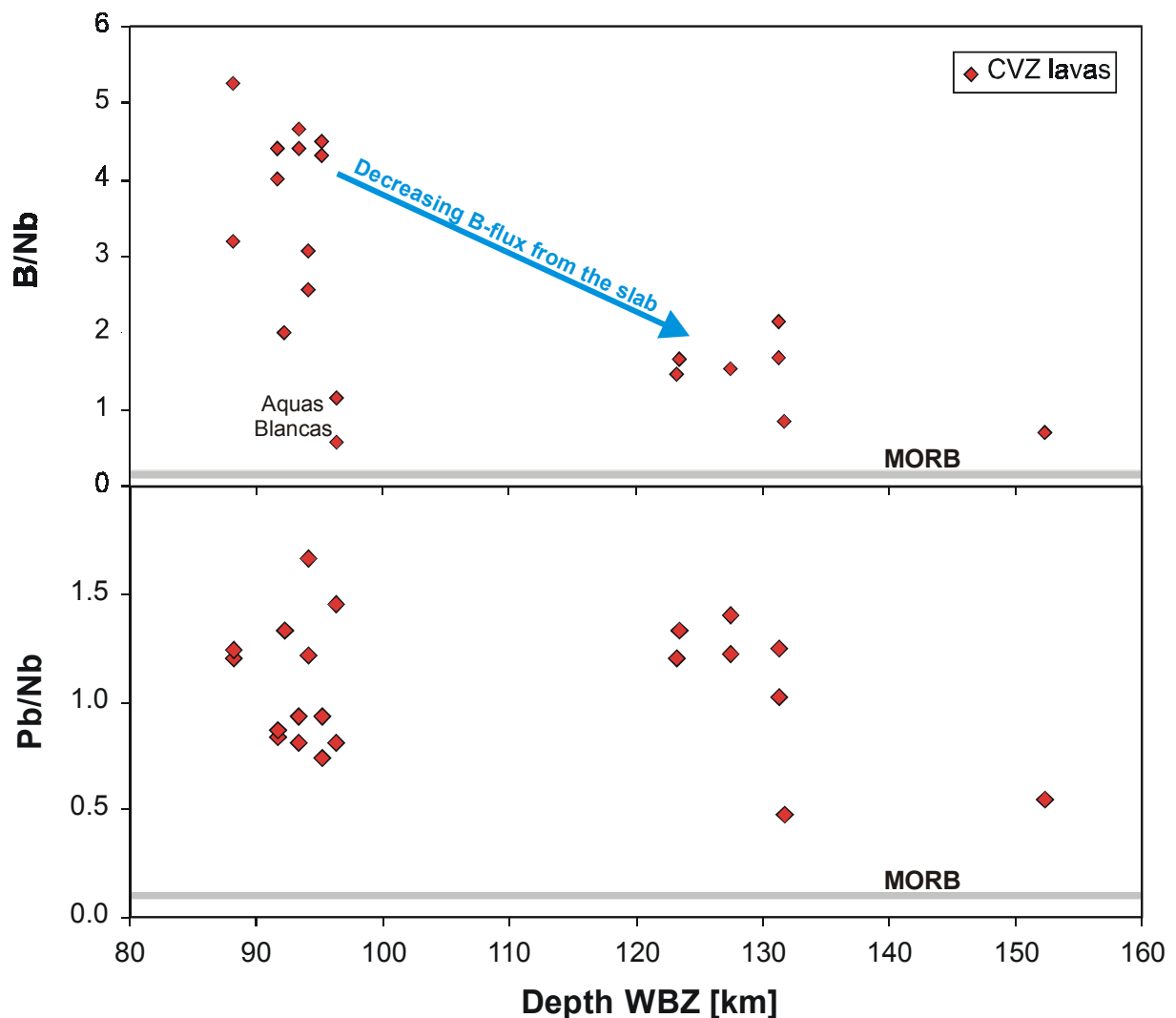


**Figure 6:** B/Nb (a) and Pb/Nb (b) vs. depth of Wadati-Benioff Zone; N-MORB values for comparison are based on data of *Chaussidon and Marty* [1995] and *Hofmann* [1988]. Arrow in diagram a) highlights the decreasing B-flux from the slab.

Strontium, Nd and Pb isotope ratios of the samples are given in Table 2 and plotted with other reference data in Figures 9 and 10. The isotope compositions are typical for CVZ arc volcanics as previously described by, e.g., *Davidson et al.* [1990, 1991], *Kay et al.*, [1994], *Aitchison et al.* [1995], and *Trumbull et al.*, [1999], with more radiogenic Sr and Pb, and less radiogenic Nd compared with MORB. The initial  $^{87}\text{Sr}/^{86}\text{Sr}$  and  $^{143}\text{Nd}/^{144}\text{Nd}$  isotope ratios vary between 0.705981 and 0.708107, and 0.512249 and 0.512481, respectively, and show a close inverse correlation (Fig. 7).

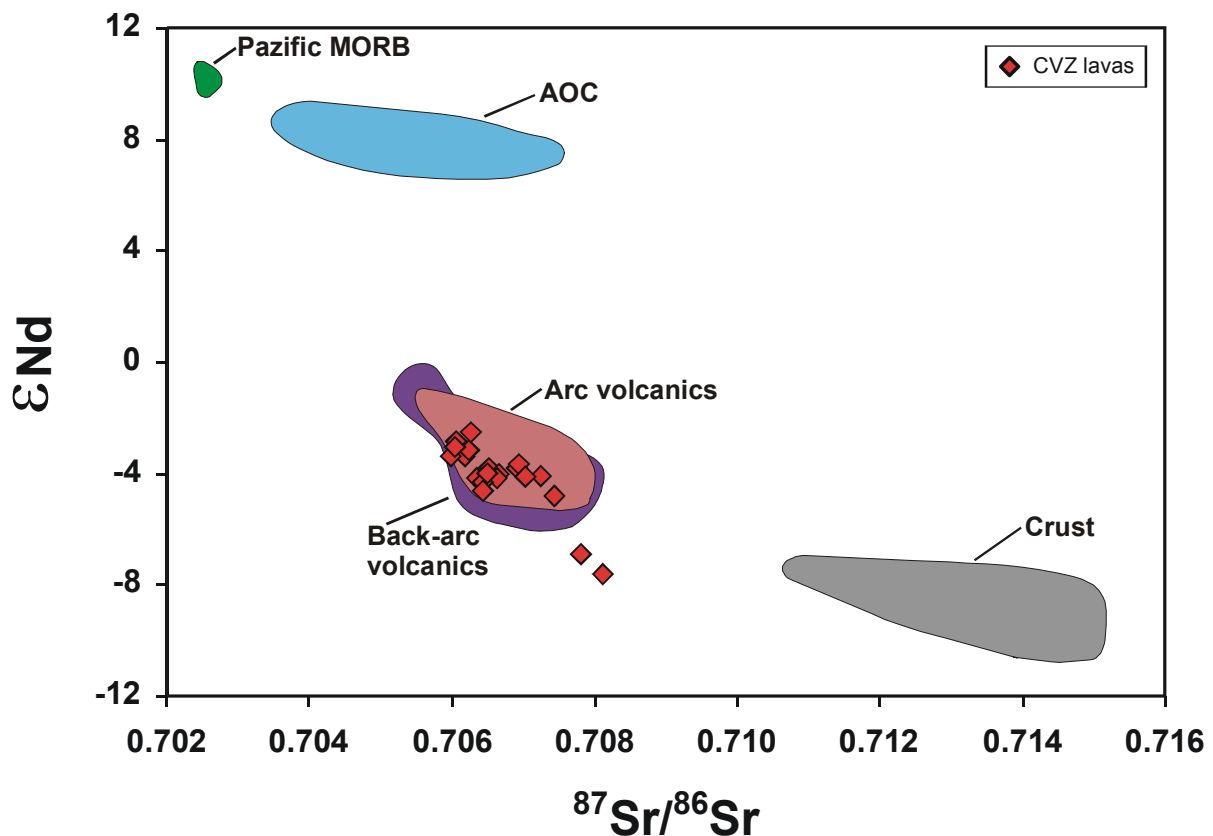


**Figure 7:** Initial  $^{87}\text{Sr}/^{86}\text{Sr}$  vs.  $\epsilon\text{Nd}$  values of CVZ volcanic rocks: Fields show composition of other volcanic rocks from the frontal arc [*Trumbull et al.*, 1999] and back-arc region [*Kay et al.*, 1994] in the study area. Also shown for comparison are the compositions of relevant reservoirs for magma genesis: Crust (Panizos ignimbrite [*Ort et al.*, 1996]), Pacific-MORB [*Regelous et al.*, 1999] and altered oceanic crust [*Staudigel et al.*, 1995].

The Pb isotope compositions are homogeneous, with  $^{206}\text{Pb}/^{204}\text{Pb}$  ratios from 18.701 to 18.887,  $^{207}\text{Pb}/^{204}\text{Pb}$  from 15.585 to 15.694 and  $^{208}\text{Pb}/^{204}\text{Pb}$  from 38.632 to 39.054. In a  $^{207}\text{Pb}/^{204}\text{Pb}$  vs.  $^{206}\text{Pb}/^{204}\text{Pb}$  diagram (Fig. 8), the data plot in a narrow compositional field below the Andean Pb-line defined from pre-Mesozoic basement data by *Lucassen et al.* [2001]. Unlike the Sr and Nd isotopes, Pb isotope ratios of the andesite-dacite samples fall in the same range as those of crustal-dominated Cenozoic ignimbrites from the CVZ [*Ort et al.*,



1996; Lindsay et al., 2001], suggesting that the Pb isotope composition of the samples is dominated by crustal-derived Pb. The radiogenic isotope ratios do not correlate with  $\delta^{11}\text{B}$ , nor is there a significant variation in Sr, Nd or Pb isotope ratios with WBZ depth across the arc.

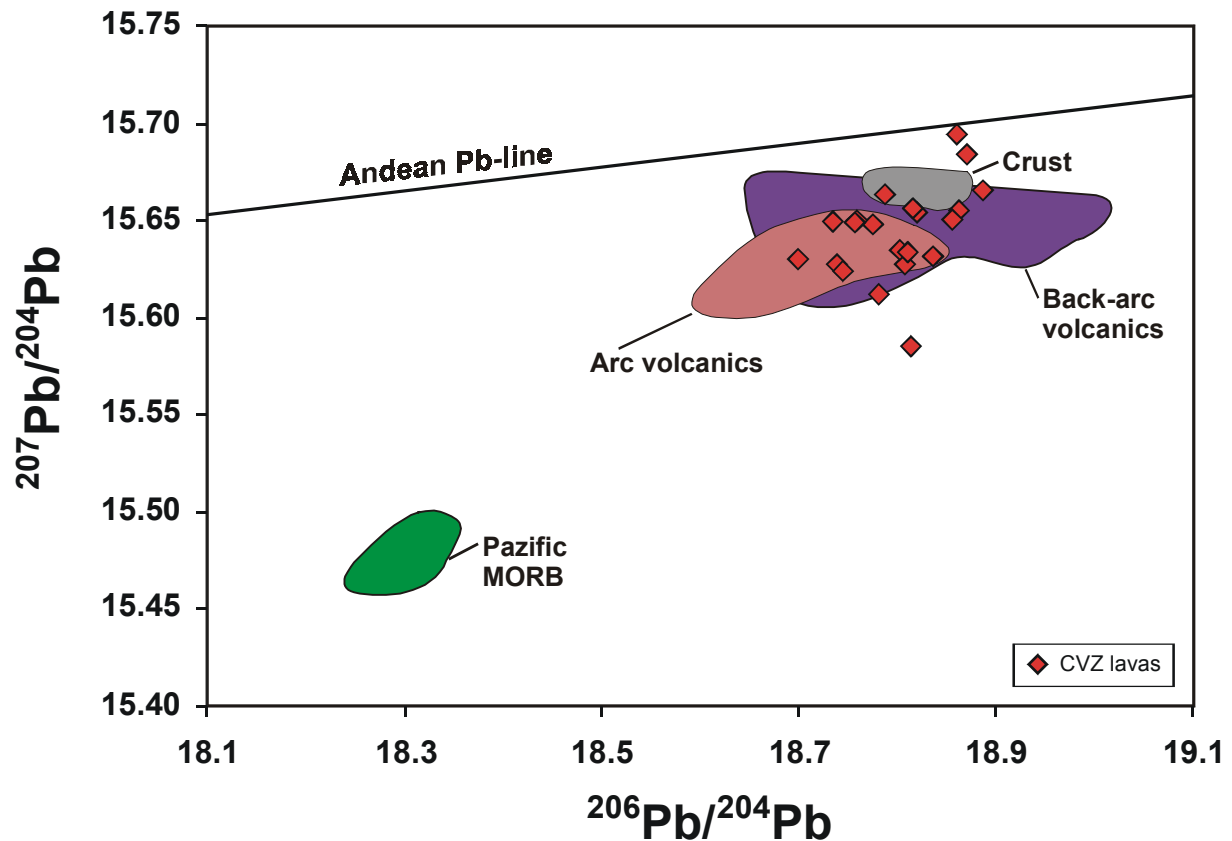


**Figure 8:**  $^{206}\text{Pb}/^{204}\text{Pb}$  vs.  $^{207}\text{Pb}/^{204}\text{Pb}$  compositions of CVZ volcanic rocks: Fields show the composition of the crust (Panizos ignimbrite [Ort et al., 1996] and Pacific-MORB [Regelous et al., 1999] for comparison along with the composition of other volcanic rocks from the frontal arc [Trumbull et al., 1999] and back-arc region [Kay et al., 1994] in the study area. The Andean Pb-line (solid line) is based on pre-Mesozoic basement compositions [Lucassen et al., 2001].

## III.6 Discussion

### III.6.1 Boron sources in CVZ magmas

A striking feature of the B-isotope data from this study of the CVZ arc rocks is the wide range of compositions present and their systematic across-arc variation. To aid in interpretation of these results, Table 3 (page 77) lists average B compositions and isotope ratios from the literature along with complementary data for Sr, Nd and Pb for relevant source reservoirs in the subducting slab, mantle wedge and continental crust. Figure 9 a shows a simplified sketch

of the subduction zone of the Central Andes along with the major source reservoirs for arc-magma genesis and Figure 9 b shows a classification diagram of these reservoirs based on their B composition.

For the subducting slab, we assume that the main B reservoir will be the AOC in the upper part, which is strongly enriched in B over MORB by seawater interaction. *Smith et al.* [1995] report a mean  $\delta^{11}\text{B}$  value of +3.4 ‰ and B concentration of 5.2 ppm for the upper 500 to 1000 m of the ocean floor basalts (Fig. 9). The B-isotope composition of marine sediments is highly variable [*Ishikawa and Nakamura*, 1993] and depends on the relative abundance of continental detritus (-13 to -8 ‰), marine smectite (+2.3 to +9.2 ‰), biogenic carbonates (+8.0 to +26.2 ‰), and biogenic silica (+2.1 to +4.5 ‰; Fig. 9). The sediment input to the sub-arc region in the Central Andes is difficult to estimate but it must be small because of the very thin sedimentary fill in the Chile trench. The paucity of continental detritus also means that pelagic components, with positive  $\delta^{11}\text{B}$  values, may dominate the sediments entering the subduction zone. Pelagic sediments on the Nazca plate were drilled at DSDP Site 320 west of Peru and a thickness of 125 m was determined with a water content of 59 % [*Plank and Langmuir*, 1998]. Even if it is assumed that this material is subducted, compaction and dewatering will reduce its thickness to a small fraction relative to the 300 to 500 m-thick layer of AOC formed by oxidative seawater interaction [*Erzinger*, 1989]. The mantle wedge is assumed to have a composition similar to Pacific MORB source following *Bourdon et al.* [2000] and *Lucassen et al.* [2002], and estimates of its B concentration and isotope ratios are from *Chaussidon and Marty* [1995] (Fig. 9). A major source of uncertainty in the reservoir compilation is the composition of the continental crust. Our estimate of the crustal composition is based on an average composition of rhyodacitic ignimbrites from the Panizos caldera in NW Argentina [*Ort et al.*, 1996], which is a typical representative of several late Miocene to Pliocene caldera complexes whose eruptions created one of the largest ignimbrite provinces on earth [*deSilva et al.*, 1989]. The estimated  $> 30,000 \text{ km}^3$  of felsic magmas in this province represent crustal melts with minor admixture of more mafic arc magmas [*Francis and Hawkesworth*, 1994; *Ort et al.*, 1996; *Lindsay et al.*, 2001]. These ignimbrites are compositionally homogeneous and not strongly fractionated, so their compositions give a good estimate of the fusible components in the crust over a wide region extending from the arc to back-arc. Determinations of B concentration and isotope ratios in the ignimbrites are generally not available.

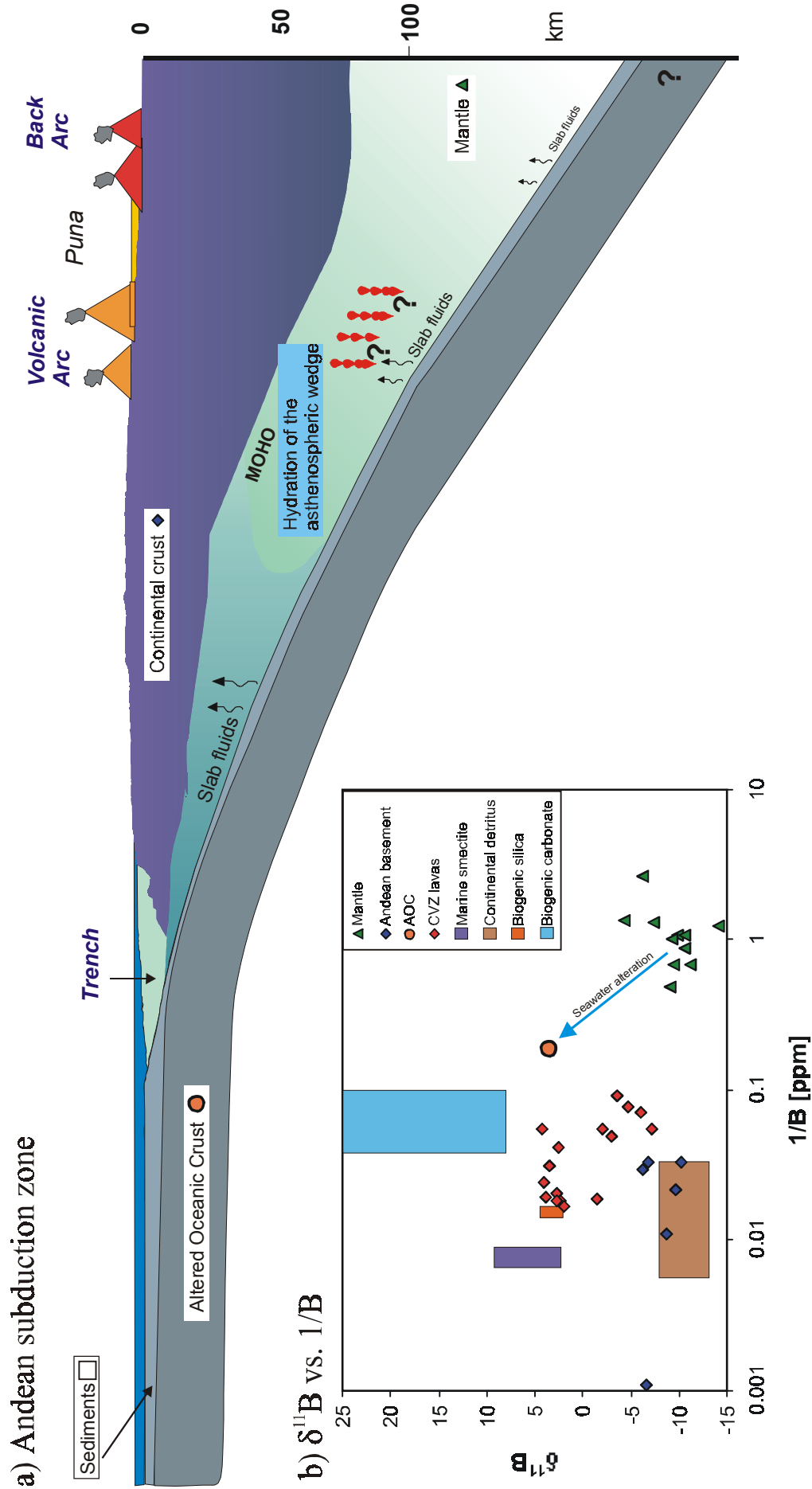


**Figure 9:** a) Simplified sketch of the Central Andean subduction zone between 21 and 27° S along with the major structural units modified after Kasemann et al. [1999]; b)  $\delta^{11}\text{B}$  vs.  $1/\text{B}$  of the source reservoirs involved in Andean magma genesis (References: Mantle [Chaussidon and Marty, 1995]; Andean basement [Kasemann et al., 2000]; AOC (altered oceanic crust) [Smith et al., 1995]; Marine sediment data [Nakamura and Ishikawa, 1993]). Blue arrow shows the effect of seawater alteration from MORB to AOC.

The only study to date, by *Schmitt et al.* [2001], determined  $\delta^{11}\text{B}$  values of melt inclusions in three ignimbrite units from the CVZ but the results are too varied (+2 to -9 ‰) to yield a useful average estimate. We therefore take the average crustal  $\delta^{11}\text{B}$  value of -8.9 ‰ determined by *Kasemann et al.* [2000] from a study of pre-Mesozoic granitoids and gneisses in the basement of the Central Andes (Fig. 9), which also agrees with the global crustal estimate of -8 to -13 ‰ by *Chaussidon and Albarède* [1992].

Extensive crustal contamination of arc magmas is a long-established feature of the CVZ, and the Sr, Nd and Pb isotope ratios of our sample set show this clearly. The Pb isotope ratios, in particular, fall in the same field as the crustal ignimbrites (Fig. 8) and appear to be entirely dominated by crustal Pb. The lack of systematic relationships between radiogenic isotope ratios and depth to the WBZ suggests that the slab-derived component does not contribute significantly to the Sr, Nd or Pb systematics in CVZ magmas or that its contribution is overprinted by crustal contamination. In terms of B, the crustal contamination is not dominant the arc magmas since the  $\delta^{11}\text{B}$  values of -7 to +4‰ for the volcanic rocks are all higher than the average value for the Andean crust (-8.9 ‰). However, the mixing and B-isotope fractionation models discussed below (see sections 6.2 and 6.3) show that only, with a static mixing approach, some crustal contamination is required to explain the  $\delta^{11}\text{B}$  values in back-arc samples (i.e., < -4 ‰), which are more negative than either MORB-source mantle or the slab components.

Most importantly, no combination of crustal and mantle-derived B can explain the positive  $\delta^{11}\text{B}$  values found in samples from the volcanic front since both reservoirs have negative  $\delta^{11}\text{B}$  and the B concentrations in the mantle are too low in any case to be of major importance. Positive  $\delta^{11}\text{B}$  values therefore require input of heavy B from the subducted Nazca plate. Although pelagic sediments could contribute to positive  $\delta^{11}\text{B}$  values, we consider the AOC reservoir to be more likely because of its greater thickness compared with any pelagic material left on the Nazca plate after subduction to sub-arc levels.

*Straub and Layne* [2002] suggested that the heavy B-isotope signature of magmas from the Izu arc may reflect a metasomatized layer of mantle just above the slab which was enriched by slab fluids generated at more shallow levels and then dragged to a sub-arc position by mantle corner flow. This mechanism could operate in the Andes setting too, but for our purposes the metasomatized mantle layer can be included as part of the "subduction component".

The intermediate  $\delta^{11}\text{B}$  values of between -7 and +4 ‰ could reflect different degrees of mixing between the slab-derived B and the crustal component, with the slab contribution decreasing progressively toward the back arc. We explore this hypothesis further with a B-isotope fractionation model and mixing models in a later sections.

The higher B concentrations and B/Nb ratios in samples from the frontal arc compared with those farther east (Fig. 6 a) give further support for a slab origin for much of the B in the CVZ arc magmas. Progressive metamorphic devolatilization of the slab will cause a decrease in slab-derived fluid flux from the arc front to the back-arc and this is consistent with the variations in B and B/Nb over a across-arc profile as observed in the Andes and other oceanic arcs [e.g., *Ishikawa and Tera, 1997; Ishikawa et al., 2001*].

### III.6.2 B-isotope fractionation, crustal contamination and the across-arc $\delta^{11}\text{B}$ variations

Systematic across-arc variations in  $\delta^{11}\text{B}$  like those found in this study have been noticed in several island arcs as well, and attributed to decreasing input of slab-derived fluid with AOC-like composition to the mantle wedge as subduction and dehydration of the slab progresses [e.g., *Ishikawa and Nakamura, 1994*]. In the continental arc setting of the Central Andes, crustal contamination could in principle cause across-arc variations if different degrees of contamination by crustal B ( $\delta^{11}\text{B} = -8.9$  ‰) were added to isotopically homogeneous primary arc magmas. However, there are no correlations of Sr, Nd and Pb isotope compositions with B-isotopes or the depth of the WBZ and therefore an increasing degree of crustal contamination from the frontal arc to the back-arc region can be ruled out.

If it is assumed that the  $\delta^{11}\text{B}$  composition of arc magmas is controlled by mixing of isotopically constant slab-derived fluid with a second component (the crust in the CVZ example), a minimum  $\delta^{11}\text{B}$  value for the fluid component can be predicted by extrapolating a linear regression of  $\delta^{11}\text{B}$  vs. Nb/B values to Nb/B = 0 [e.g., *Ishikawa and Tera, 1997*]. This approach predicts a  $\delta^{11}\text{B}$  value of +5.1 ‰ for slab-derived B (Fig. 10), which is slightly higher than the average composition of the AOC reservoir (Table 3) and lower than values obtained by the same method for the Izu- (+7.4 ‰; *Ishikawa and Nakamura [1994]*), the Kurile- (+7.0 ‰ Northern Kuriles and +6.3 ‰ Southern Kuriles; *Ishikawa and Tera [1997]*), the Mariana- (5.4 ‰; *Ishikawa and Tera [1999]*) and the Kamchatka arc (+6.2 ‰; *Ishikawa et al. [2001]*).

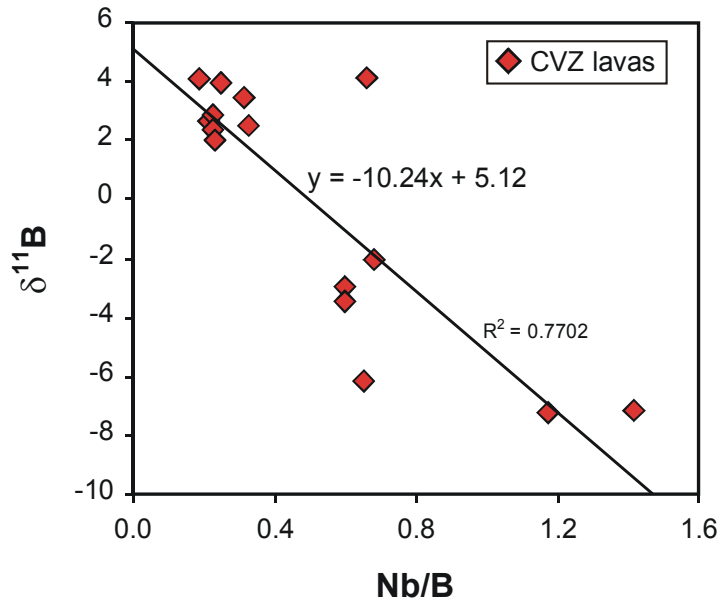


**Figure 10:** Systematic variation between  $\delta^{11}\text{B}$  vs. Nb/B. The regression line (excluding samples SALZU-96H-7 and AQUA-2-19) extrapolated to Nb/B=0 gives a model composition of slab-derived fluid of 5.1 ‰ if no isotope fractionation occurs during dehydration (see text).

However, the assumption that slab-derived fluid has a constant B-isotope composition throughout the entire subduction zone is an oversimplification because the dehydration reactions that liberate slab fluid can also cause a temperature-dependent fractionation of  $^{11}\text{B}$  and  $^{10}\text{B}$  between the fluid and residual minerals. During progressive dehydration of the downgoing slab, this B-isotope fractionation effect would cause systematically more negative  $\delta^{11}\text{B}$  compositions in slab fluid released at deeper levels [Peacock and Hervig, 1999], and this is exactly what is observed in the CVZ and other arcs (Figs. 5 and 12). We calculated the possible effect of B-isotope fractionation during progressive dehydration using the Rayleigh distillation equation (see caption to Fig. 11) following the approach of Peacock and Hervig [1999] and using the B concentrations and isotope ratios of AOC from Table 3 as the slab reservoir. The release of B from the slab is assumed to be a linear function of temperature, with 80 % loss at 750° C. Figure 11 shows the modeled composition of slab-fluid (instantaneous fluid) and resitite (mineral-resitite) as a function of temperature, with the starting  $\delta^{11}\text{B}$  value for the AOC of +3.4 ‰. Mineral-water fractionation factors ( $\alpha$ ) for B-isotopes are available for only a few phases relevant to subduction zone dehydration. We used the fractionation factors and their temperature dependence from experiments by Williams *et al.* [2001 a and b] on clay minerals, which are the main B-phases in the altered crust and/or marine sediments at least at low temperatures. The change from tetrahedral coordination of B in clay to trigonal coordination in coexisting fluid leads to extreme fractionation of B-isotopes at low temperatures, and even at the 400° - 600° C range appropriate for the sub-arc region in the CVZ, the fractionation effect may be on the order of 10 ‰ (Fig. 11).

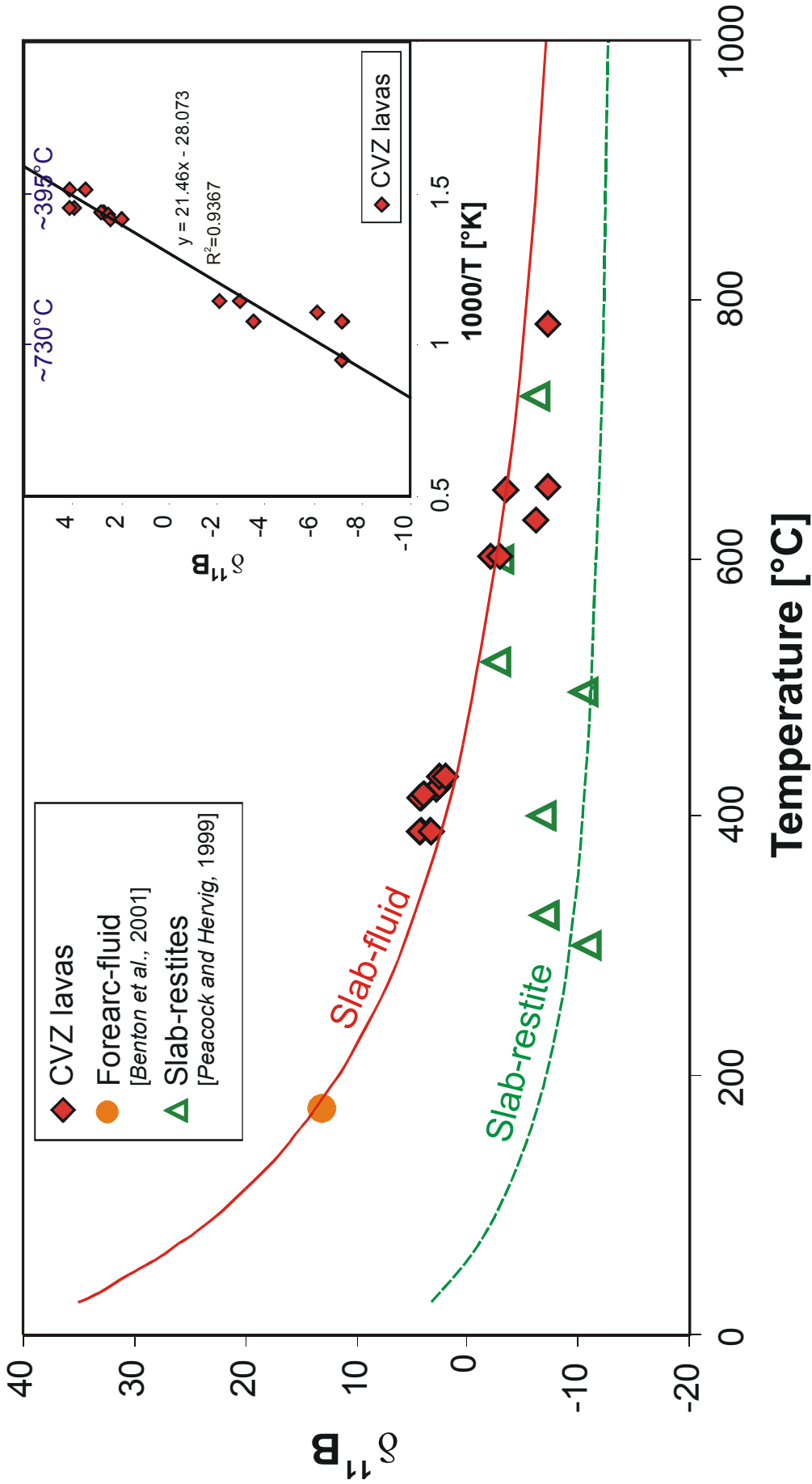


**Figure 11:** Modelled B-isotope fractionation between slab-fluid and slab-restite as a function of temperature:  $\delta^{11}\text{B}$  values of slab-fluid (red solid line) and the slab-restite (green dashed line) were calculated for different temperature increments using the Rayleigh fractionation model ( $\delta^{11}\text{B}_{\text{restite}} = \{\delta^{11}\text{B}_{\text{initial}} + 10^3\} * \{\text{B-conc.}_{\text{restite}} / \text{B-conc.}_{\text{initial}}\}^{(-1)} - 10^3$ ;  $\delta^{11}\text{B}_{\text{fluid}} = \{\delta^{11}\text{B}_{\text{restite}} + 10^3\} - 10^3$ ) and fractionation factors from Williams *et al.* [2001]. For the initial B-isotope composition of the slab, we used the average  $\delta^{11}\text{B}$  value of +3.4 ‰ from Smith *et al.* [1995]. To plot the CVZ  $\delta^{11}\text{B}$  data (red diamonds) in this model, the depths of the Wadati-Benioff Zone were translate to temperatures using the thermal model shown in Fig. 2.  $\delta^{11}\text{B}$  data and temperatures for a forearc fluid (blue circle) and slab-restites (green open triangles) were taken from Benton *et al.* [2001] and Peacock and Hervig [1999], respectively. Inset shows the linear correlation of our  $\delta^{11}\text{B}$  data vs.  $1000/T$  (see text for discussion).

The measured  $\delta^{11}\text{B}$  values of the CVZ arc volcanic rocks are plotted on Figure 11 using the thermal field in Figure 2 to translate the individual WBZ depth into temperature. Samples SALZU-96-H7 and AQUA-2-19 are not plotted here because they deviate from the across-arc trend shown by the other samples (Fig. 5) and their B-budget may not be controlled only by the slab component. The correspondence between the observed data and the model curve for slab-fluid is good, nevertheless all samples show evidence for crustal contamination.

The model fluid curve also fits with the composition of forearc slab fluid reported by *Benton et al.* [2001] from the Mariana arc at about 25 km WBZ depth (or 200° C using the thermal model in Fig. 2). The model restite curve also corresponds well with measured  $\delta^{11}\text{B}$  values of geologic samples considered to represent slab-restites from *Peacock and Hervig* [1999]. Finally, our  $\delta^{11}\text{B}$  data show a remarkably tight linear relationship with reciprocal temperature (Fig. 11 inset), which strongly supports the hypothesis that  $\delta^{11}\text{B}$  variations are caused by temperature-dependent fractionation in the slab. Note that extrapolation of the temperature vs.  $\delta^{11}\text{B}$  regression line to 25° C yields an estimate of +43 ‰ for the fluid in equilibrium with the slab at the onset of subduction. This estimate is surprisingly close to the seawater value of +39.5 ‰ although the procedure makes no assumptions about the B-composition of the slab or the B-isotope fractionation factor. The fractionation model (fluid curve in Fig. 11) predicts a fluid composition of +34 ‰ at 25° C, which is also reasonably close to the seawater value considering the uncertainties in the AOC initial composition and fractionation factor.

In summary, the correspondence between the fractionation model and observational data is excellent and this suggests that B-isotope fractionation in subduction zones may be a controlling factor in the B systematics of volcanic arcs in general. This in turn implies that B-isotope ratios of arc volcanics need not directly reflect the initial composition of B in the subducting slab, and this limits our ability to distinguish the relative contributions of B-sources in the slab such as AOC and marine sediments.

The specific effects of isotope fractionation on arc magma composition will depend on local variables like slab composition, convergence rate, angle of subduction, and the thermal structure of the subduction zone. In fact, there are important differences in the trends of across-arc variation in  $\delta^{11}\text{B}$  between the continental CVZ and the western Pacific Izu-, Kurile- and Kamchatka arcs which are built primarily on oceanic crust. When plotted against depth to the WBZ (Fig. 12), the  $\delta^{11}\text{B}$  data from the CVZ show a greater overall range, more negative values, and a steeper slope than the oceanic arcs with the exception of Kamchatka, where the



crust is relatively thick (~30 km [Gill, 1981]) and made up of accreted arc terranes. In principle, given the same initial B-composition of the subducting slab, the  $\delta^{11}\text{B}$  values of slab-derived fluids under the volcanic arc should be higher for a colder subduction zone than for hotter ones because dehydration and B-isotope fractionation of the slab at the sub-arc position will be less advanced. However, the subducting crust is Eocene or older in both the CVZ and western Pacific arcs, so all should be relatively cold slabs, and the convergence rates are also similar [Gill, 1981]. In the Central Andes, the arc is located above a shallower WBZ than in the other arcs because of the lesser dip of the slab. This factor should favor a greater slab-fluid flux and higher  $\delta^{11}\text{B}$  values in the CVZ magmas, but the opposite is observed. A viable explanation for steeper slopes of the  $\delta^{11}\text{B}$  across-arc variation in the Central Andes and possibly in the Kamchatka arc as well, is crustal contamination. If the degree of crustal contamination is nearly constant across the arc as suggested by the Sr, Nd and Pb data, and the input of slab-derived B decreases progressively away from the arc front, the effect will be a clockwise rotation of the compositional trend in Figure 12 as the crustal influence increases toward the backarc.

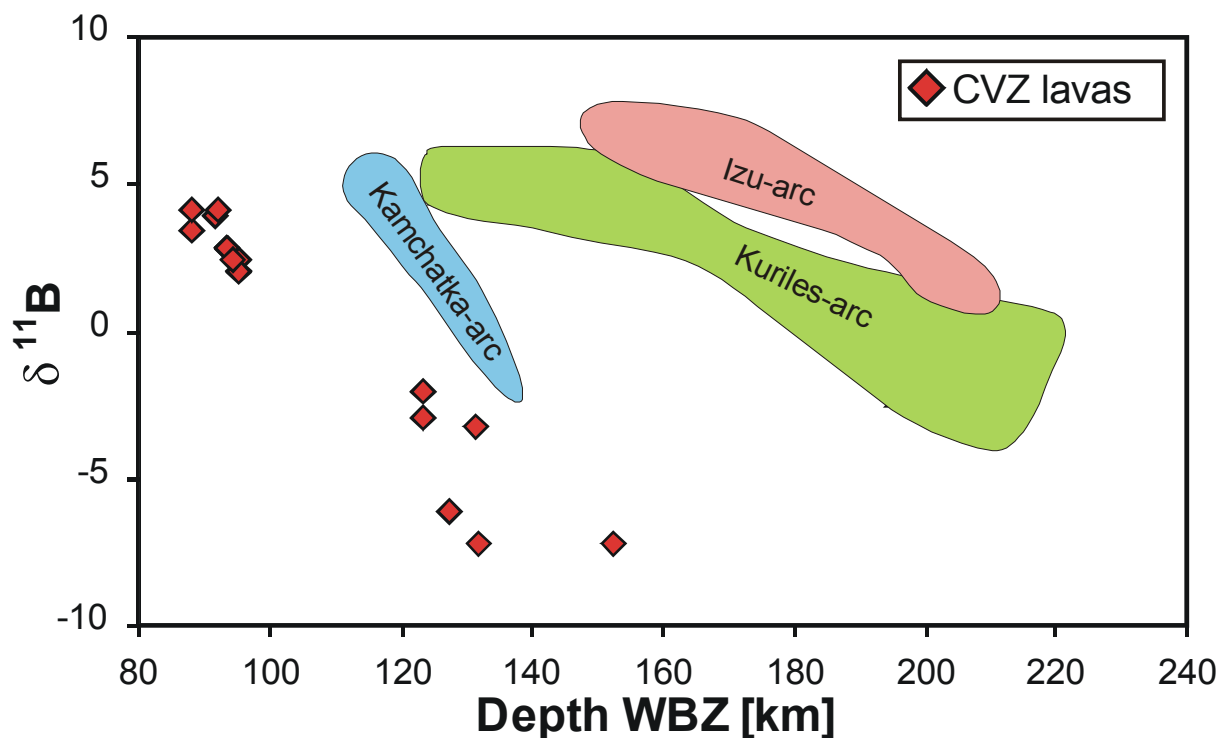


**Figure 12:** Comparison of  $\delta^{11}\text{B}$  across-arc trends ( $\delta^{11}\text{B}$  vs. Wadati-Benioff Zone) for the CVZ (excluding SALZU-96H-7 and AQUA-2-19) and west Pacific arcs (Izu- [Ishikawa and Nakamura, 1994], Kurile- [Ishikawa and Tera, 1997] and Kamchatka arc [Ishikawa and Tera, 1997]).

### III.6.3 Coupled B, Sr and Nd mixing models

The purpose of this section is to define the effect of the addition of subduction zone fluids on the composition of the fertile mantle and the effect of crustal contamination on the composition of the initial arc magmas using B - Sr and B - Nd-isotope mixing models.

We calculated two different types of models, the first (static model, Figs. 13 a and b) assuming no change in the B-isotope composition of the slab fluid with subduction depth and the other (dynamic model, Figs. 13 c and d) taking B-isotope fractionation and ongoing B-loss during dehydration into account. Both models involve three endmembers: slab-fluid derived mainly from the AOC component in the Nazca-plate, a MORB-like asthenospheric mantle wedge, and the continental crust. The reservoir compositions used and calculated element concentrations of the slab-fluid are explained in Table 3.

**Table 3:** Average reservoir compositions used for interpretation and modelling slab-fluid composition: Element concentrations are calculated based on the equation  $C_{\text{slab fluid}} = C_{\text{AOC}} * (M/F)$ , where  $C_{\text{slab fluid}}$  is the concentration of an element in the slab fluid,  $C_{\text{AOC}}$  is the original concentration of an element in the AOC, M is the mobility of an element during dehydration and F is the weight fraction of hydrous fluid extracted from the AOC, here assumed to be 1.5 % [Tatsumi and Kogiso, 1997]; mobilities for Sr and Nd are taken from Kogiso et al. [1997] and for B from Sano et al. [2001]; Sr and Nd isotope composition of the primary arc magma are calculated from a 1.5 % slab-fluid addition to the mantle (see text).

Reservoir	B (ppm)	$\delta^{11}\text{B}$ (‰)	Sr (ppm)	$^{87}\text{Sr}/^{86}\text{Sr}$	Nd (ppm)	$^{143}\text{Nd}/^{144}\text{Nd}$	$^{206}\text{Pb}/^{204}\text{Pb}$	$^{207}\text{Pb}/^{204}\text{Pb}$
MORB	0.05 <sup>a</sup>	-4.0 <sup>a</sup>	14 <sup>b</sup>	0.70255 <sup>e</sup>	1.1 <sup>b</sup>	0.513157 <sup>c</sup>	18.31 <sup>c</sup>	15.48 <sup>c</sup>
AOC	5.2 <sup>d</sup>	+3.4 <sup>d</sup>	169 <sup>e</sup>	0.70475 <sup>e</sup>	6.7 <sup>e</sup>	0.513057 <sup>e</sup>		
Slab fluid	208	+8.0 to -8.0	4589	0.70475 <sup>e</sup>	138	0.513057 <sup>e</sup>		
Arc-magma	10 to 0.1	+8.0 to -8.0	270 <sup>b</sup>	0.70357	10 <sup>b</sup>	0.513091		
Pelagic sed.	10 to 150 <sup>f</sup>	+2.1 to 26.2 <sup>f</sup>						
Andean Crust	10 <sup>g</sup>	-8.9 <sup>h</sup>	353 <sup>i</sup>	0.71428 <sup>i</sup>	42.6 <sup>i</sup>	0,512167 <sup>i</sup>	18.88 <sup>i</sup>	15.57 <sup>i</sup>

<sup>a</sup> Chaussidon and Marty [1995]; <sup>b</sup> Tatsumi [2000]; <sup>c</sup> Regelous et al. [1999]; <sup>d</sup> Smith et al. [1995]; <sup>e</sup> Staudigel et al. 1995; <sup>f</sup> Ishikawa and Nakamura [1993]; <sup>g</sup> Taylor and McLennan [1985]; <sup>h</sup> Kasemann et al. [2000]; <sup>i</sup> Ort et al. [1996];

#### Static Model

The first stage of the static model (Figs. 13 a and b) involves mixing between the MORB-like mantle wedge and a slab-derived fluid phase whose B concentration and isotope ratios are controlled by the AOC reservoir and remain constant during progressive subduction. The calculated mixing line (mantle wedge plus slab-fluid) represents the possible range of isotope

compositions in the metasomatized mantle (fertile mantle) above the slab, which is assumed to be the source of primary basaltic magmas.

The second stage of mixing involves the primary arc basaltic magmas and partial melts of the continental crust. For the  $\delta^{11}\text{B}$ ,  $^{87}\text{Sr}/^{86}\text{Sr}$  and  $^{143}\text{Nd}/^{144}\text{Nd}$  values of the primary arc basalt, we calculated the compositions resulting from addition of 1.5 wt. % slab fluid to a MORB-like mantle wedge [Tatsumi, 2000], which corresponds to a fluid/mantle ratio of 63 for B. Element concentrations of Sr and Nd in the primary magma were taken from Tatsumi [2000]. Because B concentration in primary arc-basalts are not well constrained, we used a series of concentrations (10 ppm, 1.0 ppm, 0.1 ppm) to cover the range of possible values. The crustal melt composition is based on the Panizos ignimbrite [Ort *et al.*, 1996] as described above, but we emphasize again that the ignimbrites themselves contain some component of arc andesites with the consequence that the proportion of crust estimated in the model is a maximum value.

#### *Dynamic Model*

This model uses the same assumptions of slab, mantle and crustal compositions as the static models, but also takes into account the effect of changing slab-fluid composition due to B-isotope fractionation and changes in overall fluid flux due to progressive dehydration of the slab (Figs. 13 c and d). For the first stage of the dynamic model, i.e. B-isotope fractionation by slab dehydration, we chose two extreme  $\delta^{11}\text{B}$  values to represent the range of slab fluid composition expected for the volcanic front (+8 ‰) to the back-arc (-8 ‰) based on the model in Fig. 11. In the second stage, these different slab-fluids are mixed with the MORB-like mantle wedge to calculate the composition of primary arc magmas. To simulate the effect of decreasing fluid flux with progressive subduction, we assumed a 1.5 % fluid addition to the mantle wedge at the volcanic front and only 0.15 % fluid added at the back-arc position. We also assigned the primary magmas in the arc front and backarc positions different B concentrations to simulate decreasing fluid flux: for the volcanic front 10 and 1 ppm and for the back-arc 1 and 0.1 ppm. Concentrations for Sr and Nd are the same as in the static model.

Both the static and dynamic mixing model show that the B-isotope composition of the mantle wedge can be strongly affected by very small proportions of slab fluid. Compositions are dominated by the slab component beyond about 0.15 % fluid addition and remain little changed at higher fluid fluxes. This implies that the slab fluid can continue to have a major effect on the B-isotope composition of primary arc magmas over the whole arc-profile as long as some slab fluid is produced, as predicted by the dehydration models of Kerrick and Connolly [2001].

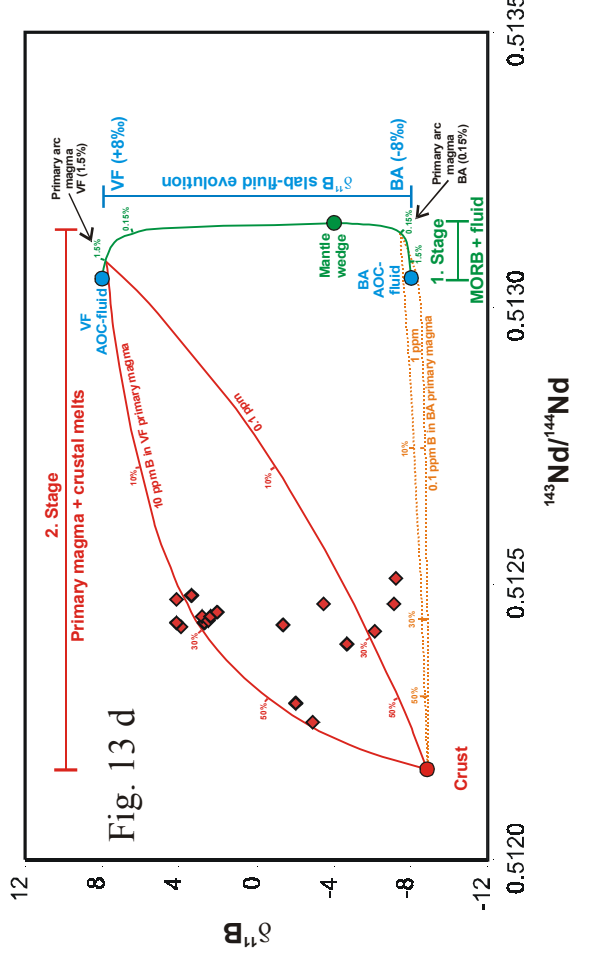
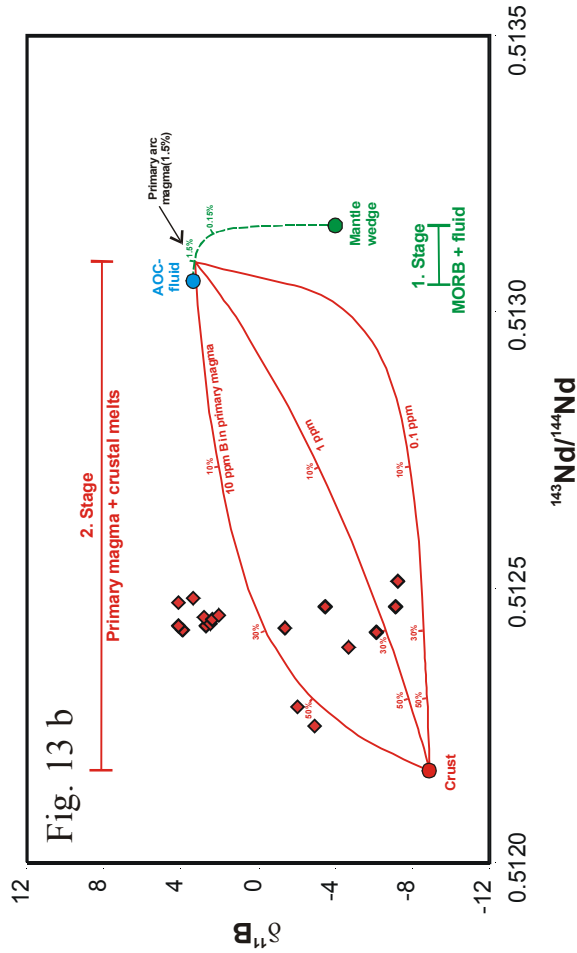
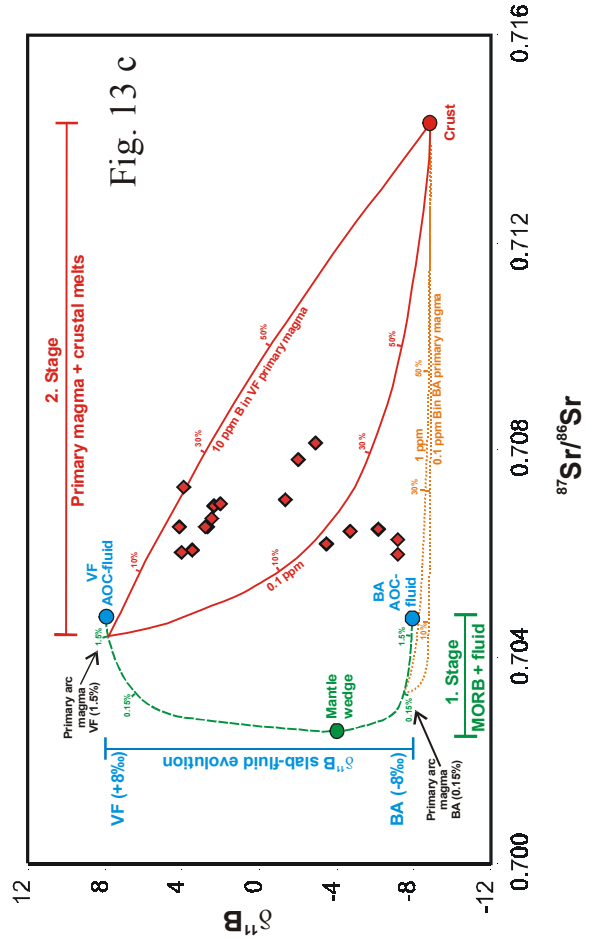
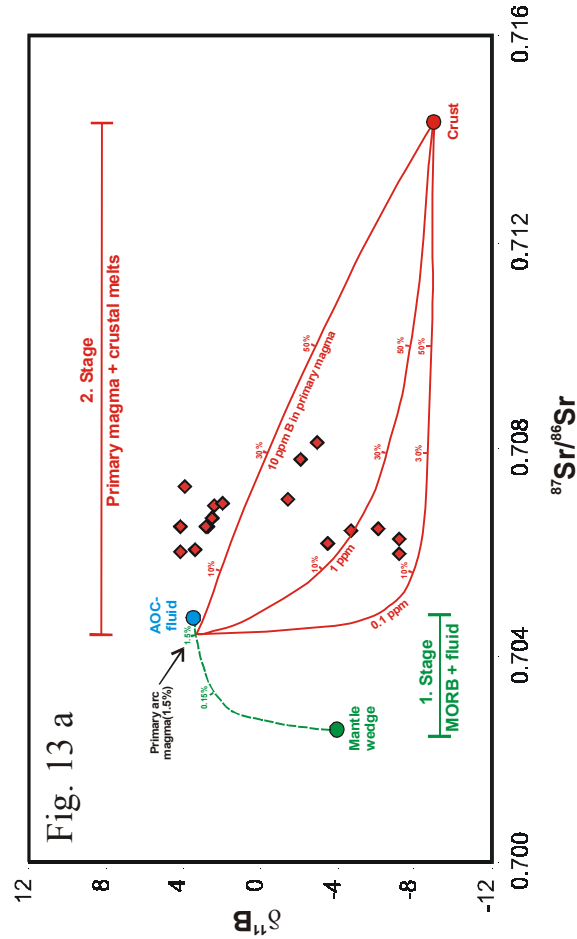


**Figure 13:** Static mixing model for B - Sr isotopes (a) and B - Nd isotopes (b) based on compositions given in Table 3 and assuming no B-isotope fractionation. The green dashed mixing line (first stage) describes the isotope composition of primary arc magma produced by mixing between the mantle wedge and AOC-derived slab fluids. Tic marks give proportion of fluid in the mantle. The three solid red mixing lines (second stage) describe the contamination of primary arc magma with crustal melts assuming B-concentrations in the arc magma of 0.1, 1 and 10 ppm. Tic marks give proportion of crustal melt in the primary magma. The primary magma composition assumes 1.5 % addition of fluid to the mantle wedge [cf. *Tatsumi, 2000*]. Dynamic mixing model for B - Sr isotopes (c) and B - Nd isotopes (d) based on compositions given in Table 3 and taking B-isotope fractionation into account. The effect of isotope fractionation is represented by two end-member fluid compositions for the volcanic front (VF;  $\delta^{11}\text{B} +8 \text{‰}$ ) and back-arc (BA;  $\delta^{11}\text{B} -8 \text{‰}$ ). The green dashed lines (first stage) describes the isotope composition of primary arc magmas produced by mixing between the mantle wedge and the two end-member slab fluids. Tic marks give proportion of fluid in the mantle. The two pairs of solid red mixing lines (second stage) describe the contamination of primary arc magmas with crustal melts. Tic marks give proportion of crustal melt to the primary magma. To account for progressive dehydration, we assume a fluid addition of 1.5 % for the frontal arc primary magmas and only 0.15 % for the back-arc. Similarly, the B concentrations for the frontal arc primary magmas are assumed to be higher (1 and 10 ppm; solid red lines) than for the back arc (0.1 to 1 ppm; dotted orange lines).

The static model fails to produce  $\delta^{11}\text{B}$  values higher than the initial AOC composition of +3.4 ‰ whereas the dynamic model is able to explain the whole range of Andean B-compositions (except LAU-94-1). It should be noted that *Spivack and Edmond [1987]* and *Smith et al. [1995]* reported  $\delta^{11}\text{B}$  values for the AOC higher than the value used here, and previous models of B-isotopes in island-arcs also call for a slab-fluid composition between +4 ‰ and +8 ‰ [*Ishikawa and Nakamura, 1994; Ishikawa and Tera, 1997; Ishikawa and Tera, 1999; Ishikawa et al., 2001*].

The static models would fit most of the Andean data only if the slab component had a  $\delta^{11}\text{B}$  value of +8 ‰, but this seems unrealistically high and furthermore, the dynamic model is physically more realistic.

The dynamic model indicates that an average addition of 15 to 30 % crustal melt to the primary arc-basalt can explain most of our data, and we note again that this is a maximum estimate since the ignimbrites on which the crustal composition is defined are impure crustal melts. The estimated degrees of crustal contamination are in good agreement with *Trumbull et al. [1999]* and *Bourdon et al. [2000]* based on radiogenic isotope data alone. Inconsistencies in the models are that the B - Sr model calculates slightly lower degrees of contamination than the B - Nd model. This may be caused by a false assumption that the average basement

compositions of Sr and Nd are constant. Note that samples from the Licancabur and Sairecabur volcanoes plot on the same B - Sr and B - Nd mixing lines as volcanoes from the arc front but at much higher degrees of crustal contamination (> 60 %). However, these samples plot along with the others on the linear  $\delta^{11}\text{B}$  vs.  $1000/T$  trend in Figure 11, which could not be the case if they had twice as much crustal contamination as the other samples. Therefore we consider it likely that there is a local variation in composition of the crust (note that Sairecabur and Licancabur are located close together, Fig. 1) and suggest that the degree of crustal contamination is approximately uniform across the arc.

In summary, the implication of the mixing models is that the very negative  $\delta^{11}\text{B}$  values of samples from the back-arc (-7 ‰) are not due to an increase in crustal-derived B, but must reflect instead a decreasing amount of fluid derived from the slab, in addition to the effect of B-isotope fractionation.

### III.7 Conclusions

This study of arc volcanic rocks from the Central Andes is the first systematic investigation of B-isotope systematics in subduction zone magmatism at a continental arc setting. The Late Miocene to Quaternary andesites and dacites studied are compositionally typical for the CVZ and show a wide range of B contents (6 - 60 ppm) and  $\delta^{11}\text{B}$  values (+4 to -7 ‰) that vary systematically across the arc. Positive  $\delta^{11}\text{B}$  values of frontal arc volcanic rocks from the CVZ requires a source enriched in  $^{11}\text{B}$  relative to the mantle (MORB) or continental crust (average CVZ basement value is -8.9 ‰) and the best explanation for this is seawater-altered upper oceanic crust from the subducted slab.

The progressive shift to more negative  $\delta^{11}\text{B}$  values towards the back-arc is attributed to a combination of two processes: (1) a changing  $\delta^{11}\text{B}$  composition of slab fluids due to B-isotope fractionation during progressive slab dehydration, and (2) a steady decrease in slab-fluid flux towards the back arc coupled with a relatively constant degree of crustal contamination in the magmas, as indicated by their Sr, Nd, Pb isotope ratios. This indicates that B in the magmas is dominated by the subducted slab component despite the presence of a 60 km thick continental crust, and it suggests that B can be used as a tracer for subduction zone processes in continental as well as oceanic settings.

The effect of B-isotope fractionation on slab-fluid composition was calculated by a Rayleigh fractionation model using mineral-fluid fractionation factors from *Williams et al.* [2001 a] coupled with a temperature model for the Central Andes subduction zone from

*Springer* [1999]. The predicted effect of fractionation is large and the agreement between calculated slab fluid composition and the composition of CVZ volcanic rocks is excellent. Combined B, Sr and Nd isotope mixing calculations for the slab fluid, a mantle wedge of MORB-source composition, and the continental crust yield a consistent solution for the B, Sr and Nd isotope data, with an average crustal input of 15 to 30 %.

Boron isotope fractionation during progressive slab dehydration should be a general feature of subduction zone processes although in detail, its effect on arc magma composition will depend on local variables like slab composition, convergence rate, angle of subduction and the thermal structure of the subduction zone. The fractionation effect will not only influence the B-isotope composition of material transferred into the crust by arc magmas, but it has also potential implications for the B-composition of restitic material recycled back into the mantle. *Chaussidon and Marty* [1995] report average  $\delta^{11}\text{B}$  values for OIB of -9.9 ‰ and -4.0 ‰ for N-MORB or -3.6 ‰ for E-MORB. The nearly 6 ‰ more negative  $\delta^{11}\text{B}$  values of OIB relative to MORB may reflect recycling of  $^{11}\text{B}$ - depleted slab-restite components into the deep mantle.

## REFERENCES

- Adam, J., and C.-D. Reuther, Crustal dynamics and active fault mechanics during subduction erosion. Application of frictional wedge analysis on to the North Chilean Forearc, *Tectonophysics*, 321, 297-325, 2000.
- Aitcheson, S. J. and A. H. Forrest, Quantification of crustal contamination in open magmatic systems, *J. Petrol.*, 35, 461-488, 1994.
- Aitcheson, S. J., R. S. Harmon, S. Moorbarth, A. Schneider, P. Soler, E. Soria-Escalante, G. Steele, I. Swainbank, and G. Wörner, Pb isotopes define basement domains in the Altiplano, central Andes, *Geology*, 23, 555-558, 1995.
- Allmendinger, R. W., T. E. Jordan, S. M. Kay, and B. L. Isacks, The evolution of the Altiplano-Puna Plateau of the central Andes, *Ann. Rev. Earth Sci.*, 25, 139-174, 1997.
- Barth, S., Boron isotope variations in nature: a synthesis. *Geol. Rundsch.*, 82, 640-651, 1993.
- Bebout, G. E., J. G. Ryan, W. P. Leeman, and A. E. Bebout, Fractionation of trace elements by subduction-zone metamorphism-effect of convergent-margin thermal evolution, *Earth Planet. Sci. Lett.*, 171, 63-81, 1999.
- Benton, L. D., J. G. Ryan, and F. Tera, Boron isotope systematics of slab fluids as inferred from a serpentine seamount, Mariana forearc, *Earth Planet. Sci. Lett.*, 187, 273-282, 2001.
- Bourdon, B., G. Wörner, and A. Zindler, U-series evidence for crustal involvement and magma residence times in the petrogenesis of Parinacota volcano, Chile, *Contrib. Mineral. Petrol.*, 139, 458-469, 2000.
- Breitlaender GmbH, Pulverproben / Festproben / Mineralische / Metallurgische / Werkstoffe, <http://www.breitlander.de>.
- Cahill, T. A., and B. L. Isacks, Seismicity and shape of the subducted Nazca plate. *J. Geophys. Res.*, 97, 17503-17529, 1992.
- Catanzaro, E. J., C. E. Champion, E. L. Garner, G. Marinenko, K. M. Sappenfield, and W. R. Shields, Standard Reference Materials: Boric acid; Isotopic, and Assay Standard Reference Materials, *US National Bureau of Standards, Spec. Publ.*, 260-17: 70pp, 1970.



- Chaussidon, M. and F. Albarède, Secular boron isotope variations in the continental crust: An ion microprobe study, *Earth Planet. Sci. Lett.*, 108, 229-241, 1992.
- Chaussidon, M., and B. Marty, Primitive boron isotope composition of the mantle, *Science*, 269: 383-386, 1995.
- Clift, P. D., E. F. Rose, N. Shimizu, G. D. Layne, A. E. Draut, and M. Regelous, Tracing the evolving flux from the subducting plate in the Tonga-Kermadec arc system using boron in volcanic glass, *Geochim. Cosmochim. Acta*, 65), 3347-3364, 2001.
- Coira, B., J. Davidson, C. Mpodozis, V. Ramos, Tectonic and magmatic evolution of the Andes of northern Argentina and Chile, *Earth Sci. Rev.*, 18, 303-322, 1982.
- Davidson, J. P., N. J. McMillan, S. Moorbath, G. Wörner, R. S. Harmon, and L. Lopez-Escobar, The Nevados de Payachata volcanic region (18°S, 69°W, N. Chile); II, Evidence for widespread crustal involvement in Andean magmatism, *Contrib. Mineral. Petrol.*, 105, 412-432, 1990.
- Davidson, J. P., R. S. Harmon, and G. Wörner, The source of central Andean magmas: some considerations, *Geol. Soc. Am. Sp. Paper*, 265, 233-244, 1991.
- deSilva, S., Altiplano-Puna Complex of the Central Andes, *Geology*, 17, 1102-1106, 1989.
- deSilva, S., and P. Francis, *Volcanos of the Central Andes*, Springer-Verlag, New York, 216pp, 1991.
- D'Orazio, M., Boron Determination in Twenty One Silicate Rock Reference Materials by Isotope Dilution ICP-MS, *Geostandard Newsletters*, 23, 21-29, 1999.
- Deyhle, A., Improvements of boron isotope analysis by positive thermal ionization mass spectrometry using static multicollection of  $\text{Cs}_2\text{BO}_2^+$  ions, *Int. J. Mass Spectrom.*, 206, 79-89, 2001.
- Erzinger, J., Chemical alteration of the oceanic crust, *Geol. Rdsch.*, 78 (3), 731-740, 1989.
- Feeley, T. C. and J. P. Davidson, Petrology of calc-alkaline lavas at Volcan Ollagüe and the origin of compositional diversity at Central Andean stratovolcanoes, *J. Petrol.* 35, 1295-1340, 1994.
- Francis, P., and C. Hawkesworth, Late Cenozoic rates of magmatic activity in the Central Andes and their relationships to continental crust formation and thickening. *Journal of the Geological Society of London*, 151, 845-854, 1994.

- Gaillardet, J., and C. J. Allégre, Boron isotopic composition of corals: Seawater or diagenesis record?, *Earth Planet. Sci. Lett.*, 136, 665-676, 1995.
- Gill, J. B., *Orogenic Andesites and Plate Tectonics*, 390pp., Springer-Verlag, New York, 1981.
- Gonfiantini, R., S. Tonarini, M. Gröning, A. Adorni-Braccesi, A. S. Al-Ammar, M. Astner, S. Bächler, R. M. Barnes, R. L. Bassett, A. Cocherie, A. Deyhle, A. Dini, G. Ferrara, J. Gaillardet, J. Grimm, C. Guerrot, U. Krähenbühl, G. Layne, D. Lemarchand, A. Meixner, D. J. Northington, M. Pennisi, E. Reiznerová, I. Rodushkin, N. Sugiura, R. Surberg, S. Tonn, M. Wiedenbeck, S. Wunderli, Y. Xiao, and T. Zack, Intercomparison of Boron Isotope and Concentration Measurements Part II: Evaluation of the results obtained, *Geostandard Newsletters*, in prep..
- Govindaraju, K., 1994 compilation of working values and sample description for 383 geostandards, *Geostandard Newsletters*, 18 (Special Issue), 158pp, 1994.
- Gregoire, D.C., Determination of Boron Isotope Ratios in Geological Materials by Inductive Coupled Plasma Mass Spectrometry, *Anal. Chem.*, 59, 2479-2484, 1987.
- GSJ (Geological Survey of Japan), Geochemical Standards DataBase, <http://www.aist.go.jp/RIODB/geostand>.
- Hawkesworth, C. J., K. Gallagher, J. M. Hergt, and F. McDermott, Mantle and slab contributions in arc magmas, *Ann. Rev. Earth Planet. Sci.*, 21, 175-204, 1993.
- Hemming, N.G., and G. N. Hanson, A procedure for the analysis of boron by thermal ionization mass spectrometry, *Chem. Geol.*, 114, 147-156, 1994.
- Hervig, R. L., G. M. Moore, L. B. Williams, S. M. Peacock, J. R. Holloway, and K. Roggensack, Isotopic and element partitioning of boron between hydrous fluid and silicate melt, *American Mineralogist*, 87, 769-774, 2002.
- Hofmann A. W., Chemical differentiation of the Earth: the relationship between mantle, continental crust, and oceanic crust, *Earth Planet. Sci. Lett.*, 90, 297-314, 1988.
- Imai, N., S. Terashima, S. Itoh, and A. Ando, 1994 compilation of analytical data for minor and trace elements in seventeen GSJ geochemical reference samples, "Igneous rock series", *Geostandard Newsletters*, 19, 135-213, 1995.

- Ishikawa, T. and E. Nakamura, Suppression of Boron Volatilization from a Hydrofluoric Acid Solution Using a Boron-Mannitol Complex, *Anal. Chem.*, 62, 2612-2616, 1990.
- Ishikawa, T. and E. Nakamura, Boron isotope systematics of marine sediments, *Earth Planet. Sci. Lett.*, 117, 567-580, 1993.
- Ishikawa, T., and E. Nakamura, Origin of the slab component in arc lavas from across-arc variation of B and Pb isotopes, *Nature*, 370, 205-208, 1994.
- Ishikawa, T. and F. Tera, Source, composition and distribution of the fluid in the Kurile mantle wedge; constraints from across-arc variations of B/Nb and B isotopes, *Earth Planet. Sci. Lett.*, 152, 123-138, 1997.
- Ishikawa, T. and F. Tera, Two isotopically distinct fluid components involved in the Mariana arc: Evidence from Nb/B ratios and B, Sr, Nd and Pb isotope systematics, *Geology*, 27, 83-86, 1999.
- Ishikawa, T., F. Tera, and T. Nakazawa, Boron isotope and trace element systematics of the three volcanic zones in the Kamchatka arc, *Geochim. Cosmochim. Acta*, 65, 4523-4537, 2001.
- Jochum, K. P., D. B. Dingwell, A. Rocholl, B. Stoll, A. W. Hoffmann, and thirty one others, The Preparation and Preliminary Characterisation of Eight Geological MPI-DING Reference Glasses for In-Situ Microanalysis. *Geostandard Newsletters*, 24, 87-133, 2000.
- Kakihana, H., M. Kotaka, S. Satoh, M. Nomura, and M. Okamoto, Fundamental studies on the separation of boron isotopes, *Bull. Chem. Soc. Japan*, 50, 158-163, 1977.
- Kasemann, S., J. Erzinger, J. G. Viramonte, and G. Franz, The boron isotope cycle of the continental crust from the Central Andes (23 – 27° S) – An overview from Paleozoic to recent, II South American Symposium on Isotope Geology, Cordoba, Argentina, Acta I, 227-231, 1999.
- Kasemann, S., J. Erzinger, and G. Franz, Boron recycling in the continental crust of the central Andes from the Palaeozoic to Mesozoic, NW Argentina, *Contrib. Mineral. Petrol.*, 140, 328-343, 2000.
- Kasemann, S., A. Meixner, A. Rocholl, T. Vennemann, M. Rosner, A. Schmitt, and M. Wiedenbeck, Boron and Oxygen Isotope Composition of Certified Reference Materials NIST SRM 610/612 and Certified Reference Materials JB-2 and JR-2, *Geostandards Newsletters*, 25, 405-416, 2001.

- Kay, S. M. and J. Abruzzi, Magmatic evidence for Neogene lithospheric evolution of the central Andean "flat-slab" between 30°S and 32°S. *Tectonophysics* 259, 15-28, 1996.
- Kay, S. M., B. Coira, and J. Viramonte, Young mafic back arc volcanic rocks as indicators of continental lithospheric delamination beneath the Argentine Puna plateau, central Andes, *J. Geophys. Res.*, 99, 24323-24339, 1994.
- Kerrick, D. M. and J. A. D. Connolly, Metamorphic devolatilization of subducted oceanic metabasalt: implications for seismicity, arc magmatism and volatile recycling, *Earth Planet. Sci. Lett.*, 189, 19-29, 2001.
- Kiss, E., Ion-exchange separation and spectrophotometric determination of boron in geological materials, *Anal. Chim. Acta*, 211, 243-256, 1988.
- Klötzli, U. S., Negative thermal ionisation mass spectrometry: A new approach to boron isotope geochemistry, *Chem. Geol.*, 101, 111-122, 1992.
- Kogiso, T., Y. Tatsumi, and S. Nakano, Trace element transport during dehydration processes in the subducted oceanic crust: 1. Experiments and implications for the origin of ocean island basalts, *Earth Planet. Sci. Lett.*, 148, 193-205, 1997.
- Lécuyer, C., P. Grandjean, B. Reynard, F. Albarède, and P. Telouk, <sup>11</sup>B/<sup>10</sup>B analysis of geological materials by ICP-MS Plasma 54: Application to the boron fractionation between brachiopod calcite and seawater, *Chem. Geol.*, 186, 45-55, 2002.
- Leemann, W.P., R. D. Vocke, E. S. Beary, and P. J. Paulsen, Precise boron isotopic analysis of aqueous samples: Ion exchange extraction and mass spectrometry, *Geochim. Et Cosmochim. Acta*, 55, 3901-3907, 1991.
- Lemarchand, D., J. Gaillardet, É. Lewin, and C. J. Allègre, The influence of rivers on marine boron isotopes and implications for reconstructing past ocean pH, *Nature*, 408, 951-954, 2000.
- Lemarchand, D., J. Gaillardet, and G. Manhès, An optimized procedure for boron separation and mass spectrometry analysis for river samples, *Chem. Geol.*, 182, 323-334, 2002.
- Lindsay, J. M., A. K. Schmitt, R. B. Trumbull., S. L. de Silva, W. Siebel, and R. Emmermann, Magmatic evolution of the La Pacana Caldera system, central Andes, Chile: compositional variation of two cogenetic, large-volume felsic ignimbrites and implications for contrasting eruption mechanisms. *J. Petrol.*, 42, 459-486, 2001.

- Lucassen, F., G. Franz, M. F. Thirlwall, and K. Mezger, Crustal Recycling of Metamorphic Basement: Late Paleozoic Granitoids of Northern Chile (~22°S). Implications for the Composition of the Andean Crust, *J. Petrol.*, 40, 1527-1551, 1999.
- Lucassen, F., R. Becchio, H. G. Wilke, G. Franz, M. F. Thirlwall, J. Viramonte, and K. Wemmer, Proterozoic-Paleozoic development of the basement of the Central Andes (18-26°S) – a mobile belt of the South American craton, *J. South Am. Earth Sci.*, 13, 697-715, 2000.
- Lucassen, F., R. Becchio, R. Harmon, S. Kasemann, G. Franz, R. Trumbull, H. G. Wilke, R. L. Romer, and P. Dulski, Composition and density model of the continental crust at an active continental margin – the Central Andes between 21° and 27°S, *Tectonophysics*, 341, 195-223, 2001.
- Lucassen, F., M. Escayola, R. L. Romer, J. Viramonte, K. Koch, and G. Franz, Isotopic composition of Late Mesozoic basic and ultrabasic rocks from the Andes (23-32°S) – implications for the Andean mantle, *Contrib. Mineral. Petrol.*, 143, 336-349, 2002.
- Matthews, S., A. Jones, and M. Gardeweg, Lascar Volcano, Northern Chile; evidence for steady-state disequilibrium, *J. Petrol.*, 35, 401-432, 1994.
- Morris, J., W. P. Leeman, and F. Tera, The subducted component in island arc lavas: constraints from Be isotopes and B/Be systematics. *Nature*, 344, 31-36, 1990.
- Nakamura, E., T. Ishikawa, J.-L. Birck, and C. J. Allègre, Precise boron isotopic analysis of natural rock samples using a boron-mannitol complex, *Chem. Geol.*, 94, 193-204, 1992.
- Nakano, T. and E. Nakamura, Static multicollecion of Cs<sub>2</sub>BO<sub>2</sub><sup>+</sup> ions for precise boron isotope analysis with positive thermal ionization mass spectrometry, *Int. J. Mass Spectrom.*, 176, 13-21, 1998.
- Naranjo, J., and P. Cornejo, Hoya Salar de la Isla-Carta Geologica de Chile, No. 72, 1:250000, Servicio National de Geologia y Minería, Santiago de Chile, 1992.
- NIST (National Institute of Standards and Technologie), Certificate of Analysis: Standard Reference Material<sup>®</sup> 952, <http://www.nist.gov/>, 1999.
- Oi, T., M. Nomura, T. Oosaka, O. Okamoto, and H. Kakhana, Boron isotopic compositions of some boron minerals, *Geochim. Cosmochim. Acta*, 53, 3189-3195, 1989.

- Ort, M. H., B. L. Coira, and M. M. Mazzoni, Generation of a crust-mantle mixture: magma sources and contamination at Cerro Panizos, central Andes, *Contrib. Mineral. Petrol.*, 123, 308-322, 1996.
- Owens, J. W., E. S. Gladney, and D. Knab, Determinations of boron in geological materials by inductively-coupled plasma emission spectrometry, *Anal. Chim. Acta*, 135, 169-172, 1982.
- Palmer, M. R. and G. H. Swihart, Boron isotope geochemistry: An overview, In: *Boron, Mineralogy, Petrology and Geochemistry* (eds. E.S. Grew and L.M. Anovitz) *Rev. Mineral.*, 33, 845-862, 1996.
- Peacock, S. M., Thermal and Petrological Structure of Subduction Zones (Overview), In: *Subduction top to bottom, Geophysical monograph*, 96, American Geophysical Union, 119-133, 1996.
- Peacock, S. M., and R. L. Hervig, Boron isotopic composition of subduction-zone metamorphic rocks, *Chem. Geol.*, 160, 281-290, 1999.
- Pearce, J. A., and D. W. Peate, Tectonic implications of the composition of volcanic arc magmas, *Annu. Rev. Earth Planet. Sci.*, 23, 251-285, 1995.
- Pearson, P. N., and M. R. Palmer, Atmospheric carbon dioxide concentrations over the past 60 million years, *Nature*, 406, 695 – 699, 2000.
- Plank, T., and C. H. Langmuir, The geochemical composition of subducting sediments and its consequences for the crust and mantle, *Chem. Geol.*, 145, 325-394, 1998.
- Ramakumar, K. L., A. R. Parab, P. S. Khodade, A. I. Almaula, S. A. Chitambar, and H. C. Jain, Determination of isotopic composition of boron, *J. Radioanal. Nucl. Chem. Lett.*, 94, 53-62, 1985.
- Regelous, M., Y. Niu, J. I. Wendt, R. Batiza, A. Greig, K. D. Collerson, Variations in the geochemistry of magmatism on the East Pazific Rise at 10°30'N since 800 ka, *Earth Planet. Sci. Lett.*, 168, 45-63, 1999.
- Rehkämper, M., M. Schönbächler, and C. H. Stirling, Multiple collector ICP-MS: introduction to instrumentation, measurement techniques and analytical capabilities, *Geostandard Newsletters*, 25, 23-40, 2001.

- Romer, R. L., H. L. Förster, and C. Breitkreuz, Intracontinental extensional magmatism with a subduction fingerprint: the late Carboniferous Halle Volcanic Complex (Germany), *Contrib. Mineral. Petrol.*, 141, 201-221, 2001.
- Rose, E. F., N. Shimizu, G. D. Layne, and T. L. Grove, Melt Production Beneath Mt. Shasta from Boron Data in Primitive Melt Inclusions, *Science*, 293, 281-283, 2001.
- Sano, T., T. Hasenaka, A. Shimaoka, C. Yonezawa, and T. Fukuoka, Boron contents in Japan trench sediments and Iwate basaltic lavas, Northeast Japan arc: estimations of sediment-derived fluid contribution in the mantle wedge, *Earth Planet. Sci. Lett.*, 186, 187-198, 2001.
- Scheuber, E., A. J. Bogdanic, and K. J. Reutter, Tectonic development of the north Chilean Andes in relation to plate convergence and magmatism since the Jurassic. In: Reutter, K.-J. (ed) *Tectonics of the Southern Central Andes*, Springer-Verlag, New York, pp. 121-139, 1994.
- Schmitt, A. K., S. Kasemann, A. Meixner, and D. Rhede, Boron in central Andean ignimbrites: implications for crustal boron cycles in an active continental margin. *Chem. Geol.*, 183, 333-347, 2001.
- Schwarcz, H. P., E. K. Agyei, and C. C. McMullen, Boron isotope fractionation during clay adsorption from seawater, *Earth Planet. Sci. Lett.*, 6, 1-5, 1969.
- Smith, H. J., A. J. Spivack, H. Staudigel, and R. H. Hart, The boron isotopic composition of the altered oceanic crust, *Chem. Geol.*, 126, 119-135, 1995.
- Smith, H. J., W. P. Leeman, J. Davidson, and A. J. Spivack, The B isotopic composition of arc lavas from Martinique, Lesser Antilles, *Earth Planet. Sci. Lett.*, 146, 303-314, 1997.
- Spivack, A. J., and J. M. Edmond, Determinations of boron isotope ratios by thermal ionization mass spectrometry of cesium metaborate cation. *Anal. Chem.*, 58, 31-35, 1986.
- Spivack, A. J., and J. M. Edmond, Boron exchange between seawater and the oceanic crust, *Geochim. Cosmochim. Acta*, 51, 1033-1043, 1987.
- Springer, M., Interpretation of heat-flow density in the Central Andes, *Tectonophysics*, 306, 377-395, 1999.

- Staudigel, H., G. R. Davies, S. R. Hart, K. M. Marchant, and B. M. Smith, Large scale isotopic Sr, Nd and O isotopic anatomy of altered oceanic crust: DSDP / ODP sites 417 / 418, *Earth Planet. Sci. Lett.*, 130, 169-185, 1995.
- Stern, C., Role of subduction erosion in the generation of Andean magmas, *Geology*, 19, 78 – 81, 1991.
- Straub, S. M., and G. D. Layne, The systematics of boron isotopes in Izu arc front volcanic rocks, *Earth Planet. Sci. Lett.*, 198, 25-39, 2002.
- Sun, S. S., and W. F. Mc Donough, Chemical and isotopic systematics of oceanic basalts: implications for mantle composition and processes. In: Saunders, A. D., M. J. Norry (eds.), *Magmatism in ocean basins, Geol. Soc. London Spec. Pub.*, 42, pp. 313-345, 1989.
- Swihart, G. R., Instrumental techniques for boron isotope analysis, In: *Boron, Mineralogy, Petrology and Geochemistry (eds. E.S. Grew and L.M. Anovitz) Rev. Mineral.*, 33, 845-862, 1996.
- Tatsumi, Y., Continental crust formation by crustal delamination in subduction zones and complementary accumulation of the enriched mantle I component in the mantle, *Geochem. Geophys. Geosyst.*, vol. 1, Paper number 2000GC000010, 2000.
- Tatsumi, Y., and S. Eggins, Subduction Zone Magmatism, *FRONTIERS IN EARTH SCIENCES*, Blackwell Scientific Publications, Oxford, pp. 1-211, 1995.
- Tatsumi, Y., and T. Kogiso, Trace element transport during dehydration processes in the subducted oceanic crust, 2, Origin of chemical characteristics in arc magmas, *Earth Planet. Sci. Lett.*, 148, 207-222, 1997.
- Taylor, S. R. and S. M. McLennan, *The Continental Crust: its Composition and Evolution, Geoscience Texts*, Blackwell Scientific Publications, Oxford, pp. 9-95, 1985.
- The ANCORP Working Group, Seismic reflection image revealing offset of Andean subduction-zone earthquake locations into the oceanic mantle, *Nature*, 397, 341-34, 1999,
- Tonarini, S., W. P. Leeman, and G. Ferrara, Boron isotopic variations in lavas of the Aeolian volcanic arc, South Italy, *J. of Volcanol. Geotherm. Res.*, 110, 155-170, 2001.
- Tonarini, S., M. Pennisi, and W. P. Leeman, Precise boron isotopic analysis of complex silicate (rock) samples using alkali carbonate fusion and ion-exchange separation, *Chem. Geol.*, 142, 129-137, 1997.



- Tonarini, S., M. Pennisi, A. Adorni-Braccesi, A. Dini, G. Ferrara, R. Gonfiantini, M. Wiedenbeck, and M. Gröning, Intercomparison of boron isotope and concentration measurements. Part I: Selection, preparation and homogeneity tests of the intercomparison materials, *Geostandard Newsletters*, in prep..
- Trumbull, R. B., and M. Chaussidon, Chemical and boron isotopic composition of magmatic and hydrothermal tourmalines from the Sinceni granite-pegmatite system in Swaziland, *Chem. Geol.*, 153, 125-137, 1999.
- Trumbull, R. B., R. Wittenbrink, K. Hahne, R. Emmermann, W. Büch, H. Gerstenberger, and W. Siebel, Evidence for late Miocene to Recent contamination of arc andesites by crustal melts in the Chilean Andes 25-26°S and its geodynamic implications, *J. South Am. Earth Sci.*, 12, 135-155, 1999.
- Vengosch, A., A. R. Chivas, and J. M. McCulloch, Direct determination of boron and chlorine isotopic compositions in geological materials by negative thermal-ionization mass-spectrometry, *Chem. Geol.*, 79, 333-343, 1989.
- Walker, J. A., T. N. Moulds, M. Zentilli, and M. D. Feigenson, Spatial and temporal variations in volcanics of the Andean Central Volcanic Zone (26° to 28°S), *Geological Society of America Special Paper*, 265, 139-155, 1991.
- Williams, L. B., R. L. Hervig, J. R. Holloway, and I. Hutcheon, B isotope geochemistry during diagenesis. Part I. Experimental determination of fractionation during illitization of smectite, *Geochim. Et Cosmochim. Acta*, 65, 1769-1782, 2001 a.
- Williams, L. B., R. L. Hervig and I. Hutcheon, Boron isotope geochemistry during diagenesis. Part II. Applications to organic-rich sediments *Geochim. Et Cosmochim. Acta*, 65, 1783-1794, 2001 b.
- Wittenbrink, R., Zeitliche Variationen der Magmengenese miozäner bis quartärer Vulkanite im südlichen Bereich der Zentralen vulkanischen Zone der Anden (CVZ, 25°-26°S, 67°-69°W), *Berliner Geowissenschaftliche Abhandlungen*, Reihe A 193 (in German with English summary), 135pp, 1997.
- Xiao, Y.-K., and L. Wang, Effect of NO<sub>3</sub><sup>-</sup> on the isotopic measurement of boron, *Int. J. Mass Spectrom.*, 178, 213-220, 1998.

- Xiao, Y.-K., E. S. Beary, and J. D. Fassett, An improved method for the high precision isotopic measurement of boron by thermal ionization mass spectrometry, *Int. J. Mass Spectrom. Ion. Processes*, 85, 203-213, 1988.
- Xiao, Y.-K., H.-Z. Wie, Y.-M. Zhou, Y.-H. Wang, and W.-G. Liu, Investigation of characteristics of non-reductive thermal ion emission of various graphites in thermal ionization mass spectrometry, *Anal. Chim. Acta*, 420, 95-101, 2000.
- Yamazaki, H., Matrix effects in SIMS analysis of high-dose boron implanted silicon wafers, *Nuclear Instruments and Methods in Physics Research B*, 134, 121-125, 1998.
- Yuan, X., S. V. Sobolev, and R. Kind, Moho topography in the Central Andes and its geodynamic implications. *Earth Planet. Sci. Lett.*, 199, 389-402, 2002.
- Zeininger, H., and K. G. Heumann, Boron isotope ratio measurement by negative thermal ionization mass spectrometry, *Int. J. Mass Spectrom. Ion Phys.*, 48, 377-380, 1983.
- Zuleger, E., and J. Erzinger, Determination of the REE and Y in silicate materials with ICP-AES, *Fresenius Z. Anal. Chem.*, 322, 140-143, 1988.

# APPENDIX

- Appendix 1** (List of replicate  $\text{Cs}_2\text{BO}_2^+$ -measurements of NIST SRM 951)
- Appendix 2** (List of individual boron isotope analyses of Andean arc volcanics)
- Appendix 3** (Sample list of investigated Andean arc volcanics)
- Appendix 4** (List of main and trace element concentrations)
- Appendix 5** (Danksagung)
- Appendix 6** (Curriculum vitae)

**Appendix 1:** List of individual  $\text{Cs}_2\text{BO}_2^+$ -measurements of NIST SRM 951

Sample	Date	$^{11}\text{B}/^{10}\text{B}$	1SD	2 SD (mean)	Blocks
NBS 951 (Pos. 1)	30300	4.05393	0.00104	0.00073	8
NBS 951 (Pos. 2)	30300	4.05435	0.00038	0.00027	8
NBS 951 (Pos. 1)	140400	4.05473	0.00065	0.00041	10
NBS 951 (Pos. 12)	80500	4.05361	0.00068	0.00052	7
NBS 951 (Pos. 11)	200600	4.05398	0.00043	0.00029	9
NBS 951 (Pos. 13)	200600	4.05519	0.00078	0.00059	7
NBS 951 (Pos. 11)	220600	4.05463	0.00068	0.00052	7
NBS 951 (Pos. 13)	220600	4.05636	0.00084	0.00064	7
NBS 951 (Pos. 13)	170700	4.05494	0.00065	0.00043	9
NBS 951 (Pos. 12)	170700	4.05493	0.00122	0.00081	9
NBS 951 (Pos. 13)	190700	4.05541	0.00097	0.00062	10
NBS 951 (Pos. 11)	110800	4.05362	0.00056	0.00039	8
NBS 951 (Pos. 13)	110800	4.05482	0.00076	0.00057	7
NBS 951 (Pos. 12)	130800	4.05433	0.00049	0.00031	10
NBS 951 (Pos. 11)	20900	4.05564	0.00134	0.00085	10
NBS 951 (Pos. 12)	20900	4.05483	0.00080	0.00053	9
NBS 951 (Pos. 13)	20900	4.05580	0.00057	0.00036	10
NBS 951 (Pos. 11)	160900	4.05481	0.00054	0.00038	8
NBS 951 (Pos. 11)	270900	4.05410	0.00062	0.00041	9
NBS 951 (Pos. 12)	270900	4.05431	0.00060	0.00038	10
NBS 951 (Pos. 13)	270900	4.05427	0.00125	0.00088	8
NBS 951 (Pos. 1)	101100	4.05499	0.00084	0.00096	3
NBS 951 (Pos. 2)	101100	4.05524	0.00016	0.00014	5
NBS 951 (Pos. 11)	111100	4.05383	0.00090	0.00060	9
NBS 951 (Pos. 12)	111100	4.05527	0.00090	0.00064	8
NBS 951 (Pos. 12)	131100	4.05460	0.00113	0.00092	6
NBS 951 (Pos. 13)	131100	4.05442	0.00071	0.00047	9
NBS 951 (Pos. 9)	141100	4.05439	0.00067	0.00048	8
NBS 951 (Pos. 7)	151100	4.05423	0.00061	0.00054	5
NBS 951 (Pos. 12)	221100	4.05320	0.00030	0.00027	5
NBS 951 (Pos. 12)	291100	4.05366	0.00046	0.00046	4
NBS 951 (Pos. 12)	271200	4.05385	0.00073	0.00046	10
NBS 951 (Pos. 12)	28II1200	4.05339	0.00073	0.00085	3
NBS 951 (Pos. 13)	28II1200	4.05385	0.00060	0.00069	3
NBS 951 (Pos. 10)	30201	4.05347	0.00034	0.00039	3
NBS 951 (Pos. 11)	30201	4.05446	0.00066	0.00054	6
NBS 951 (Pos. 12)	40201	4.05383	0.00103	0.00119	3
NBS 951 (Pos. 13)	40201	4.05460	0.00085	0.00085	4
NBS 951 (Pos. 5)	70201	4.05318	0.00050	0.00050	4
NBS 951 (Pos. 6)	70201	4.05272	0.00056	0.00045	6
NBS 951 (Pos. 12)	130201	4.05255	0.00056	0.00050	5
NBS 951 (Pos. 13)	130201	4.05282	0.00042	0.00042	4
NBS 951 (Pos. 8)	150201	4.05381	0.00078	0.00078	4
NBS 951 (Pos. 12)	240201	4.05364	0.00076	0.00068	5
NBS 951 (Pos. 13)	240201	4.05345	0.00074	0.00066	5
NBS 951 (Pos. 7)	10301	4.05562	0.00129	0.00064	16
NBS 951 (Pos. 5)	210501	4.05459	0.00613	0.00046	7
NBS 951 (Pos. 6)	210501	4.05449	0.00083	0.00083	4
NBS 951 (Pos. 6)	260501	4.05377	0.00051	0.00036	8
NBS 951 (Pos. 13)	270501	4.05481	0.00067	0.00077	3

## Appendix 1: Continued

Sample	Date	$^{11}\text{B}/^{10}\text{B}$	1SD	2 SD (mean)	Blocks
NBS 951 (Pos. 1)	30601	4.05353	0.00013	0.00013	4
NBS 951 (Pos. 2)	30601	4.05353	0.00055	0.00055	4
NBS 951 (Pos. 3)	30601	4.05413	0.00048	0.00022	19
NBS 951 (Pos. 4)	30601	4.05447	0.00034	0.00030	5
NBS 951 (Pos. 11)	300601	4.05419	0.00090	0.00042	19
NBS 951 (Pos. 12)	300601	4.05387	0.00046	0.00035	7
NBS 951 (Pos. 13)	300601	4.05420	0.00043	0.00030	8
NBS 951 (Pos. 12)	260701	4.05552	0.00085	0.00039	19
NBS 951 (Pos. 13)	260701	4.05306	0.00037	0.00030	6
NBS 951 (Pos. 12)	80801	4.05396	0.00049	0.00049	4
NBS 951 (Pos. 13)	80801	4.05433	0.00038	0.00018	18
NBS 951 (Pos. 13)	141101	4.05322	0.00028	0.00023	6
NBS 951 (Pos. 12)	151101	4.05371	0.00056	0.00050	5
NBS 951 (Pos. 1)	161101	4.05350	0.00061	0.00027	20
NBS 951 (Pos. 1)	191101	4.05331	0.00072	0.00033	19
NBS 951 (Pos. 1)	211101	4.05335	0.00074	0.00033	20
NBS 951 (Pos. 1)	231101	4.05476	0.00093	0.00049	14
NBS 951 (Pos. 1)	251101	4.05431	0.00033	0.00030	5
NBS 951 (Pos. 11)	251101	4.05498	0.00095	0.00072	7
NBS 951 (Pos. 1)	280102	4.05423	0.00083	0.00038	19
NBS 951 (Pos. 12)	300102	4.05347	0.00101	0.00054	14
NBS 951 (Pos. 1)	310102	4.05490	0.00069	0.00033	18
NBS 951 (Pos. 1)	40202	4.05335	0.00081	0.00036	20
NBS 951 (Pos. 1)	50202	4.05439	0.00096	0.00043	20
NBS 951 (Pos. 6)	70202	4.05444	0.00094	0.00052	13
NBS 951 (Pos. 7)	70202	4.05308	0.00057	0.00027	18
NBS 951 (Pos. 10)	100202	4.05492	0.00093	0.00059	10
NBS 951 (Pos. 12)	190202	4.05438	0.00030	0.00021	8
NBS 951 (Pos. 13)	190202	4.05290	0.00081	0.00039	17
NBS 951 (Pos. 1)	200202	4.05373	0.00080	0.00056	8
NBS 951 (Pos. 11)	40302	4.05390	0.00136	0.00070	15
NBS 951 (Pos. 12)	40302	4.05362	0.00099	0.00081	6
NBS 951 (Pos. 9)	50302	4.05304	0.00068	0.00036	14
	<b>Mean</b>	<b>4.05416</b>			
	<b>1Sd Promill</b>	<b>0.00077</b>			
	<b>1RSD [‰]</b>	<b>0.19044</b>			

**Appendix 2:** Compilation of all measured  $^{11}\text{B}/^{10}\text{B}$  ratios, the concurrently determined value for the NIST SRM 951 (NIST 951(unpro.)) and normalised  $\delta^{11}\text{B}$  values along with the in-run precisions (calculated on the basis of the block averages) and external reproducibilities of the  $\delta^{11}\text{B}$  values.

Sample	Chemistry	$^{11}\text{B}/^{10}\text{B}$	Measured		$\delta^{11}\text{B}$ mean		1SD [‰]
			2RSD mean	NIST 951 <sub>(unpro.)</sub>	run	mean	
CDA-2-21	K <sub>2</sub> CO <sub>3</sub> 1	4.06702	0.00077	4.05331	3.38		
		4.06621	0.00036	4.05331	3.18	3.28	0.14
	K <sub>2</sub> CO <sub>3</sub> 2	4.06265	0.00035	4.05364	2.22		
		4.06331	0.00035	4.05373	2.36	2.29	0.10
<b>Mean CDA-2-21</b>					<b>2.79</b>	<b>0.70</b>	
CDA-1-4	K <sub>2</sub> CO <sub>3</sub> 1	4.06560	0.00063	4.05331	3.03		
		4.06666	0.00069	4.05331	3.29	3.16	0.18
	K <sub>2</sub> CO <sub>3</sub> 2	4.06382	0.00030	4.05364	2.51		
		4.06401	0.00046	4.05373	2.54	2.52	0.02
<b>Mean CDA-1-4</b>					<b>2.84</b>	<b>0.45</b>	
LULL-KH3	K <sub>2</sub> CO <sub>3</sub>	4.06607	0.00042	4.05331	3.15		
		4.06681	0.00043	4.05331	3.33	3.24	0.13
	HF1	4.06265	0.00017	4.05335	2.29		
		4.06124	0.00109	4.05376	1.84	2.07	0.32
	HF 2	4.06188	0.00858	4.05322	2.13		
		4.06220	0.00059	4.05350	2.15	2.14	0.01
<b>Mean LULL-KH3</b>					<b>2.48</b>	<b>0.66</b>	
LAST-KH2	K <sub>2</sub> CO <sub>3</sub>	4.06556	0.00089	4.05512	2.58	2.58	
		4.06368	0.00110	4.05362	2.48		
	HF	4.06220	0.00119	4.05422	1.97	2.23	0.36
<b>Mean LAST-KH2</b>					<b>2.40</b>	<b>0.25</b>	
LAST-RW3	K <sub>2</sub> CO <sub>3</sub>	4.06492	0.00071	4.05331	2.86		
		4.06667	0.00100	4.05331	3.30	3.08	0.31
	HF 1	4.06032	0.00046	4.05414	1.52	1.52	
	HF 2	4.06174	0.00200	4.05347	2.04		
		4.05645	0.00109	4.05347	0.73	1.39	0.92
<b>Mean LAST-RW3</b>					<b>2.00</b>	<b>0.94</b>	
LAU-94-1	K <sub>2</sub> CO <sub>3</sub>	4.07202	0.00038	4.05433	4.36	4.36	
		4.06734	0.00106	4.05322	3.48		
	HF	4.07248	0.00072	4.05464	4.40	3.94	0.65
<b>Mean LAU-94-1</b>					<b>4.15</b>	<b>0.30</b>	
LIC-5/1/7	K <sub>2</sub> CO <sub>3</sub>	4.04601	0.00175	4.05433	-2.05	-2.05	
		4.04319	0.00080	4.05322	-2.48		
	HF	4.04799	0.00047	4.05464	-1.64	-2.06	0.59
<b>Mean LIC-5/1/7</b>					<b>-2.06</b>	<b>0.00</b>	
LULL-KH3	K <sub>2</sub> CO <sub>3</sub> 1	4.06607	0.00042	4.05331	3.15		
		4.06681	0.00043	4.05331	3.33	3.24	0.13
	K <sub>2</sub> CO <sub>3</sub> 2	4.06265	0.00017	4.05335	2.29		
		4.06124	0.00109	4.05376	1.84	2.07	0.32
	HF 1	4.06188	0.00086	4.05322	2.13		
		4.06220	0.00059	4.05350	2.15	2.14	0.01
<b>Mean LULL-KH3</b>					<b>2.48</b>	<b>0.66</b>	

## Appendix 2: Continued

Sample	Chemistry	$^{11}\text{B}/^{10}\text{B}$	Measured		$\delta^{11}\text{B}$ mean		1SD [‰]		
			2RSD mean	NIST 951 <sub>(unpro.)</sub>	run	mean			
OVER-2-10B	K <sub>2</sub> CO <sub>3</sub>	4.03786	0.00059	4.05376	-3.92				
		4.03953	0.00045	4.05376	-3.51	-3.72	0.29		
	HF	4.04521	0.00038	4.05366	-2.08				
		4.04038	0.00180	4.05295	-3.10				
		4.04226	0.00381	4.05414	-2.93	-2.71	0.54		
<b>Mean OVER-2-10B</b>					<b>-3.21</b>	<b>0.72</b>			
SAIR-2-3	K <sub>2</sub> CO <sub>3</sub>	4.04301	0.00027	4.05335	-2.55				
		4.04347	0.00026	4.05476	-2.79	-2.67	0.17		
	HF	4.03882	0.00103	4.05322	-3.55				
		4.04145	0.00074	4.05350	-2.97	-3.26	0.41		
		<b>Mean SAIR-2-3</b>					<b>-2.97</b>	<b>0.42</b>	
SAL-ZU-96H-7	K <sub>2</sub> CO <sub>3</sub>	4.04893	0.00309	4.05455	-1.38	-1.38			
		4.05057	0.00152	4.05362	-0.75				
	HF	4.04568	0.00111	4.05396	-2.04	-1.40	0.91		
		<b>Mean SAL-ZU-96H-7</b>					<b>-1.39</b>	<b>0.01</b>	
SAL-ZU-96H-14	K <sub>2</sub> CO <sub>3</sub>	4.07029	0.00088	4.05331	4.19				
		4.06972	0.00028	4.05331	4.05	4.12	0.10		
	HF	4.06944	0.00064	4.05414	3.77	3.77			
		<b>Mean SAL-ZU-96H-14</b>					<b>3.95</b>	<b>0.24</b>	
TC-2-3	K <sub>2</sub> CO <sub>3</sub>	4.07092	0.00089	4.05347	4.30				
		4.07436	0.00122	4.05490	4.80				
		4.07282	0.00159	4.05376	4.70				
		4.06942	0.00028	4.05376	3.86	4.42	0.43		
	HF	4.07258	0.00073	4.05269	4.91				
		4.06619	0.00050	4.05355	3.12				
		4.06890	0.00052	4.05562	3.27	3.77	0.99		
		<b>MeanTC-2-3</b>					<b>4.09</b>	<b>0.46</b>	

**Appendix 3:** Sample list of investigated Andean arc-volcanic rocks (WBZ = Depth of the Wadati-Benioff Zone)

<b>Sample</b>	<b>Locality</b>	<b>Latitude</b>	<b>Longitude</b>	<b>WBZ [km]</b>	<b>Age</b>
CDA-2-21	Cordon del Azufre	25°20` S	68°36` W	93	Quaternary
CDA-1-4	Cordon del Azufre	25°20` S	68°36` W	93	Quaternary
LLUL-KH3	Llullaillacu	24°43` S	68°32` W	94	Quaternary
LLUL-RW-1	Llullaillacu	24°43` S	68°32` W	94	Quaternary
LAST-KH2	Lastarria	25°10` S	68°30` W	95	Quaternary
132-LAST RW 3	Lastarria	25°10` S	68°30` W	95	Quaternary
LIC-5/1/7	Licancabur	22°50` S	67°53` W	123	Quaternary
SAIR-2-3	Sairecapur	22°44` S	67°53` W	123	Quaternary
LASC-2-13	Lascar	23°22` S	67°44` W	127	1993
LASC-2-15A	Lascar	23°22` S	67°44` W	127	1993
OVER-2-10B	Cerro Overo	23°21` S	67°40` W	131	Quaternary
179-OVER-1-02	Cerro Overo	23°21` S	67°40` W	131	Quaternary
RIN 1	Pie del Rincon	23°54` S	67°17` W	152	Pliocene
AN 01M	Salar de Antofalla	26°07` S	67°25` W	132	Pliocene
CACO-94-1	Chaco	25°25` S	68°59` W	88	Miocene
TC-2-3	Chaco	25°25` S	68°59` W	88	Miocene
SAL-ZU-96H-7	Sierra Gorbea	25°30` S	68°45` W	92	Pliocene
SAL-ZU-96H-14	Sierra Gorbea	25°30` S	68°45` W	92	Pliocene
LAU-94-1	Near San Parada	26°18` S	68°42` W	92	Miocene
AQUA-2-19	Aguas Blancas	25°41` S	68°30` W	96	Miocene
AQUA-94-29A	Aguas Blancas	25°41` S	68°30` W	96	Miocene



**Appendix 4: List of main and trace element concentrations**

<b>Sample</b>	<b>CDA-2-21</b>	<b>CDA-1-4</b>	<b>LLUL-KH3</b>	<b>LLUL-RW-1</b>	<b>Last-KH-2</b>	<b>LAST-RW-3</b>	<b>LIC-5/1/7</b>
<b>SiO<sub>2</sub></b>	58.4	58.1	65.4	67.3	59.6	61.0	59.2
<b>TiO<sub>2</sub></b>	0.95	0.87	0.72	0.72	0.96	0.97	1.13
<b>Al<sub>2</sub>O<sub>3</sub></b>	16.61	16.95	16.23	14.72	16.34	15.44	17.66
<b>Fe<sub>2</sub>O<sub>3(t)</sub></b>	7.32	7.42	3.80	3.99	6.09	6.47	6.39
<b>MnO</b>	0.11	0.11	0.05	0.05	0.09	0.09	0.09
<b>MgO</b>	3.68	3.62	1.53	1.43	3.60	3.45	1.87
<b>CaO</b>	6.49	6.74	3.90	3.83	6.00	5.94	6.34
<b>Na<sub>2</sub>O</b>	3.41	3.25	4.42	4.37	3.52	3.37	3.42
<b>K<sub>2</sub>O</b>	2.40	2.32	2.76	2.86	2.55	2.61	2.53
<b>P<sub>2</sub>O<sub>5</sub></b>	0.20	0.21	0.23	0.26	0.24	0.25	0.25
<b>H<sub>2</sub>O</b>	0.60		0.61		0.53		
<b>CO<sub>2</sub></b>	0.05		0.04		0.03		
<b>Total</b>	100.19	99.55	99.71	99.52	99.56	99.55	98.87
<b>Li</b>	21		27		24		16
<b>B</b>	54	49	24	22	54	60	18
<b>Sc</b>	18	17	5.2		14	13	16.2
<b>V</b>	177	151	85	117	145	159	174
<b>Cr</b>	34	49	24	17	75	83	
<b>Co</b>	20		10	8	22	20	15
<b>Ni</b>	14	10	14	7	35	32	5
<b>Cu</b>	38	81	49	43	44	35	19
<b>Zn</b>	86	72	76	67	82	73	85
<b>Ga</b>	20		23		22		22
<b>Rb</b>	109	91	73	87	117	119	80
<b>Sr</b>	492	539	635	635	532	531	427
<b>Y</b>	23	22	8		19	18	27.6
<b>Zr</b>	190	154	210	214	194	167	198
<b>Nb</b>	11.6	11.1	7.8		12.0	13.9	12.3
<b>Sb</b>	0.67		0.18		0.75		0.25
<b>Cs</b>	8.5	7.5	1.7		9.3	7.4	2.6
<b>Ba</b>	465	440	754	809	476	497	645
<b>La</b>	34	32	35		37	36	32
<b>Ce</b>	73	68	72		72	77	68
<b>Pr</b>	8.2	7.8	8.1		9.2	8.5	8.3
<b>Nd</b>	32	31	31		35	33	31
<b>Sm</b>	6.2	5.9	5.1		6.6	6.6	6.5
<b>Eu</b>	1.4	1.4	1.3		1.4	1.4	1.5
<b>Gd</b>	5.7	5.1	3.5		5.4	5.0	6.1
<b>Tb</b>	0.85	0.79	0.42		0.66	0.78	0.98
<b>Dy</b>	4.6	4.4	1.9		3.7	3.8	5.5
<b>Ho</b>	0.86	0.82	0.33		0.70	0.65	0.96
<b>Er</b>	2.4	2.3	0.8		1.8	1.8	2.9
<b>Tm</b>	0.35	0.33			0.26	0.25	0.44
<b>Yb</b>	2.2	2.1	0.6		1.6	1.6	2.7
<b>Lu</b>	0.33	0.30	0.10		0.24	0.23	0.40
<b>Hf</b>	4.3	4.3	4.5		4.4	4.3	
<b>Ta</b>	0.80	2.55	0.44		0.93	1.69	0.92
<b>W</b>	2.5		0.4		2.7		
<b>Tl</b>	0.35		0.30		0.42		0.50
<b>Pb</b>	10.8	9.0	13.0		11.3	10.3	14.8
<b>Bi</b>					0.06		0.06
<b>Th</b>	20.7	20.6	5.9		21.4	23.4	8.7
<b>U</b>	5.9	4.4	1.1		6.3	6.4	2.5

## Appendix 4: Continued

Sample	SAIR-2-3	LASC-2-13	LASC-2-15A	OVER-2-10B	OVER-1-02	AN01M	RIN 1
SiO2	62.0	58.4	58.5	53.9	54.9	53.7	52.9
TiO2	0.88	0.76	0.80	0.97	0.98	1.42	1.22
Al2O3	15.70	16.10	16.50	15.66	15.33	16.30	15.80
Fe2O3 <sub>(t)</sub>	5.27	7.26	6.85	8.21	8.57	7.53	7.95
MnO	0.08	0.12	0.12	0.12	0.14	0.13	0.13
MgO	2.84	4.87	4.37	7.50	6.96	6.75	7.53
CaO	5.00	7.20	6.80	7.63	8.17	7.23	8.06
Na2O	3.63	3.01	3.50	2.94	3.03	3.36	2.99
K2O	2.78	1.62	1.69	1.20	1.29	2.10	1.84
P2O5	0.22	0.18	0.19	0.19	0.21	0.32	0.36
H2O	0.64	0.37	0.40			0.37	0.58
CO2	0.06	0.07	0.05			0.03	0.07
<b>Total</b>	<b>99.10</b>	<b>99.96</b>	<b>99.77</b>	<b>98.28</b>	<b>99.57</b>	<b>99.24</b>	<b>99.43</b>
Li	25	19	26	14		17	12
B	20	29	14	11	14	18	10
Sc	13	24	20	23		22	22
V	135	176	177			195	193
Cr	42	116	72			197	324
Co	14	25	21	31	28	32	36
Ni	10	36	32	136	125	124	142
Cu	19	55	53	57		51	43
Zn	90	80	90			78	76
Ga	22	19	19	19	19	21	21
Rb	102	56	68	42	37	61	53
Sr	441	432	464	477	467	583	628
Y	17	19	20	17	17	20	19
Zr	182	128	135	199	100	188	170
Nb	12.0	7.2	9.0	6.8	6.5	21.1	14.2
Sb	0.41	0.60	0.53	0.40		0.14	0.09
Cs	4.4	4.0	5.5	2.3	1.0	2.1	1.3
Ba	642	378	396	320	331	488	442
La	36	19	21	15	16	33	31
Ce	73	40	44	34	35	67	63
Pr	8.6	4.9	5.1	4.4	4.3	7.8	7.6
Nd	32	20	21	19	18	31	30
Sm	6.1	4.1	4.3	4.1	4.2	6.1	5.9
Eu	1.3	1.1	1.1	1.1	1.2	1.6	1.5
Gd	4.9	3.8	4.0	3.7	3.7	5.2	5.0
Tb	0.75	0.66	0.60	0.63	0.63	0.77	0.73
Dy	3.6	3.7	3.7	3.4	3.3	4.1	3.9
Ho	0.63	0.72	0.71	0.64	0.65	0.72	0.74
Er	1.7	2.2	2.1	1.8	1.8	2.1	2.0
Tm	0.23	0.33	0.32		0.28	0.28	0.27
Yb	1.6	2.1	2.1	1.7	1.7	1.9	1.7
Lu	0.23	0.32	0.32	0.26	0.26	0.26	0.27
Hf	4.1		2.8			4.7	4.3
Ta	0.86	0.63	0.84	0.63	1.00	1.27	0.80
W	1.3		1.7				
Tl	0.57	0.31	0.31	0.22			
Pb	16.0	10.1	11.0	8.5	6.7	10.0	7.7
Bi	0.07	0.11	0.06	0.15			
Th	14.0	6.1	7.1	4.0	2.5	6.3	7.2
U	3.4	2.3	2.5	1.5	0.9	1.4	1.4

## Appendix 4: Continued

Sample	SAL-ZU-7	SAL-ZU-14	LAU-94-1	AQUA-2-19	AQUA-94-29A	CACO-94-1	TC-2-3
SiO <sub>2</sub>	56.9	63.0	60.5	57.7	61.4	61.5	59.2
TiO <sub>2</sub>	1.04	0.75	0.94	1.20	0.97	0.75	0.77
Al <sub>2</sub> O <sub>3</sub>	16.95	16.08	17.19	17.08	16.38	17.30	17.70
Fe <sub>2</sub> O <sub>3</sub> (t)	7.50	5.36	5.49	7.09	5.55	4.97	5.54
MnO	0.11	0.08	0.07	0.10	0.07	0.08	0.09
MgO	3.76	2.39	2.70	3.24	2.73	2.10	3.49
CaO	6.84	4.88	5.38	6.50	5.26	5.52	6.10
Na <sub>2</sub> O	3.12	3.17	4.30	4.05	4.11	3.89	3.95
K <sub>2</sub> O	2.10	3.23	2.61	2.06	2.82	2.15	1.90
P <sub>2</sub> O <sub>5</sub>	0.21	0.17	0.27	0.30	0.27	0.19	0.19
H <sub>2</sub> O	0.97	0.62	0.52	0.76		1.32	
CO <sub>2</sub>	0.04	0.04	0.05	0.12		0.04	
<b>Total</b>	<b>99.58</b>	<b>99.76</b>	<b>99.99</b>	<b>100.23</b>	<b>99.57</b>	<b>99.80</b>	<b>98.93</b>
Li	20	24	21	17	19	12	20
B	53	51	18	13	6	32	41
Sc	15	11	9.8	11.2	11	12	18
V	174	117	117	152	116		145
Cr	42	17	60	38	49	11	75
Co	25	15.2	20	22	20	18	20
Ni	24	13	21	22	20	27	33
Cu	44	16	46	32	32	60	
Zn	93	77	92	102	93		77
Ga	23	21	26	20		22	24
Rb	96	165	91	52	85	78	64
Sr	439	374	594	775	668	557	523
Y	21	20	10.9	13	11	14	13
Zr	175	180	239	210	228	194	166
Nb	12.0	12.7	9.0	11.1	11.0	10.0	7.8
Sb	0.66	0.73		0.07		0.11	0.34
Cs	8.0	14.0	1.8	1.1	1.5	2.4	2.5
Ba	427	472	801	601	831	583	490
La	28	34	40	37	53	31	23
Ce	59	70	74	74	102	66	50
Pr	7.1	8.1	9.0	8.7	11.0	7.0	5.8
Nd	27	29	33	33	39	26	23
Sm	5.6	5.6	5.8	6.0	6.2	4.5	4.5
Eu	1.4	1.1	1.5	1.6	1.5	1.3	1.1
Gd	5.1	4.8	4.0	4.5	4.5	5.0	3.9
Tb	0.70	0.75	0.50	0.63	0.52	0.44	0.51
Dy	4.1	4.0	2.5	3.1	2.7	2.7	3.1
Ho	0.78	0.82	0.51	0.53	0.50	0.32	0.52
Er	2.1	2.1	1.1	1.4	1.2	1.4	1.7
Tm	0.31	0.34	0.14	0.18	0.17		0.20
Yb	1.8	2.0	0.9	1.1	1.0	1.1	1.4
Lu	0.28	0.31	0.14	0.16	0.16		0.19
Hf	5.0	2.1	6.5	5.5	6.1	5.4	4.2
Ta	0.84	1.10	0.30	0.50	0.30	0.50	0.54
W	2.8	3.9	0.3	0.4	0.4	0.5	0.7
Tl	0.54	0.34	0.10	0.19	0.10	0.10	0.31
Pb	10.0	11.0	12.0	9.0	16.0	12.0	9.7
Bi	0.01	0.07		0.08	0.09		0.07
Th	19.0	34.0	12.0	6.3	14.0	7.6	6.7
U	5.1	8.9	1.3	1.2	2.0	1.3	1.3

**Appendix 5:****Danksagung**

Mein besonderer Dank gilt Herrn Prof. Jörg Erzinger. Durch seine stete Hilfsbereitschaft in wissenschaftlicher als auch organisatorischer Sicht war es mir möglich das Projekt in der vorliegenden Form abzuschließen.

Herrn Prof. Gerhard Franz danke ich für seine kreativen Anregungen in Bezug auf den Fortgang der Arbeit und die informativen Diskussionen zur Interpretation der Daten.

Bei Herrn Prof. Roland Oberhänsli bedanke ich mich für die Übernahme des Referates.

Meinen Kollegen Dr. Robert Trumbull, Dr. Alexander Rocholl, Dr. Michael Wiedenbeck und Dr. Thomas Wiersberg danke ich für ihre stete Diskussionsbereitschaft während der Anfertigung dieser Arbeit.

Herrn Dr. Rolf L. Romer danke ich für die Einführung und Unterstützung bei den nasschemischen und massenspektrometrischen Methoden.

Frau Anette Meixner danke ich für eine exzellente Zusammenarbeit während des Aufbaus der  $\text{Cs}_2\text{BO}_2^+$ -Graphit Methode und die immer noch andauernden anregenden Diskussionen in Bezug auf die Verbesserung der Bor- und Lithiumanalytik.

Herrn Dr. Knut Hahne, Herrn Peter Pilz und Herrn Dr. Klaus Peter Jochum danke ich für die Bereitstellung der Proben.

Für die Unterstützung bei der Analytik danke ich Frau Sabine Tonn, Frau Heike Rothe und Herrn Rudolf Naumann.

Meinen Freunden Janet McFarland und Tobias Zisik danke ich für die Hilfe bei der Korrektur des englischen Manuskriptes.

Bei meinen Eltern Ruth und Erich und meiner Schwester Cornelia bedanke ich mich für den großartigen familiären Rückhalt. Sie haben mich sowohl immer wieder motiviert als auch von schwerwiegenden Entscheidung abgehalten, die ich im Nachhinein vielleicht bereut hätte – aber wer kann das schon genau wissen!

Die vorliegende Arbeit wurde von der Deutschen Forschungsgemeinschaft im Rahmen des Sonderforschungsbereiches 267 „Deformationsprozesse in den Anden“ finanziert.

**Appendix 6:****Curriculum vitae**

Name: Martin Siegfried Rosner  
Born: 14.07.1972 Kassel, Germany  
Citizenship: German

**School:**

1979 – 1983 Primary school in Habichtswald/Doernberg  
1983 – 1989 Secondary school in Zierenberg  
1989 – 1992 High school (Gymnasium) at the Jakob-Grimm-Schule in Kassel

**University:**

1992 – 1999 Study of Geology/Paleontology at the Georg-August-University of Göttingen  
Degree: Diploma in Geology/Paleontology  
Title: Die retrograde Entwicklungsgeschichte der Vesser-Zone und des Schwarzburger Sattels, NW` Saxothuringikum, abgeleitet aus K/Ar-Altersdatierungen an Mineralfeinfraktionen

**Carrer:**

1999 – 2002 Scientific employee (doctoral student) in the project “Boron as a tracer for transport processes” in the framework of the DFG Collaborative Research Center SFB 267 “Deformation processes in the Andes” at the GeoForschungsZentrum Potsdam  
2002 – 2003 Scientific employee in the project “Boron and lithium cycling in the Tonga subduction zone” in the framework of the DFG Schwerpunktprogramm “Ocean Drilling Programm, ODP” at the GeoForschungsZentrum Potsdam